Doctoral Thesis

Electromagnetic Properties and Double Negative Characteristics of Hybrid Granular Composite Materials in the Microwave Frequency Range

MASSANGO HERIETA

D152496

Curriculum and Instruction Sciences

Graduate School of Education

Hiroshima University

Japan

2018

Doctoral Thesis

Electromagnetic Properties and Double Negative Characteristics of Hybrid Granular Composite Materials in the Microwave Frequency Range

Presented to

Graduate School of Education

Hiroshima University

In Partial Fulfillment of the Requirements for the Degree of

Doctor of Philosophy

By

MASSANGO HERIETA

D152496

Curriculum and Instruction Sciences

Graduate School of Education

Hiroshima University

Japan

2018

Electromagnetic Properties and Double Negative Characteristics of Hybrid Granular Composite Materials in the Microwave Frequency Range

Doctoral Thesis

Written by HERIETA MASSANGO

D152496

Accepted by the board of examiners of Curriculum and Instruction Sciences

Graduate School of Education, Hiroshima University

On January 10, 2018, and declared to have fulfilled the requirement of acquiring a Ph.D Degree

Board of Examiners

……

Prof. Dr. Takanori Tsutaoka

……..….. ……..……..

(Prof. Dr. Nobuyoshi Koga) (Prof. Dr. Hirofumi Yamasaki)

……..….. ……..……..

(Prof. Dr. Takashi Umeda) (Prof. Dr. Norio Ogita)

January 10, 2018

Abstract

It has theoretical predicted and experimentally demonstrated that the Double Negative (DNG) or Left-Handed (LH) composite materials show interesting electromagnetic properties that can lead to a diversity of optical or microwave applications.

A number of studies to realize the Epsilons Negative (ENG) and Mu Negative (MNG) properties of "real" materials have been carried out using composite structures including metallic, magnetic or dielectric particles, fibers in the host materials and by artificial periodic structure of printed metal patterns or strip lines as well. The MNG spectrum can be obtained by the magnetic resonance of ferromagnetic materials. The ENG property in the Radio Frequency (RF) to microwave frequency range is obtained by metal granular composite; the low frequency plasmonic (LFP) state with the ENG spectrum can be realized in the electrically percolated metal granular composite materials. To achieve the simultaneously negative permittivity and permeability in the RF to microwave range, it is required to make a coexistence of the LFP state and the ferromagnetic resonance in the composite structure of the single or multi particle system.

Very few works exist on the realization of DNG characteristics in granular composite materials using the combination of "real" randomly distributed conductive and magnetic particles, and of these few works, the DNG characteristic was realized in RF frequency range up to 1 GHz.

In this thesis, the experimental results of the combination of Cu metal particles with different ferromagnetic particles FeNi, FeCo, Ni-Zn Ferrite and Mn-Zn Ferrite embedded in a host Polyphenylene Sulfide (PPS) resin powder, forming hybrid composite materials to achieve the DNG characteristic are presented.

The results analyses of electric permittivity and magnetic permeability spectrum measurements showed the frequency regions where the values are negative; the ENG and MNG proprieties have been obtained in the microwave frequency range. The DNG characteristic, the region where ENG and MNG are overlapped was observed in frequency range up to 10 GHz.

Acknowledgements

First of all I would like to express my gratitude to the Japanese Government and Ministry of Education, Culture, Sport, Science and Technology (MEXT) for the great opportunity to upgrade my academic skills through the Monbukagakusho scholarship.

I am deeply indebted to my academic supervisor Takanori Tsutaoka for his academic support; guidance and encouragement that have been very valuable to me and to his family for their worm welcome to Japan and affection

I am very grateful to Professor Toshinobu Maehara, Professor Takashi Umeda, Professor Nobuyoshi Koga, Professor Hirofumi Yamasak and Professor Norio Ogita for their valuable support and advice.

I would like to thank all professors and colleagues of Science Education major in Hiroshima University and my research roommates for their unconditional help and support during my study.

My deeply thank to Professor Rogério J. Uthui for his effort and encouragement to continue my studies, Professor Mário S. Balói, Professor Alberto Cupane and Professor Urâneo S. Mahanjane for their support, effort and encouragement for me to study in japan. I am also very grateful to all my colleagues at the Pedagogical University of Mozambique for their encouragement and support.

Last but not least, I would like to express my profound gratitude to my adorable son and my whole family members for their love, encouragement and support.

Dedication

I dedicate this thesis to my son Henrique José Muianga, to my parents and family for the encouragement and unconditional support.

Contents

List of Figures

List of tables

List of abbreviations

Abbreviation	Full word
ENG	Epsilon Negative
MNG	Mu Negative
LH	Left-Handed
RH	Right Handed
DNG	Double Negative
TW	Tin-Wire
SRR	Split-Ring Resonator
DNMs	Double Negative Materials
EM	Electromagnetic
RF	Radio Frequency
LFP	Low Frequency Plasmonic
NRI	Negative refractive Index
ZIM	Zero Index Materials
MMs	Metamaterials
DPS	Double Positive
SNG	Single Negative
MGA	Maxwell Garnet Approximation
CMA	Coherent Model Approximation
DWV	Domain Wall Vibration
GRS	Gyro Spin Rotation

MR	Magnetic Resonance

Chapter 1: Introduction

1.1. Conceptualization of the study

For decades, it was set the sign of index of refraction of materials to be positive and associate it with transparent materials. The idea of attributing a negative sign to refractive index of materials was seems to be unnecessary. However, if we take a look, light consists of electric and magnetic fields interacting each other and from the Maxwell relation, refractive index is related to the electric permittivity and magnetic permeability. If both the effective electric permittivity and magnetic permeability are negative, the refractive index will be negative. Hence, it was necessary to think again of index of refraction of a material having negative sign.

V. G. Veselago was who first hypothesized that composite materials can be designed to produce any value of electric permittivity and magnetic permeability [1]. V.G. Veselago demonstrated that negative refraction can occur if both the effective electric permittivity and magnetic permeability of a material are negative and these materials will show unusual electromagnetic wave propagation phenomenon. Years later, J. B. Pendry demonstrate that systems having a negative refractive index can produce sharper images, with a potential to resolve subwavelength feature [2]. Smith et al. also demonstrate that an effective LH material leads to unusual electromagnetic wave propagation and also demonstrate frequency regions where the sign of refractive index must in fact be negative in this material [3]. Because no natural material would show such property of negative index of refraction, the main thought was maybe it was possible to manufacture artificial material which can show this property. Walser, introduced the name metamaterials for a description of manmade materials designed to produce

an optimized combination not available in nature, these effective composite materials could respond to specific excitation [4].

In a very potent way, metamaterials ignited the world at the beginning of the last decade driving by the idea of embracing negative refractive index materials.

The novel of LH materials it was theoretical curiosity until Shelby and his group experimentally demonstrated a negative refraction in the microwave frequency using a metamaterial compose of an array of copper thin-wire (TW) and split-ring resonators (SRR) confirming the previous hypothesis, demonstrations and simulation [5]. Using a combination of array of copper split ring resonator and wires, they fabricate a prism-shaped sample that exhibited a frequency band where the effective index of refraction was negative. Just before the experimental demonstration of negative refractive index by Shelby; J. B. Pendry, demonstrate that a three dimensional array of intersecting thin-wire could be used to create negative values of permittivity [6] and also demonstrated that a periodic array of SRR could produce an effective value of permeability [7].

The LH structures were first fabricated to respond at frequencies of microwave [5, 8], years letter at terahertz range [9]. Since then, various researchers concentrated on developing materials of LH using SRR with a negative index of refraction capable of high-frequency magnetic response [10, 11].

Various materials composed of periodic arrays of unit cells with various novel structures were proposed to achieve the LH or DNG properties. The development of double negative materials (DNMs) with simultaneous negative value of permittivity and permeability can lead to

a diversity of optical or microwave applications such as modulators [12], super lenses [2], microwave couplers [13] and antennas [14].

Since the DNG properties in metamaterials originate from artificial structures rather than directly from natural materials. Therefore, it is also interesting to investigate the possibilities of realizing the DNG properties from the point of "real" random materials rather than periodic artificial structures. It has been proven that many "real" materials possess single negative permittivity [15-18] or negative permeability [19-23]. We can say that the double negative property can be realized in composites consisting of randomly distributed particles that can provide negative permittivity ε component and particles providing negative permeability μ component. Following this idea, composites consisting with metallic particles, providing negative ε below its plasma frequency hosted in a negative μ matrix will be presented as promises candidates for DNG composite materials. However, the coexistence of single negative permittivity and permeability spectra was observed in single submicron Ni granular composite materials [24]. This result implies that there is a possibility to create DNG single particle composite material using micron or nanometer sized ferromagnetic metal particles with the oxide layer.

As the DNG granular composite materials, the combination of conductive and magnetic particles such as Cu/YIG [25], Ag/ $Y_3Fe_5O_{12}$ [26] , Co/Al_2O_3 [27] , Fe/Al_2O_3 [28] have been investigated in the RF frequency range up to 1 GHz. We have been investigated the microwave DNG properties in the hybrid composite materials combining ferromagnetic particles with cupper particles YIG/Cu under external magnetic field [29] and in the absence of external magnetic field [30-32] in the RF frequency range up to 20 GHz.

In the present thesis, cupper particles were selected to provide negative ε. The complex permittivity spectra of Cu granular composite materials have been studied and the low frequency plasmonic state was found in the percolation threshold metal particle cluster in the microwave range [18]. In general negative μ can be obtained by magnetic resonance of ferromagnetic particles. The $Fe_{53}Ni_{47,}$ $Fe_{50}Co_{50,}$ Ni-Zn Ferrite, Mn-Zn Ferrite particles have been selected to provide negative μ. The permalloy $Fe_{53}Ni_{47}$, Permendur $Fe_{50}Co_{50}$ have been proved to be able to generate negative μ [31, 33] and Ferrite Ni-Zn and Mn-Zn to be potential candidates to generate negative μ [34, 35].

1.2. Purpose of the study

The central theme of this thesis is to design and investigate the possibilities of realizing the double negative properties DNG, simultaneous negative values of permittivity ε and permeability μ by using the combination of random granular composite materials in the microwave frequency range.

1.3. Significance of the study

Actually few works exist on the realization of DNG characteristic using granular composite materials especially in frequency range above 1GHz [25, 26, 28, 36]. In this thesis the results of electric permittivity and magnetic permeability analysis in frequency range up to 20 GHz and simultaneous negative permittivity and negative permeability, DNG characteristic up to above 1 GHz will be presented.

The experimental results on DNG properties in granular composite materials have great significance for the realization of LH materials which are needed for different applications such as the construction of electromagnetic wave absorbers, frequency selective shielding, small microwave antennas and others.

1.4. Composition of the thesis

As said before, the central theme of this thesis is to design and analyze the electromagnetic properties of granular composite materials with the main purpose of realizing the DNG characteristic in the RF frequency range up to 20 GHz. The thesis is organized into five chapters starting from the current chapter one which intends to give a brief introduction of the historical development of LH materials and the motivation of this study.

The second chapter describes the theory behind the negative refractive index materials. The basic concepts involving the materials response to the electromagnetic (EM) waves and the mechanisms to get the DNG characteristic. In generally these responses are governed by two frequency dependent parameters, permittivity ε that describes the response of the material to the electric component and permeability μ to the magnetic component. The concept involving the models that were used to evaluate the frequency dispersion of permittivity, Drude and Lorentz models and the mixing theory.

The third chapter deals with the experimental methodology, detailing all steps since the sample preparation process to the measurements. Based on "real" random materials, hybrid composite materials consisting of metallic Cu and magnetic FeNi, FeCo, NiZn Ferrite MnZn Ferrite particles are fabricated. The concept of transmission line approach and volume fraction

of particles is discussed. The relative complex permittivity ε_r and permeability μ_r of the composite materials were measured by the transmission/reflection method using a coaxial line cell and a network analyzer in the frequency range from 10 MHz to 20 GHz. The electrical conductivity of composite materials was measured by the two terminal method using an impedance analyzer in the frequency range from 1 kHz to 40 MHz.

The fourth chapter, the results and discussion will be presented. In this chapter experimental results based on theory previously reviewed is discussed. The materials developed was analyzed by measuring the electrical conductivity in frequency range from 1 kHz to 40 MHz and complex permittivity and permeability spectra in the frequency range from 10 MHz to 20 GHz using a network analyzer and a transmission line approach. Since the developed composite contains two particles having metallic and magnetic particles, the electrical percolation effect is determined by the volume fraction of metallic particles. Increasing the metallic particles the conductivity is enhanced, LFP state is achieved and the negative permittivity takes place. The negative permeability is realized by the magnetic resonance of ferromagnetic particles. We showed that the DNG characteristic is realized in the materials that we produced. The DNG characteristic is realized in frequencies up to 10 GHz. Further the complex permittivity spectra are fitted by using Drude and Lorentz models.

The fifth chapter which is the last chapter of this thesis is reserved to the conclusion. This chapter presents a summary of findings and stresses the contribution of this work for farther investigations on the development of LH materials. The quasi-isotropic Negative Refractive Index (NRI) or Zero Index Material (ZIM) can be realized using the DNG granular composite materials. The calculated NRI spectrum for the x = 0.24 in $(Cu_xFeNi_{1-x})_{0.85}PPS_{0.15}$, Cu/FeNi

composite as function of frequency was examined and the NRI was obtained from 200 MHz to 1.8 GHz.

References

[1] V.G. Veselago, The electrrodynamics of substances with simultaneously negative value of e and m, Soviet Physics Usp., 10 (1968) 509-514.

[2] J.B. Pendry, Negative refraction makes a perfect lens, Phys Rev Lett, 85 (2000) 3966-3969.

[3] David R. Smith, N. Kroll, Negative Refractive Index in Left-Handed Materials, PHYSICAL REVIEW LETTERS, 85 (2000) 2933-2936.

[4] R. M. Walser, Metamaterials: What are they? What are they good for?, 2000.

[5] R.A. Shelby, D.R. Smith, S. Schultz, Experimental verification of a negative index of refraction, Science, 292 (2001) 77-79.

[6] J.B. Pendry, A.J. Holden, D.J. Robbins, W.J. Stewart, Low frequency plasmons in thin-wire structures, J Phys-Condens Mat, 10 (1998) 4785-4809.

[7] J.B. Pendry, A.J. Holden, D.J. Robbins, W.J. Stewart, Magnetism from conductors and enhanced nonlinear phenomena, IEEE Transactions on Microwave Theory and Techniques, 47 (1999) 2075-2084.

[8] K.B. Alici, E. Özbay, Radiation properties of a split ring resonator and monopole composite, physica status solidi (b), 244 (2007) 1192-1196.

[9] T.J. Yen, W.J. Padilla, N. Fang, D.C. Vier, D.R. Smith, J.B. Pendry, D.N. Basov, X. Zhang, Terahertz Magnetic Response from Artificial Materials, Science, 303 (2004) 1494-1496.

[10] N. Katsarakis, T. Koschny, M. Kafesaki, E.N. Economou, C.M. Soukoulis, Electric coupling to the magnetic resonance of split ring resonators, Applied Physics Letters, 84 (2004) 2943-2945.

[11] A.B. Movchan, S. Guenneau, Split-ring resonators and localized modes, Physical Review B, 70 (2004) 125116.

[12] J.-S. Li, Terahertz wave modulator based on optically controllable metamaterial, Optics & Laser Technology, 43 (2011) 102-105.

[13] R. Islam, F. Elek, G.V. Eleftheriades, Coupled-line metamaterial coupler having co-directional phase but contra-directional power flow, Electronics Letters, 40 (2004) 315.

[14] R.D. Ziolkowski, N. Engheta, in: N. Engheta, R.W. Ziolkowski (Eds.) Metamaterials - Physics and Engineering Explorations-, A John Wiley & Sons, Inc., 2006, pp. 8.

[15] B. Li, G. Sui, W.-H. Zhong, Single Negative Metamaterials in Unstructured Polymer Nanocomposites Toward Selectable and Controllable Negative Permittivity, Advanced Materials, 21 (2009) 4176-4180.

[16] Z.C. Shi, R.H. Fan, Z.D. Zhang, H.Y. Gong, J. Ouyang, Y.J. Bai, X.H. Zhang, L.W. Yin, Experimental and theoretical investigation on the high frequency dielectric properties of Ag/Al2O3 composites, Applied Physics Letters, 99 (2011) 032903.

[17] M. Gao, Z.C. Shi, R.H. Fan, L. Qian, Z.D. Zhang, J.Y. Guo, High-Frequency Negative Permittivity from Fe/Al2O3 Composites with High Metal Contents, J Am Ceram Soc, 95 (2012) 67-70.

[18] T. Tsutaoka, T. Kasagi, S. Yamamoto, K. Hatakeyama, Low frequency plasmonic state and negative permittivity spectra of coagulated Cu granular composite materials in the percolation threshold, Applied Physics Letters, 102 (2013) 181904.

[19] T. Kasagi, T. Tsutaoka, K. Hatakeyama, Negative permeability spectra in Permalloy granular composite materials, Applied Physics Letters, 88 (2006) 172502.

[20] T. Tsutaoka, T. Kasagi, K. Hatakeyama, Permeability spectra of Yittrium Iron Garnet and its granular composite materials under dc magnetic field, J Appl Phys, 110 (2011) 053909.

[21] A. Pimenov, A. Loidl, K. Gehrke, V. Moshnyaga, K. Samwer, Negative Refraction Observed in a Metallic Ferromagnet in the Gigahertz Frequency Range, Physical Review Letters, 98 (2007) 197401.

[22] Z.-C. Shi, R.-H. Fan, Z.-D. Ahang, L. Qian, M. Gao, M. Zhang, L.-T. Zheng, X.-H. Zhang, L.-W. Yin, Randome Composites of Nickel Networks Supported by poros Alumina Toward Double Negative Materials, Advanced Materials, 24 (2012) 2349-2352.

[23] T. Kasagi, T. Tsutaoka, K. Hatakeyama, Electromagnetic properties of Permendur granular composite materials containing flaky particles, J Appl Phys, 116 (2014) 153901.

[24] H. Massango, T. Tsutaoka, T. Kasagi, S. Yamamoto, K. Hatekeyama, coexistence of gyromagnetic resonance and low frequency plasma state in the submicron ni granular composite materials, J Appl Phys, 121 (2017) 103902-103901-103902-103902.

[25] K. Sun, Z.-d. Zhang, R.-h. Fan, M. Chen, C.-b. Cheng, Q. Hou, X.-h. Zhang, Y. Liu, Random copper/yttrium iron garnet composites with tunable negative electromagnetic parameters prepared by in situ synthesis, RSC Adv., 5 (2015) 61155-61160.

[26] Z.C. Shi, R.H. Fan, Z.D. Zhang, K.L. Yan, X.H. Zhang, K. Sun, X.F. Liu, C.G. Wang, Experimental realization of simultaneous negative permittivity and permeability in Ag/Y3Fe5O12 random composites, Journal of Materials Chemistry C, 1 (2013) 1633-1637.

[27] X.-a. Wang, Z.-c. Shi, M. Chen, R.-h. Fan, K.-l. Yan, K. Sun, S.-b. Pan, M.-x. Yu, Tunable Electromagnetic Properties in Co/Al2O3 Cermets Prepared by Wet Chemical Method, J Am Ceram Soc, 97 (2014) 3223-3229.

[28] Z.-c. Shi, R.-h. Fan, K.-l. Yan, K. Sun, M. Zhang, C.-g. Wang, X.-f. Liu, X.-h. Zhang, Preparation of Iron Networks Hosted in Porous Alumina with Tunable Negative Permittivity and Permeability, Advanced Functional Materials, 23 (2013) 4123-4132.

[29] T. Tsutaoka, K. Fukuyama, H. Kinoshita, T. Kasagi, S. Yamamoto, K. Hatakeyama, Negative permittivity and permeability spectra of Cu/yttrium iron garnet hybrid granular composite materials in the microwave frequency range, Applied Physics Letters, 103 (2013) 261906.

[30] T. Tsutaoka, H. Massango, T. Kasagi, S. Yamamoto, K. Hatakeyama, Double negative electromagnetic properties of percolated Fe53Ni47/Cu granular composites, Applied Physics Letters, 108 (2016) 191904.

[31] H. Massango, T. Tsutaoka, T. Kasagi, Electromagnetic properties of Fe53Ni47 nd Fe53Ni47/Cu granular composite materials in the microwave range, Mater. Res. Express, 3 (2016).

[32] H. Massango, T. Tsutaoka, T. Kasagi, S. Yamamoto, K. Hatakeyama, Complex permeability and permitivitty spectra of percolated Fe50Co50/Cu granular composites, J Magn Magn Mater, 442 (2017) 403-408.

[33] T. Kasagi, T. Tsutaoka, A. Tsurunaga, K. Hatakeyama, High-frequency permeability of Fe-Co and Co granular composite materials, Journal of the Korean Physical Society, 62 (2013) 2113-2117.

[34] T. Nakamura, T. Tsutaoka, K. Hatakeyama, Frequency dispersion of permeability in ferrite composite materials, J Magn Magn Mater, 138 (1994) 319-328.

[35] T. Tsutaoka, T. Kasagi, K. Hatakeyama, M.Y. Koledintseva, Analysis of the Permeability Spectra of Spinel Ferrite Composites Using Mixing Rules, in: IEEE International Symposium on Electromagnetic Compatibility, , IEEE, Denver, 2013, pp. 545 - 550.

[36] X.-a. Wang, Z.-c. Shi, M. Chen, R.-h. Fan, K.-l. Yan, K. Sun, S.-b. Pan, M.-x. Yu, Tunable Electromagnetic Properties in Co/Al2O3 Cermets Prepared by Wet Chemical Method, 97 (2014) 3223-3229.

Chapter 2: Theory on metamaterials - Review

2.1. Electromagnetic response of materials

In general electromagnetic (EM) response in homogeneous materials is predominantly governed by the two parameters, permittivity ε and permeability μ. Both parameters are typically frequency-dependent complex quantities and are described by

$$\varepsilon_r(\omega) = \varepsilon_r'(\omega) - j\varepsilon_r''(\omega) \quad 2.1$$

$$\mu_r(\omega) = \mu_r'(\omega) - j\mu_r''(\omega) \quad 2.2$$

Where ε_r and μ_r are the relative complex permittivity and permeability; ε_r' and μ_r' the real parts and ε_r'' and μ_r'' imaginary parts of ε_r and μ_r respectively. Other quantity commonly used to describe the EM wave propagation is the index of refraction that is defined in terms of ε and μ.

$$n(\omega) = \sqrt{\varepsilon_r(\omega)\mu_r(\omega)} \quad 2.3$$

The index of refraction provides a measure of the speed of EM wave as it propagates within a material. Also provides a measure of the deflection of a beam of light as it crosses the interface between two materials having different values for their refractive index. If a material were found that has negative values of ε and μ, then its refractive index would be negative. Fig. (2.1) illustrates the comparison of deflection of an incident beam on a conventional material and or in a left-handed material. The incident beam θ_1 from the air enters and refracts in a convention material θ_2 or metamaterial $-\theta_2$.

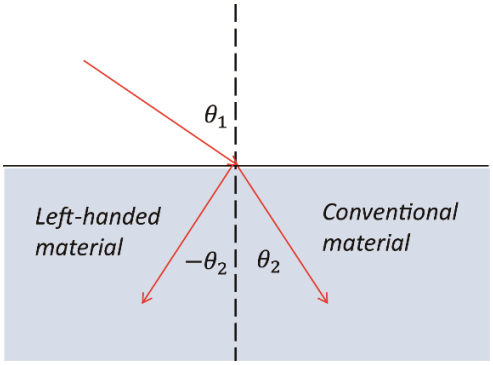

Figure 2.1. A comparison of refractive index in a negative material to that in a conventional material with positive refractive index. The incident beam θ_1 from the air enters and refracts in a convention material θ_2 or metamaterial$-\theta_2$.

In negative medium, $n = -1$ the expression of permittivity and permeability can be derived using polar coordinates in terms of magnitude and phase π of both μ and ε.

$$\varepsilon_r = \varepsilon_r' - j\varepsilon_r'' = |\varepsilon_r| e^{-j\theta_\varepsilon} \qquad 2.4$$

$$\mu_r = \mu_r' - j\mu_r'' = |\mu_r| e^{-j\theta_\mu} \qquad 2.5$$

$$\mathrm{n} = \sqrt{|\varepsilon_r||\mu_r|}\, e^{-j\theta_n} \qquad 2.6$$

Where $\theta_n = (\theta_\varepsilon + \theta_\mu)/2$ is the total phase of ε_r and μ_r. Such LH materials with both negative values of ε and μ or $n = -1$ have never been found in nature. However because artificial materials metamaterials, MMs can have controlled magnetic and electric response over a broad frequency range, it is possible to achieve the condition $\varepsilon < 0$ and $\mu < 0$ in artificial composite

materials. To understand these artificial composite medium or MMs, it is necessary to understand the materials response to the EM waves.

2.1.Classification of metamaterials

Metamaterials can be classified in terms of their permittivity and permeability. In general there is four possible sigh combination $(+,+)$, $(-,+)$, $(+,-)$ and $(-,-)$ of the ε and μ pair as shown in Fig. (2.2).

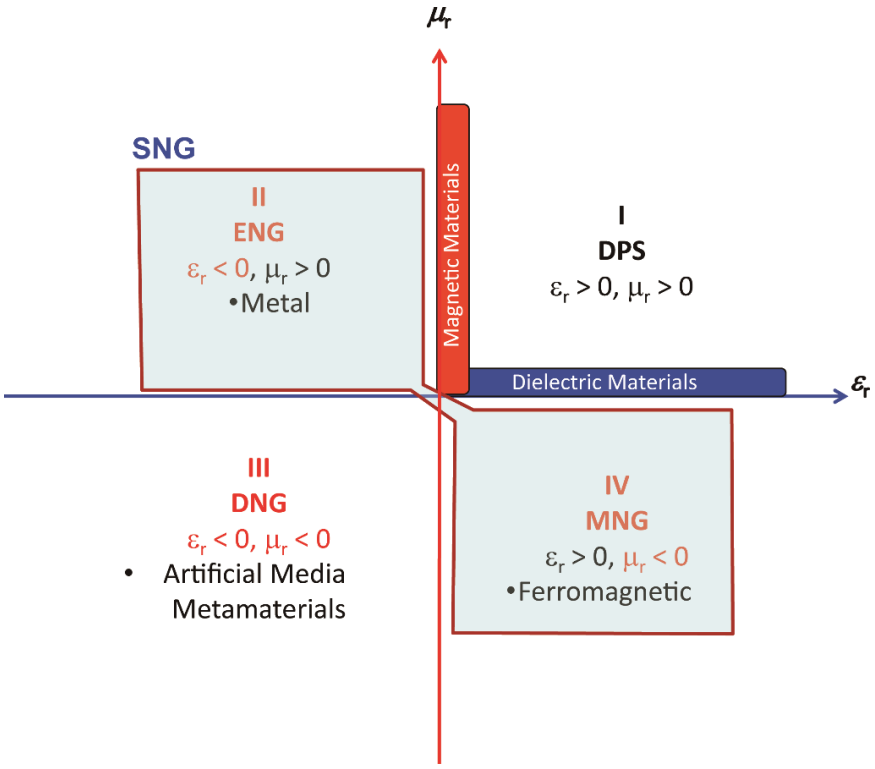

Figure 2.2. Classification of electromagnetic materials by their permittivity-permeability.

The first combination $\varepsilon > 0$ and $\mu > 0$, $(+,+)$ double positive (DPS) materials is well known in conventional materials, all our everyday transparent materials. In these materials the

index of refraction is positive and real, the electromagnetic waves can propagate in these materials. In this group, dielectric material have high permittivity ε and magnetic materials have high permeability μ.

The second and third combinations correspond to the single negative (SNG) materials, $(-,+)$, $\varepsilon < 0$ and $\mu > 0$, ENG metallic materials or $(+,-)$, $\varepsilon > 0$ and $\mu < 0$, MNG ferromagnetic materials. The electromagnetic response of materials in the visible and near-ultraviolet regions is dominated by negative ε concept.

The last combination $(-,-)$, $\varepsilon < 0$ and $\mu < 0$ constitutes a new class of materials, DNG materials. No natural materials have been found with simultaneous values of negative ε and μ. Artificial materials have been use to get these properties. These DNG materials can have interested LH properties that can lead to a development of several microwave devices.

2.2. Metamaterials

Metamaterials are artificial homogeneous structures with unusual electromagnetic properties not readily available in nature. The term "metamaterials" was coined by Walser, he described the metamaterials as manmade materials designed to produce an optimized combination not available in nature [1]. Metamaterials are constructed with two or more materials at a macroscopic level, their size and spacing is much smaller relatively to the scale of spatial variation of exciting field. The materials are used to control and manipulate the electromagnetic parameters. Hence, metamaterials can be designed to produce any value of electric permittivity and magnetic permeability.

2.3. Left-handiness of metamaterials from Maxwell equations

A LH material is an electromagnetic medium with simultaneous negative ε and μ. The DNG properties result in the propagation of electromagnetic waves exhibiting antiparallel phase and group velocity or LH waves. Starting from the Maxwell equations,

$$\nabla \mathrm{x} E = -\frac{\partial B}{\partial t} \qquad 2.7$$

$$\nabla \mathrm{x} \mathrm{H} = \frac{\partial D}{\partial t} \qquad 2.8$$

$$\nabla \cdot \mathrm{D} = \rho_e \qquad 2.9$$

$$\nabla \cdot \mathrm{B} = \rho_m \qquad 2.10$$

where E is the electric field intensity, H the magnetic field intensity D is the electric flux density and B the magnetic flus density. In linear medium, ε and μ are not depending on E and H,

$$\mathrm{D} = \varepsilon_0 E + P = \varepsilon_0 (1 + \chi_e) E = \varepsilon_0 \varepsilon_r E = \varepsilon E \qquad 2.11$$

$$\mathrm{B} = \mu_0 H + M = \mu_0 (1 + \chi_m) H = \mu_0 \mu_r H = \mu H \qquad 2.12$$

where $\mathrm{P} = \varepsilon_0 \chi_e$ and $\mathrm{M} = \mu_0 \chi_m$ are the electric and magnetic polarization, χ_e and χ_m the electric and magnetic susceptibilities, ε_0 and μ_0 are the permittivity and permeability of free space

respectively and $\varepsilon_r = 1 + \chi_e$ and $\mu_r = 1 + \chi_m$ are the permittivity and permeability of the material considered.

Assuming harmonic fields with the time dependence $e^{+j\omega t}$, Maxwell`s equations can be written as,

$$\nabla \mathrm{x} \mathrm{E} = -\mathrm{j}\omega\mu\mathrm{H} \qquad 2.13$$

$$\nabla \mathrm{x} \mathrm{H} = \mathrm{j}\omega\mathrm{E} \qquad 2.14$$

$$\nabla \cdot \mathrm{D} = \rho_e \qquad 2.15$$

$$\nabla \cdot \mathrm{B} = \rho_m \qquad 2.16$$

Considering a loss-less medium in regions without sources; Fig. (2.3) shows a vector triad $\vec{E}, \vec{H}, \vec{k}$ and Poynting vector $\vec{S}$. Vector $\vec{S}$ always forms a RH set with vectors $\vec{E}$ and $\vec{H}$.

$$\vec{S} = \vec{E} \mathrm{x} \vec{H}$$

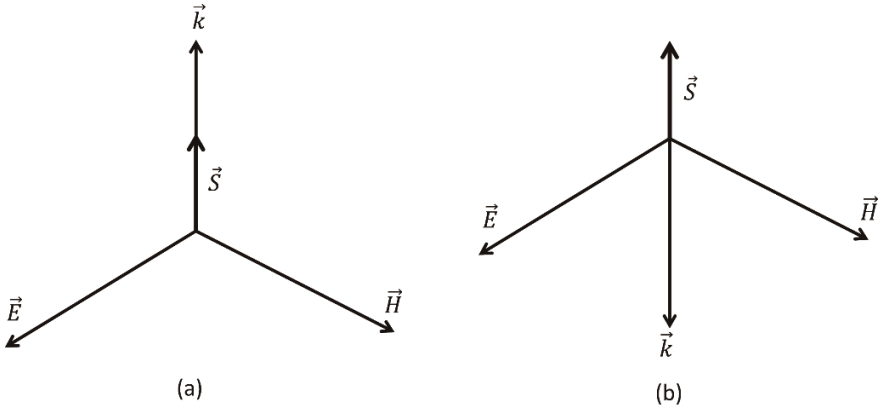

Figure 2.3. The wave triad $\vec{E}, \vec{H}, \vec{k}$ vectors (a) in a RH material and (b) LH material

Vector $\vec{k}$ ($k = \sqrt{\mu\varepsilon}$) is always in the direction of $\vec{S}$ vector. In the case of right handed (RH) medium, $\varepsilon > 0$ and $\mu > 0$. The vectors $\vec{E}$, $\vec{H}$ and $\vec{k}$ forms a RH.

$$\vec{k}x\vec{E} = +\omega\mu\vec{H} \qquad 2.17$$

$$\vec{k}x\vec{H} = -\omega\varepsilon\vec{E} \qquad 2.18$$

Which built a RH triad shown in Fig. 2.3(a). In contrast, in the case of a LH medium, $\varepsilon < 0$ and $\mu < 0$, and sice $|\varepsilon| = -\varepsilon > 0$ and $|\mu| = -\mu > 0$. The direction of propagation is reversed the vectors $\vec{E}$, $\vec{H}$ and $\vec{k}$ forms a LH system.

$$\vec{k}x\vec{E} = -\omega|\mu|\vec{H} \qquad 2.19$$

$$\vec{k}x\vec{H} = +\omega|\varepsilon|\vec{E} \qquad 2.20$$

Which built a LH triad shown in Fig. 2.3(b). Frequency being always a positive quantity, the phase velocity in a LH medium is opposite to the phase velocity in RH medium. The wave number k is positive in RH medium; it is negative in a LH medium. Fig.2.4. shown an example of Doppler Effect in a RH and LH medium.

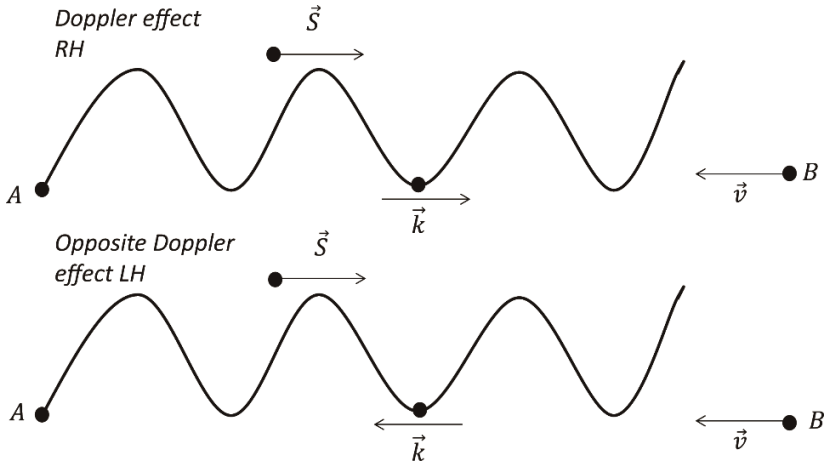

Figure 2.4. Doppler effect in a convectional RH and in a LH mediums.

In a RH medium the wave vector number $\vec{k}$ is positive and goes outward propagation from the source. In a LH, $\vec{k}$ is negative and the wave goes inward propagation to the source.

2.4. Left Handed media entropy condition

In a dispersive medium, the field intensity $\bar{E}/\bar{H}$ ($\bar{E}$ and $\bar{H}$ are the electric and magnetic field vectors) creates the flux density $\bar{D}/\bar{B}$ ($\bar{D}$ and $\bar{B}$ are the electric and magnetic flux density vector) by inducing oscillation of bound electrons in the atoms of the medium. These electrons respond to the excitation of the field $\bar{E}/\bar{H}$ with various delays to produce the collective response $\bar{D}/\bar{B}$ of the system. As a consequence, a time delay exists between the cause and the effect, and arbitrary field intensity $\bar{E}(t)/\bar{H}(t)$ induces flux density $\bar{D}(t)/\bar{B}(t)$ that are superposition of the effects of $\bar{E}(t`)/\bar{H}(t`)$ at all times $t' \ll t$.

$$\bar{D} = \varepsilon(t) * \bar{E}(r,t) = \int_{-\infty}^{t} \varepsilon(t-t')\bar{E}(r,t')dt' \qquad 2.21$$

$$\bar{B} = \mu(t) * \bar{H}(r,t) = \int_{-\infty}^{t} \mu(t-t')\bar{H}(r,t')dt' \qquad 2.22$$

The S Poynting vector in terms of the real field can be expressed as

$$\bar{S}(r,t) = \bar{E}(r,t)\mathrm{x}\bar{H}(r,t) \qquad 2.23$$

Thus, the divergence of Poynting vector is

$$\nabla \cdot \bar{S} = \left[\bar{E} \cdot \frac{\partial \overline{D}}{\partial t} + \bar{H} \frac{\partial \bar{B}}{\partial t}\right] \quad 2.24$$

In a quasi-harmonic fields wich mean resonance frequency ω_0,

$$\nabla \cdot \bar{S} = -\frac{1}{4}\left[\bar{E} \cdot \frac{\partial \overline{D}^*}{\partial t} + \bar{E}^* \cdot \frac{\partial \overline{D}}{\partial t} + \bar{H} \frac{\partial \overline{B}^*}{\partial t} + \bar{H}^* \cdot \frac{\partial \bar{B}}{\partial t}\right] \quad 2.25$$

where * defines a convector/dual vector; $\overline{D}$ and $\bar{B}$ components are expanded in its Fourier series to,

$$\frac{\partial \overline{D}}{\partial t} = j\omega\varepsilon(\omega)\bar{E} + \frac{d(\omega\varepsilon)}{d\omega}\frac{\partial \bar{E}}{\partial t}e^{j\omega t} \quad 2.26$$

$$\frac{\partial \bar{B}}{\partial t} = j\omega\mu(\omega)\overline{H} + \frac{d(\omega\mu)}{d\omega}\frac{\partial \overline{H}}{\partial t}e^{j\omega t} \quad 2.27$$

Substituting these expressions in Eq. (2.25)

$$\nabla \cdot \bar{S} = -\frac{1}{4}\left[\frac{d(\omega\varepsilon)}{d\omega}\frac{\partial(\bar{E} \cdot \bar{E}^*)}{\partial t} + \frac{d(\omega\mu)}{d\omega}\frac{\partial(\overline{H} \cdot \overline{H}^*)}{\partial t}\right] \quad 2.28$$

The internal energy per unit volume in the medium

$$\bar{W} = -\int \nabla \cdot \bar{s} dt \qquad 2.29$$

$$\bar{W} = \frac{1}{4}\left[\frac{d(\omega\varepsilon)}{d\omega}\bar{E}^2 + \frac{d(\omega\mu)}{d\omega}\bar{H}^2\right] \qquad 2.30$$

If the external supply of electromagnetic energy is cut off, $\bar{W} > 0$ this leads to

$$\frac{d(\omega\varepsilon)}{d\omega} > 0 \text{ and } \frac{d(\omega\mu)}{d\omega} > 0 \qquad 2.31$$

In a nondispersive medium Eq. (2.31), simultaneous negative permittivity and permeability are physically impossible since they would violate the low of entropy. However, in a dispersive medium simultaneous negative permittivity and permeability can occur; for this, permittivity and permeability must be positive in some frequency regions in order to compensate for their negative parts. A LH material is necessarily a dispersive medium with frequency dependent constative parameters.

2.5. Dielectric permittivity ε and magnetic permeability μ of materials

The permeability and permittivity dispersion in a material can be described by the Lorentz model for dielectric permittivity and magnetic permeability and Drude models for metals.

2.5.1. Lorentz model for dielectric permittivity and magnetic permeability

In dielectric materials, electrons are tightly bound to the nucleus. The ion-electron dipoles are constantly oscillating, but the charges are kept in equilibrium state by the Coulomb force.

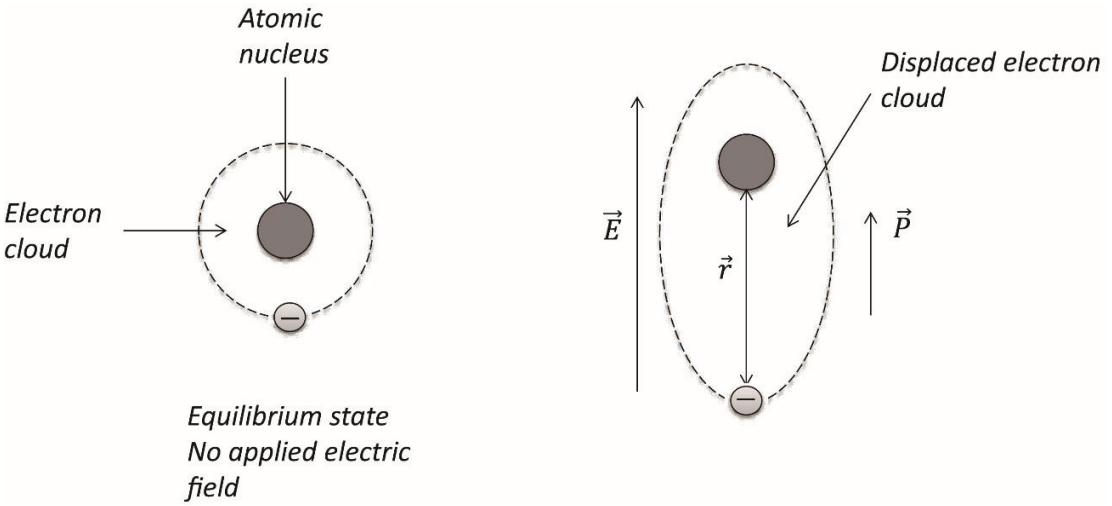

Figure 2.5. Lorentz model for dielectrics. In dialectic material electric dipole is in equilibrium state. Electric polarization arises when the external electric field E is applied and the electron nucleus is displaced.

When an external field E is applied, electron bound to the nucleus would be pushed in the direction opposite to the applied field as illustrated in Fig. (2.5). The electric field will act as a driving force applied to the oscillating dipole and the overall displacement of the cloud of electrons e^- is $\vec{r}$. Then we can describe the distance between the electron and an ion using the Lorentz equation of motion,

$$m_e \frac{d^2\vec{r}}{dt^2} + m_e \Gamma \frac{d\vec{r}}{dt} + m_e \omega_0^2 = -q\vec{E} \quad 2.32$$

where m_e is the mass of electron, Γ is the damping constant and ω_0 the natural frequency, $m_e \frac{d^2\vec{r}}{dt^2}$ is the acceleration force, $m_e \Gamma \frac{d\vec{r}}{dt}$ frictional force, $m_e \omega_0^2$ restoring force and $-q\vec{E}$ the driving force. After performing the Fourier transformation,

$$(-m_e \omega^2 - j\omega m_e \Gamma + m_e \omega_0^2)\vec{r} = -q\vec{E} \quad 2.33$$

The displacement is then

$$\vec{r} = -\frac{q}{m_e} \frac{\vec{E}}{\omega_0^2 - \omega^2 - j\omega\Gamma} \quad 2.34$$

The dipole moment is given by

$$\vec{M} = -q\vec{r} \quad 2.35$$

$$\vec{M} = \frac{q^2}{m_e} \frac{\vec{E}}{\omega_0^2 - \omega^2 - j\omega\Gamma} \quad 2.36$$

And the Lorentz polarizability,

$$\vec{M} = \alpha\vec{E} \quad 2.37$$

$$\alpha = \frac{q^2}{m_e} \frac{1}{\omega_0^2 - \omega^2 - j\omega\Gamma} \quad 2.38$$

The polarization per unit volume of electrons cloud around the nucleus in a material is defined as

$$\vec{P} = \frac{1}{V} \sum_V \overrightarrow{M_i} \quad 2.39$$

Where $\overrightarrow{M_i}$ is the average dipole moment over all atoms in a material. The statistical approach is used to compute the average of the randomness to the polarized atoms,

$$\vec{P} = N\langle\vec{M}\rangle \tag{2.40}$$

where N is the number of atom per unit volume. Recalling from the Maxwell's equation with material polarization and combining with Eq. (2.37) and (2.38), leads to an equation to calculate the susceptibility,

$$\vec{P} = \varepsilon_0\chi\vec{E} \tag{2.39}$$

$$N\langle\vec{M}\rangle = \varepsilon_0\chi\vec{E}$$

$$\chi = \frac{N\alpha}{\varepsilon_0}$$

$$\chi = \frac{Nq^2}{\varepsilon_0 m_e}\frac{1}{\omega_0^2 - \omega^2 - j\omega\Gamma} \tag{2.40}$$

where $\frac{Nq^2}{\varepsilon_0 m_e} = \omega_p^2$ is the plasma frequency. The susceptibility of a dielectric material is then,

$$\chi = \frac{\omega_p^2}{\omega_0^2 - \omega^2 - j\omega\Gamma} \tag{2.41}$$

Since the complex permittivity for a dielectric material as defined in the beginning of the this chapter

$$\varepsilon_r = 1 + \chi \tag{2.42}$$

The dielectric function for a material takes the following formula,

$$\varepsilon_r = 1 + \frac{\omega_{pe}^2}{\omega_{0e}^2 - \omega^2 - j\omega\Gamma_e} \tag{2.43}$$

The Eq. (2.43), is the Lorenz dispersion formula to classify the dielectric materials. Where

$$\omega_{pe}^2 = \frac{n_0 e^2}{m\varepsilon_0} \tag{2.44}$$

is the electric angular plasma frequency (where e and m are the electric charge and mass of the conduction electron, n_0 is the conduction electron's number density). ω_{0e} is the electric angular resonance frequency, ω angular frequency of the electric field and Γ_e the electric damping. Splitting the equation into real and imaginary parts, it follows:

$$\varepsilon_r = 1 + \frac{\omega_p^2}{(\omega_0^2 - \omega^2) - j\omega\Gamma} \frac{(\omega_0^2 - \omega^2) + j\omega\Gamma}{(\omega_0^2 - \omega^2) + j\omega\Gamma}$$

$$\varepsilon_r = 1 + \frac{\omega_p^2(\omega_0^2 - \omega^2) + j\omega\Gamma\omega_p^2}{(\omega_0^2 - \omega^2)^2 + \omega^2\Gamma^2}$$

$$\varepsilon_r = 1 + \frac{\omega_p^2(\omega_0^2 - \omega^2)}{(\omega_0^2 - \omega^2)^2 + \omega^2\Gamma^2} + \frac{j\omega_p^2\omega\Gamma}{(\omega_0^2 - \omega^2)^2 + \omega^2\Gamma^2} \tag{2.45}$$

$$\varepsilon_r' = 1 + \frac{\omega_p^2(\omega_0^2 - \omega^2)}{(\omega_0^2 - \omega^2)^2 + \omega^2\Gamma^2} \tag{2.46}$$

$$\varepsilon_r'' = \frac{\omega_p^2\omega\Gamma}{(\omega_0^2 - \omega^2)^2 + \omega^2\Gamma^2} \tag{2.47}$$

The imaginary part in the equation only exists if there is loss. Fig. (2.6) below shows the typical Lorentz response curves for relative complex permittivity real ε_r' and imaginary parts ε_r''. At low

frequencies, below the plasma frequency far from the resonance, the materials has a DC offset, the permittivity is almost constant up to frequencies near ω_0 and the loss is very low.

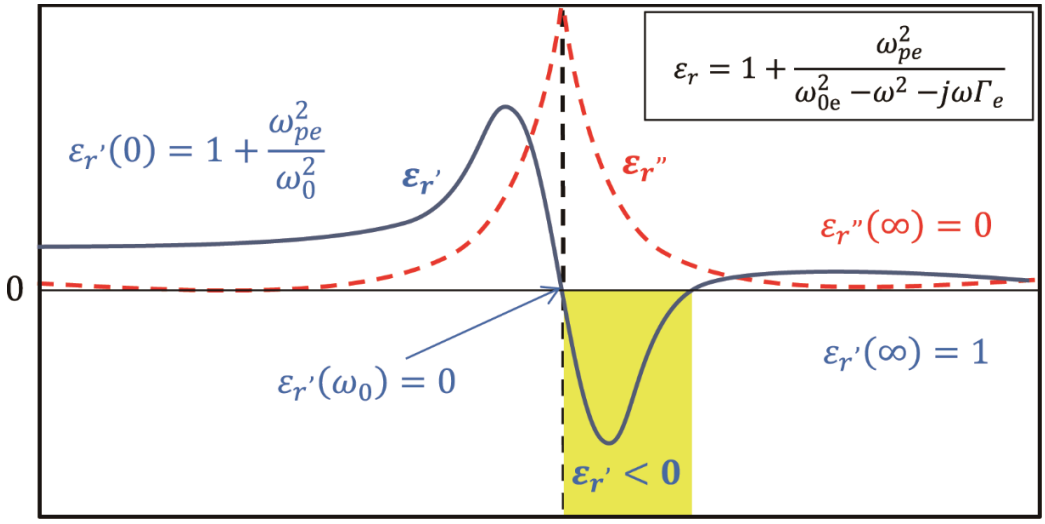

Figure 2.6. Relative complex permittivity dispersion curves – Lorentz model for dielectrics

The loss becomes high near the ω_0 and ε_r' can be negative. The width of ε_r'' will be determined by the electric damping Γ rate. The width increases with the damping and the curve shows the maximum amplitude ε_{rmax}'' at $\omega = \omega_0$.

The Lorentz model for magnetic permeability is similar to the Lorentz model to electric permittivity except the fact that instead of electric field we deal with magnetic field, so that from Eq. (2.43) we have,

$$\mu_r = 1 + \frac{\omega_{pm}^2}{\omega_{0m}^2 - \omega^2 - j\omega\Gamma_m} \qquad 2.48$$

Where ω_{pm} is the magnetic plasma frequency, ω_{0m} is the magnetic angular resonance frequency, ω angular frequency of the electric field Γ_m the magnetic damping. Splitting the equation into real and imaginary parts, it follows

$$\mu_r' = 1 + \frac{\omega_{pm}^2(\omega_{0m}^2 - \omega^2)}{(\omega_{0m}^2 - \omega^2)^2 + \omega^2\Gamma_m^2} \qquad 2.49$$

$$\mu_r'' = \frac{\omega_{pm}^2 \omega\Gamma}{(\omega_{0m}^2 - \omega^2)^2 + \omega^2\Gamma_m^2} \qquad 2.50$$

The Fig. (2.7) shows the typical Lorentz response curves for relative complex permeability real μ_r' and imaginary parts μ_r''. The similar happens as in the case of Lorentz permeability response.

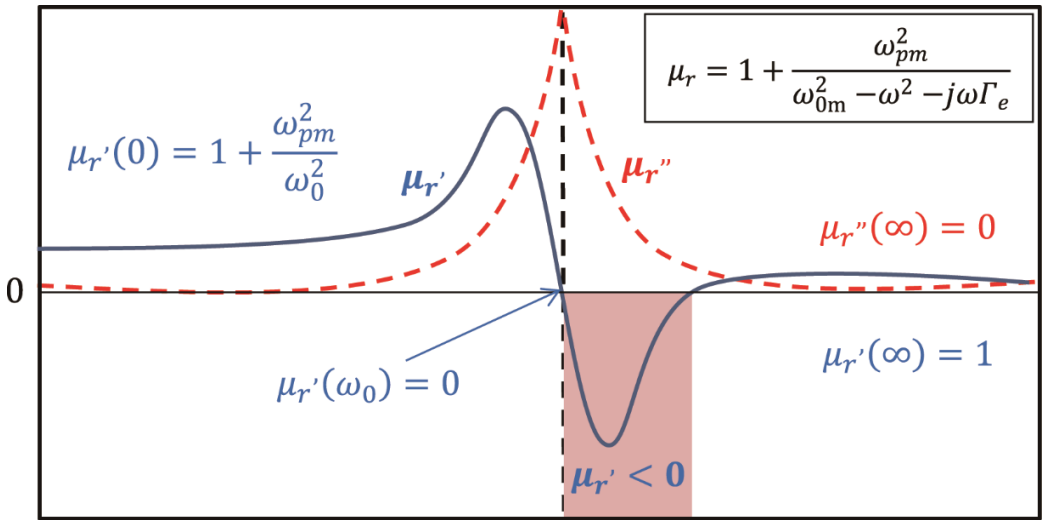

Figure 2.7. Relative complex permeability dispersion curves – Lorentz model

In summary, most materials tend to be transmissive below resonance frequency, at the resonance are very absorbing, become reflective above the resonance and transmissive again above the plasma frequency away from resonance frequency.

2.5.2. Drude model for metals

The Drude model is especial case of Lorentz model. In the Lorentz model the electrons are bound tightly to their nucleus and hence will not be free to move around and contribute to the materials conduction while in the Drude model, the behavior of electron may be treated classically.

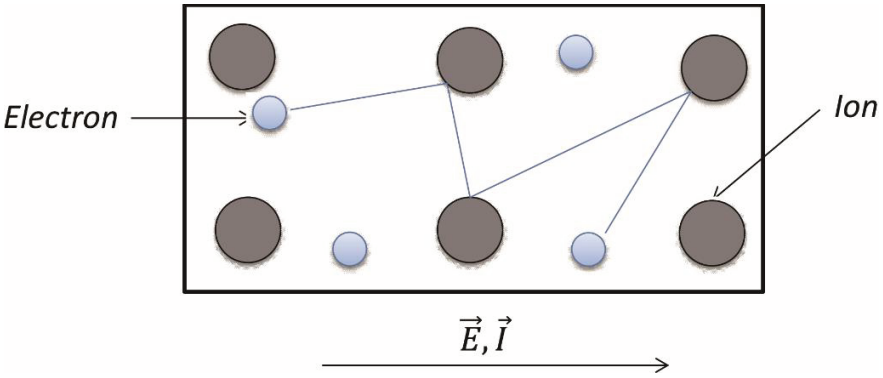

Figure 2.8. Drude model for metals, electrons are free to move colliding and bouncing between stationary ions.

Electrons are free to move colliding and bouncing and re-bouncing in relatively static positive ions since they are not bound to the nucleus making in this way the electrical conduction. The number of atoms per unit volume N is now interpreted as a charge density and m_e the

effective mass of electrons. For Drude model, the restoring force is negligible and there is no natural frequency. So is assuming that $\omega_0 = 0$, from Eq.(2.43) we have,

$$\varepsilon_r = 1 - \frac{\omega_{pe}^2}{\omega^2 + j\omega\Gamma_e} \tag{2.51}$$

Splitting the equation into real and imaginary parts, it follows

$$\varepsilon_r' = 1 - \frac{\omega_{pe}^2}{\omega^2 + \Gamma_e^2} \tag{2.52}$$

$$\varepsilon_r'' = \frac{\omega_{pe}^2\Gamma_e}{\omega(\omega^2 + \Gamma_e^2)} \tag{2.53}$$

The Fig. (2.9) shows the typical Drude response curves for relative complex permittivity real ε_r' and imaginary parts ε_r''. At low frequencies, below the plasma frequency, $\omega < \omega_p$ the dielectric constant is mostly imaginary and metals behave like good conductors. Then the real part ε_r' is negative and the electric field cannot penetrate the material that is totally refractive. An incident wave of frequency less than the plasma frequency, which is incident to the plasma will not be propagate through the plasma but will be totally reflected.

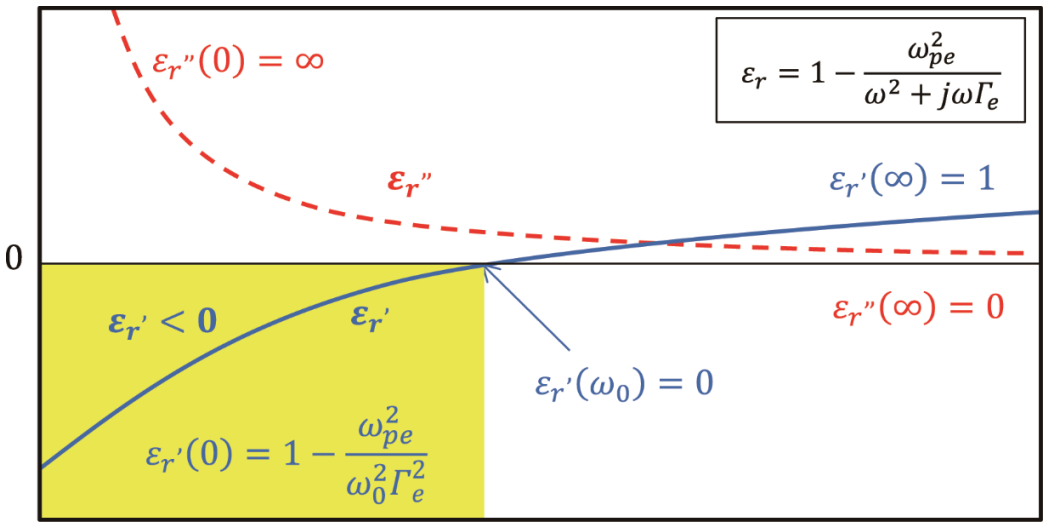

Figure 2.9. Relative complex permittivity dispersion curves – Drude model for metals

Near the plasma frequency, both ε_r' and ε_r'' are significant and the loss is too high in the metal. In the case of $\omega = \omega_0 = \sqrt{\omega_{pe}^2 - \Gamma_e^2}$, ε_r' is zero and all electrons oscillate in phase through the material. Meanwhile, at high frequencies above the plasma frequency the metal become transparent. Basically there is no loss and no absorption.

2.6. Composite medium with simultaneous negative permittivity and permeability

A period structure Fig. (2.10(c)) composed by unit cell of metallic Tiny Wires (TW) Fig. (2.10(a)) and Split Ring Resonators (SRR) Fig. (2.10(a)) were proposed to achieve effective negative permittivity and effective negative permeability. The electric and magnetic properties in TW and SRR were investigated by Pendry[2, 3].

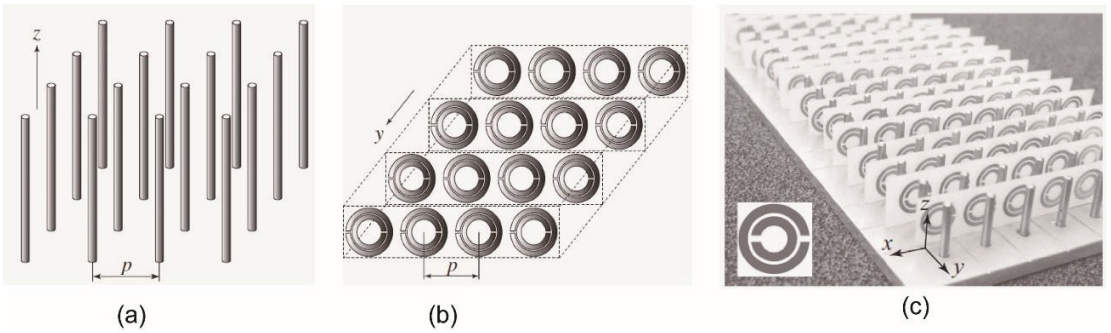

Figure 2.10. First metamaterials proposed by Pendry. (a) metal tine wire (TW) to produce negative permittivity and (b) splint ring resonator that produces negative permeability. The first combination of TW and SRR used to demonstrate the first LH properties (c)

The TW can produce the desired electric response. Electric field E is applied along the wires, induced electric current along the wires generate electric dipole moment. From Eq. (2.52) negative permittivity $\varepsilon_r < 0$ can be achieved for $\omega^2 < \omega_{pe}^2 - \Gamma_e^2$. In the case of $\Gamma = 0$, negative permittivity is realized when $\omega^2 < \omega_{pe}^2$. The SRR can be seen as a LC circuit with the resonance frequency $\omega_0 = \sqrt{1/LC}$, a time varying external magnetic field will induce circulating current across the rings. Charges in the gaps of the rings will be stored as a capacitance. For frequencies below ω_0, currents in the SRR will keep up by the driving forces produced by the external magnetic field and the response will be positive. Increasing the rate of external magnetic field, the current in SRR can no longer keep up and probably being delayed resulting in an out of phase and negative response. From Eq. (2.48) the magnetic response of the SRR is,

$$\mu_r = 1 + \frac{F\omega^2}{\omega_{0m}^2 - \omega^2 - j\omega\Gamma_m} \qquad 2.54$$

where $\omega_{pm} = \omega_{0m}/\sqrt{1-F}$ is the magnetic plasma frequency, where $F = \pi(r/P)^2$ is the geometrical factor of the inner ring. Negative permeability $\mu_r < 0$ will be realized under condition $\omega_{0m} < \omega < \omega_{pm}$.

To fabricate such artificial materials, the size and spacing P of the elements SRR and TW should be much smaller than the electromagnetic wavelength of interest ($P \ll \lambda$) so that the incident radiation cannot distinguish the collection of elements from a homogeneous material.

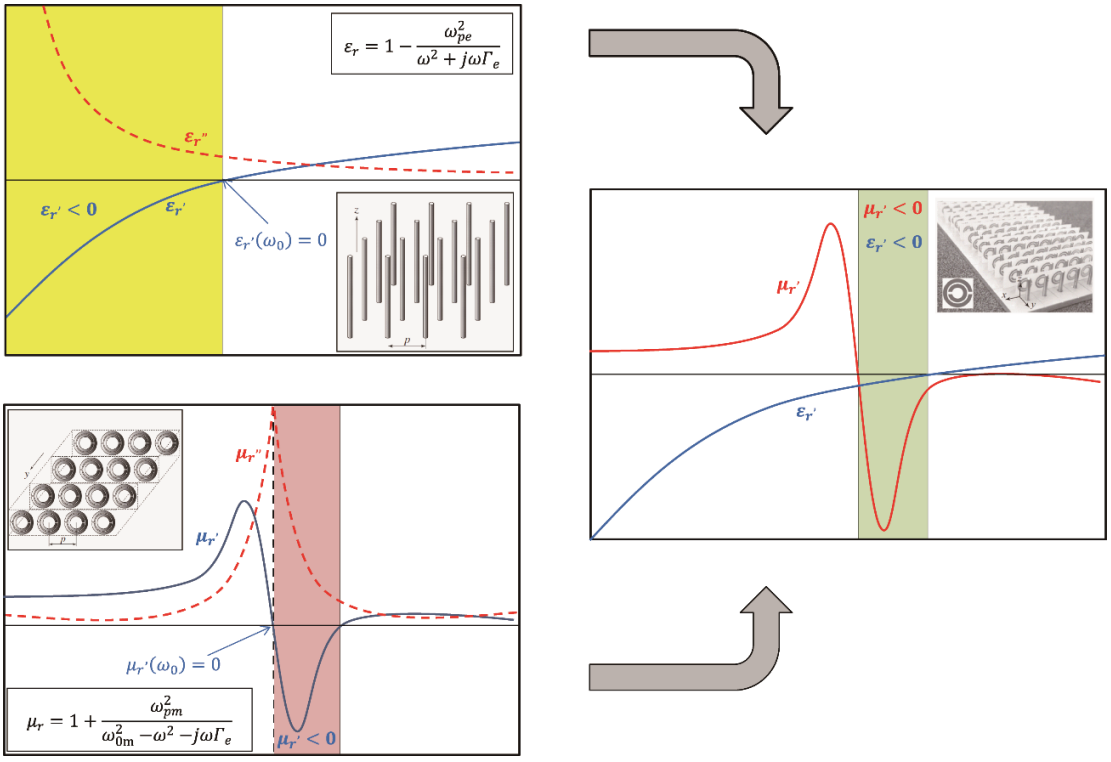

Figure 2.11. The combination of TW and SRR to produce a LH or DNG composite metamaterial with simultaneous negative μ_r' and ε_r'

Having identified the materials that would show $\varepsilon_r < 0$ and $\mu_r < 0$, both can be combined Fig. (2.10(c)) and produce a metamaterial that could show the region in microwave frequency

that negative permittivity and negative permeability are overlapped forming in that way a LH or a DNG metamaterial as illustrated in Fig. (2.11).

The first experimental demonstration of negative refraction was performed by Shelb et al. [4]. A prism shaped metamaterial composed of SRR and TW embedded in a circuit board was fabricated and used to demonstrate LH properties. A beam of microwave radiation incident on the prism was observed to refract to the opposite side of the surface normal. This prism would show regions of frequencies in which the refractive index is negative, confirming for the first time the existence of negative refractive index.

2.7. Ferromagnetic permeability

2.7.1. Magnetic response of magnetization

A material with constant magnetization M and volume V acts just like a magnetic dipole when placed in an external magnetic field H. The magnetic flux density is given by,

$$\mathrm{B} = \mu_0 H + M \qquad 2.55$$

The magnetic moment is related to the magnetic susceptibility χ_m; $M = \chi_m H$, so the magnetic flux can be rewrite as

$$\mathrm{B} = (\mu_0 + \chi_m) H \qquad 2.56$$

$$B = \mu H \quad (2.57)$$

$$\mu = \mu_0 + \chi_m \quad (2.58)$$

$$\frac{\mu}{\mu_0} = 1 + \frac{\chi_m}{\mu_0} \quad (2.59)$$

In ferromagnetic materials, the frequency dispersion of relative permeability can be express in terms of relative susceptibility χ_r,

$$\mu_r = 1 + \chi_r \quad (2.60)$$

2.7.2. Frequency dispersion of relative permeability

In ferromagnetic materials, the frequency dispersion of relative permeability can be attributed to the domain wall (DW) vibration and gyromagnetic spin rotation by Lorentz and Landau-Lifshitz-Gilbert [5, 6].

$$\mu_r = 1 + \chi_d + \chi_s \quad (2.61)$$

Where χ_d is the domain wall susceptibility and χ_s the gyromagnetic spin susceptibility.

2.7.2.1. Domain wall resonance

When external field is applied to the multi-domain ferromagnetic, saturation magnetization can be achieved through the domain wall motion

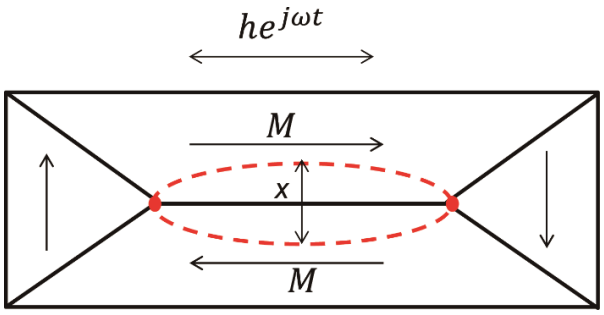

Figure 2.12. Schematic representation of domain wall motion, the direction of magnetization changes by 180^0 and 90^0

From the equation of motion

$$\rho\frac{d^2x}{dt^2} + \beta\frac{dx}{dt} + k_d x = 2M_{d_s}H \qquad 2.62$$

Where ρ is the effective mass of DW, k_d the elastic constant of the DW, β the damping factor and M_{d_s} saturation magnetization. The right hand side in the equation represents the external force that is produced by H. When the DW displacement is x, change of $\overline{M}$ can be

$$\mathrm{M} = M_{d_s}nx \qquad 2.63$$

$$x = \frac{M}{M_{d_s} n} \tag{2.64}$$

Where n is the number of DW per unit volume. Replacing the x in the equation of motion the following equation is obtained,

$$\frac{\rho}{M_{d_s} n} \frac{d^2 M}{dt^2} + \frac{\beta}{M_{d_s} n} \frac{dM}{dt} + \frac{k_d}{M_{d_s} n} M = 2 M_{d_s} H \tag{2.65}$$

$$\rho \frac{d^2 M}{dt^2} + \beta \frac{dM}{dt} + k_d M = 2 M_{d_s}^2 n H \tag{2.66}$$

The excitation $H = h_0 e^{j\omega t}$ and the response $M = M_0 e^{j\omega t}$; replacing H and M in the Eq. (2.66) and make necessary derivation we get

$$\rho \frac{d^2 M_0 e^{j\omega t}}{dt^2} + \beta \frac{d M_0 e^{j\omega t}}{dt} + k_d M_0 e^{j\omega t} = 2 M_{d_s}^2 n h_0 e^{j\omega t}$$

$$\rho j^2 \omega^2 M_0 e^{j\omega t} + \beta \mathrm{j}\omega M_0 e^{j\omega t} + k_d M_0 e^{j\omega t} = 2 M_{d_s}^2 n h_0 e^{j\omega t}$$

$$(-\rho\omega^2 + j\beta\omega + k_d) M_0 e^{j\omega t} = 2 M_{d_s}^2 n h_0 e^{j\omega t}$$

$$M_0 = \frac{2M_{d_s}^2 n h_0}{-\rho\omega^2 + j\beta\omega + k_d} \quad 2.67$$

Since the domain wall susceptibility is $\chi_d = M_0/h_0$ then,

$$\chi_d = \frac{2M_{d_s}^2 n}{k_d - \rho\omega^2 + j\beta\omega} \quad 2.68$$

When $\omega = 0$,

$$\chi_{d_0} = \frac{2M_{d_s}^2 n}{k_d} \quad 2.69$$

So that

$$\chi_d = \frac{\chi_{d_0} k_d}{k_d - \rho\omega^2 + j\omega\beta} \quad 2.70$$

Divided the equation by the effective mass of the domain wall ρ, we get

$$\chi_d = \frac{\chi_{d_0} k_d/\rho}{(k_d - \rho\omega^2 + j\omega\beta)/\rho} \quad 2.71$$

Where $k_d/\rho = \omega_d^2$ is the resonance frequency, $\beta/\rho = \beta$ is the damping constant. Then,

$$\chi_d = \frac{\chi_{d_0}\omega_d^2}{\omega_d^2 - \omega^2 + j\omega\beta} \tag{2.72}$$

Eq. (2.72) is the Domain wall susceptibility for ferromagnetic particles

The DW susceptibility can be express in terms of real and imaginary parts,

$$\chi_d = \frac{\chi_{d_0}\omega_d^2}{\omega_d^2 - \omega^2 + j\omega\beta} \cdot \frac{\omega_d^2 - \omega^2 - j\omega\beta}{\omega_d^2 - \omega^2 - j\omega\beta} \tag{2.73}$$

$$\chi_d = \frac{\chi_{d_0}\omega_d^2(\omega_d^2 - \omega^2)}{(\omega_d^2 - \omega^2)^2 + \omega^2\beta^2} - j\frac{\omega\beta\chi_{d_0}\omega_d^2}{(\omega_d^2 - \omega^2)^2 + \omega^2\beta^2} \tag{2.74}$$

From the Eq. (2.62), if $d^2x/dt = 0$, that means no inertia term, $\omega = \omega_0$, and if $\beta \gg 1$, that is the case of overdamped oscillation, that means $(\omega_d^2 + j\omega\beta) \gg \omega^2$. In this case the approximation ω^2 can be neglected. From Eq. (2.72) we get

$$\chi_d = \frac{\chi_{d_0}\omega_d^2}{\omega_d^2 + j\omega\beta} \tag{2.75}$$

$$\chi_d = \frac{\chi_{d_0}}{1 + j\omega \frac{\beta}{\omega_d^2}} \qquad 2.76$$

Where $\omega_d^2/\beta = \omega_{relax}$ is the relaxation frequency, the relaxation susceptibility is then,

$$\chi_{relax} = \frac{\chi_{d_0}}{1 + j\frac{\omega}{\omega_{relax}}} \qquad 2.77$$

Eq. (2.77) is the Debye type relaxation.

2.7.2.2. Spin rotation

The magnetic properties of a material are due to the existence of magnetic dipole moments, which arise from electron spin. In a magnetic material a large fraction of the electron spin are oriented in random directions and the magnetic moment is small. Applying the external magnetic field, will cause the dipole moments to align in same direction and produce a large overall magnetic moment. Removing the external field, the material can stay permanently magnetized due to the existence of exchange forces that keeps the electron spins aligned.

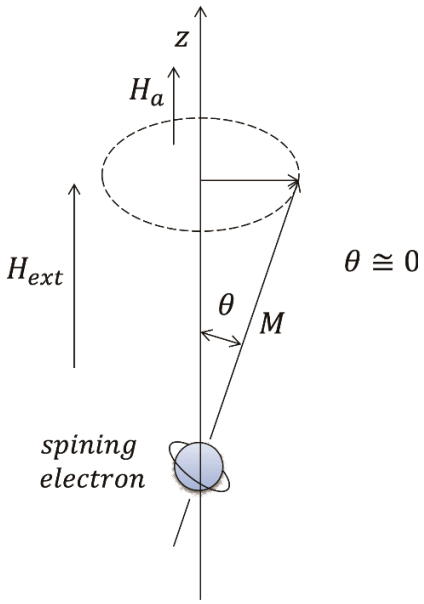

Figure 2.13. Spin magnetic dipole moment and angular momentum vectors for a spinning electron under external field H_{ext}.

The magnetization *M* can vary internally in a ferromagnetic material but its magnitude in each point is the same to the saturation magnetization M_s. From the Landau-Liftshitz equation that predicts the rotation of the magnetization in response to the torques it follows:

$$\frac{dM}{dt} = -\gamma_s(MxH_{ext}) + \frac{\alpha}{M_s}\left(Mx\frac{dM}{dt}\right) \qquad 2.78$$

Where M is the magnetization (magnetic moment per unit volume), H_{ext} is the external magnetic field, α is the Landau-Lifshitz phenomenological damping parameter and γ_s is the Landau-Lifshitz electron gyromagnetic ratio (the ratio of magnetic dipole moment to the mechanical

angular momentum). The equation can be solved in order to show that the magnetic vector processes around the field H_a. The matrixes M and H_{eff} are given by

$$\mathrm{M} = \begin{pmatrix} m_x \\ m_y \\ m_z \end{pmatrix} = \begin{pmatrix} m_x \\ m_y \\ M_s \end{pmatrix} \tag{2.79}$$

$$H_{eff} = \begin{pmatrix} h_x \\ h_y \\ h_z \end{pmatrix} = \begin{pmatrix} m_x \\ m_y \\ H_a \end{pmatrix} \tag{2.80}$$

Writing M and H_{eff} in term of their vector components gives,

$$\frac{dm_x}{dt} = -\gamma_g\left(m_y H_a - M_s h_y\right) - \frac{\alpha}{M_s} M_s \frac{dm_y}{dt} \tag{2.81}$$

$$\frac{dm_y}{dt} = -\gamma_g(M_s h_x - m_x H_a) + \frac{\alpha}{M_s} M_s \frac{dm_x}{dt} \tag{2.82}$$

$$\frac{dm_z}{dt} = 0 \tag{2.83}$$

Where γ_g is the gyromagnetic ratio, M_s is the magnetization, m_x and m_y are the components of the magnetization, and h_x and h_y the components of the magnetic field H_a is the magnetic field

parallel to the easy direction. H_a is referred to have an anisotropic field. The resonance occurs at an external field less by H_a than in the isotropic case. If the magnetization $dM_s/dt = 0$, the components x and y of the magnetic field are $h_x = h_y = h_0 e^{jwt}$ and $m_x = m_{x_0} e^{jwt}$, $m_y = m_{y_0} e^{jwt}$, $\gamma_g H_a = \omega_s$

We use Eq.(2.80) and (2.81) to obtain two equation for m_x and m_y.

$$\mathrm{j}\omega m_x = -\omega_s m_y + \gamma_g M_s h_y - \alpha j \omega m_y \qquad 2.84$$

$$\mathrm{j}\omega m_y = -\gamma_g M_s h_x + \omega_s m_x - \alpha j \omega m_x \qquad 2.85$$

The Eq. (2.83) shows that m_z is a constant, so we have the following relation,

$$m_x = -\frac{\gamma_g M_s(\omega_s + j\alpha\omega)}{(\omega_s + j\alpha\omega)^2 - \omega^2} h_x + j\frac{\omega\gamma_g M_s}{(\omega_s + j\alpha\omega)^2 - \omega^2} h_y \qquad 2.86$$

$$m_y = \frac{\gamma_g M_s(\omega_s + j\alpha\omega)}{(\omega_s + j\alpha\omega)^2 - \omega^2} h_y + j\frac{\omega\gamma_g M_s}{(\omega_s + j\alpha\omega)^2 - \omega^2} h_x \qquad 2.87$$

Then

$$\chi = \frac{\gamma_g M_s(\omega_s + j\alpha\omega)}{(\omega_s + j\alpha\omega)^2 - \omega^2} \quad 2.88$$

$$\mathrm{k} = -\frac{\omega\gamma_g M_s}{(\omega_s + j\alpha\omega)^2 - \omega^2} \quad 2.89$$

The relative permeability can be express in terms of magnetic spin susceptibility χ_s,

$$\chi_s = 1 + \chi \quad 2.90$$

$$\chi_s = 1 + \frac{\gamma_g M_s(\omega_s + j\alpha\omega)}{(\omega_s + j\alpha\omega)^2 - \omega^2} \quad 2.91$$

If we put $\chi_{s_0} = \gamma_g M_s/\omega_s$ and $\gamma_g M_s = \chi_{s_0}\omega_s$, then we get

$$\chi_s = 1 + \frac{\chi_{s_0}\omega_s(\omega_s + j\alpha\omega)}{(\omega_s + j\alpha\omega)^2 - \omega^2} \quad 2.92$$

Eq. (2.92) is the magnetic spin rotation susceptibility for ferromagnetic particles.

The permeability dispersion in magnetic composite materials can be attributed to the contribution of both domain wall resonance and spin resonance. From the Eq. (2.61), it follows.

$$\mu_r = 1 + \frac{\chi_{d_0}\omega_d^2}{\omega_d^2 - \omega^2 + j\omega\beta} + \frac{\chi_{s_0}\omega_s(\omega_s + j\alpha\omega)}{(\omega_s + j\alpha\omega)^2 - \omega^2} \quad 2.93$$

Where χ_{d_0} and χ_{s_0} are the static magnetic susceptibilities of each component, α and β are their damping factors, $\omega_d = 2\pi f_d$ and $\omega_s = 2\pi f_s$ are the resonance angular frequencies $\omega = 2\pi f$ is the angular frequency of the applied electromagnetic field.

If the damping factors or resonance frequencies are very large, the resonance type dispersion formula, Eq. (2.93) can be represented in the two Debye type relaxation form,

$$\mu_r = 1 + \frac{\chi_{d_0}}{1 + j\frac{\omega}{\omega_{d-rel}}} + \frac{\chi_{s_0}}{1 + j\frac{\omega}{\omega_{s-rel}}} \qquad 2.94$$

Where $\omega_{d-rel} = 2\pi f_{d-rel}$ and $\omega_{s-rel} = 2\pi f_{s-rel}$ are the relaxation angular frequencies of DW and Spin components,

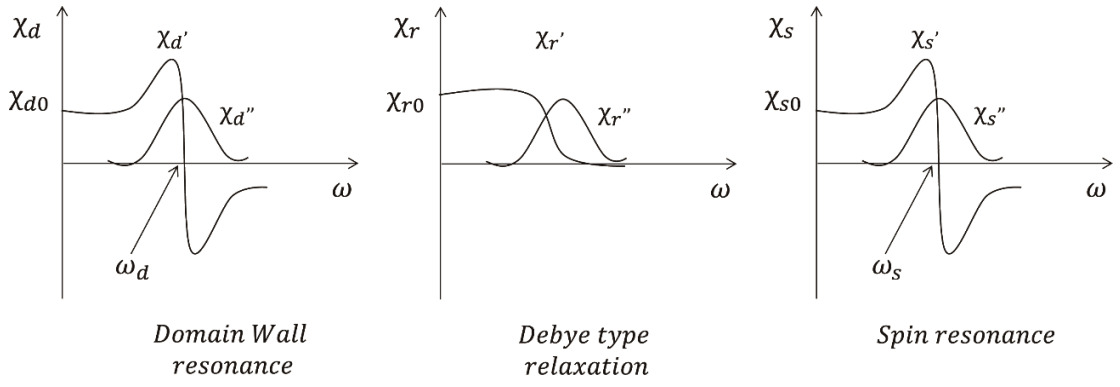

Figure 2.14. Dispersion curves of magnetic susceptibilities, domain wall susceptibility χ_d, Deby type relaxation susceptibility χ_r and spin susceptibility χ_s

2.8. Mixing theory of permittivity and permeability

2.8.1. Effective medium approximation

Composite materials are constituted of two or more materials that are mixed together to build up the materials. The schematic configuration of a composite material is shown in Fig. (2.15). Hence, the composite materials are inhomogeneous. The calculation of each constitute value is nearly impossible. However, effective medium approximation has been developed to describe the composite material as a whole. Maxwell Garnett [7] has developed a homogenization theory to approximate a complex electromagnetic medium.

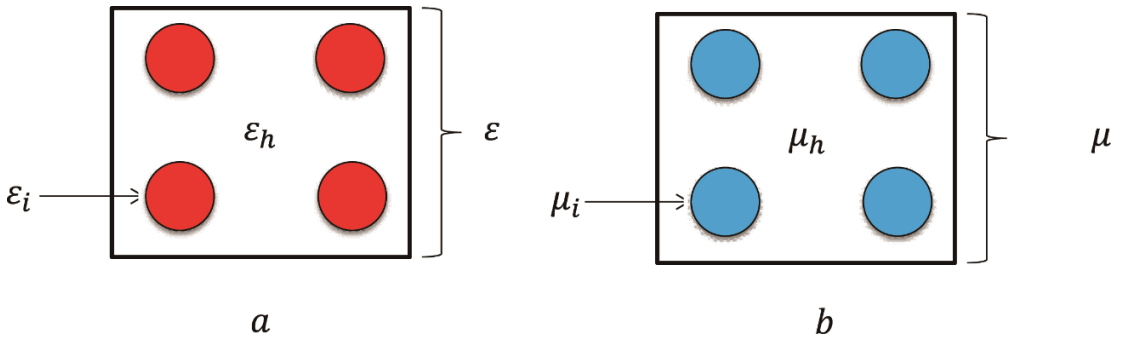

Figure 2.15. Composite materials, (a) metallic particles embedded in a host material and (b) magnetic particles in a host. Two mixing rules Maxwell Garnet Approximation (MGA) and Coherent Model approximation (CMA) to analyze the variation dielectric permittivity and magnetic permeability.

The Maxwell Garnett mixing formula, Maxwell Garnet Approximation (MGA) gives the effective permittivity and effective permeability of this effective medium. Another mixing formula, the Coherent Model Approximation (CMA), is used to analyze the complex permeability.

2.8.1.1. Maxell Garnett Approximation (MGA)

Maxwell Garnett Approximation is based on the Clausius-Mossotti relation for dielectrics composites [7, 8] so that,

$$\frac{\varepsilon_r - 1}{\varepsilon_r + 2} = A\varphi \qquad 2.95$$

$$\varepsilon_r = \frac{\varepsilon}{\varepsilon_0} \qquad 2.96$$

$$\frac{\varepsilon - \varepsilon_0}{\varepsilon + 2\varepsilon_0} = A\varphi \qquad 2.97$$

Where ε is the permittivity of the composite material , ε_0 is the permittivity in vacuum φ is the volume fraction of the inclusion and A is the volume filling factor.

When $\varphi = 0$ the permittivity is considered to be the host permittivity in the composite materials $\varepsilon = \varepsilon_h$ so that,

$$\frac{\varepsilon_h - \varepsilon_0}{\varepsilon_h + 2\varepsilon_0} = 0 \qquad 2.98$$

When $\varphi = 1$ the composite materials is already in the percolated state and the embedded particles occupies almost the all composite volume $\varepsilon = \varepsilon_i$.

$$\frac{\varepsilon_i - \varepsilon_0}{\varepsilon_i + 2\varepsilon_0} = A \qquad 2.99$$

Rewriting the Eq. (2.95) replacing A, we have

$$\frac{\varepsilon - \varepsilon_0}{\varepsilon + 2\varepsilon_0} = \varphi \frac{\varepsilon_i - \varepsilon_0}{\varepsilon_i + 2\varepsilon_0} \qquad 2.100$$

In the normal common materials the low state is vacuum and ε_0 is the permittivity of vacuum. Since we are treat a composite material where the low state is a host. The ε_0 should be replaced by ε_h in Eq. (2.100). So we get

$$\frac{\varepsilon - \varepsilon_h}{\varepsilon + 2\varepsilon_h} = \varphi \frac{\varepsilon_i - \varepsilon_h}{\varepsilon_i + 2\varepsilon_h} \qquad 2.101$$

Where ε is the permittivity of the composite material, ε_i the permittivity of the inclusion and ε_h the permittivity of the host material. From Eq.(2.101) the effective permittivity is then

$$\frac{\frac{\varepsilon}{\varepsilon_0} - \frac{\varepsilon_h}{\varepsilon_0}}{\frac{\varepsilon}{\varepsilon_0} + 2\frac{\varepsilon_h}{\varepsilon_0}} = \varphi \frac{\frac{\varepsilon}{\varepsilon_0} - \frac{\varepsilon_h}{\varepsilon_0}}{\frac{\varepsilon}{\varepsilon_0} + 2\frac{\varepsilon_h}{\varepsilon_0}}$$

$$\frac{\varepsilon_r - \varepsilon_{rh}}{\varepsilon_r + 2\varepsilon_{rh}} = \varphi \frac{\varepsilon_{ri} - \varepsilon_{rh}}{\varepsilon_{ri} + 2\varepsilon_{rh}} \qquad 2.102$$

The Eq. (2.102) yield the following mixing formulas of permittivity

$$\varepsilon_r = \frac{\varepsilon_{rh}(1+2\varphi)\varepsilon_{ri} + 2\varepsilon_{rh}^2(1-\varphi)}{\varepsilon_{rh}(2+\varphi) + \varepsilon_{ri}(1-\varphi)} \qquad 2.103$$

The Maxwell Garnett mixing formula for effective permittivity.

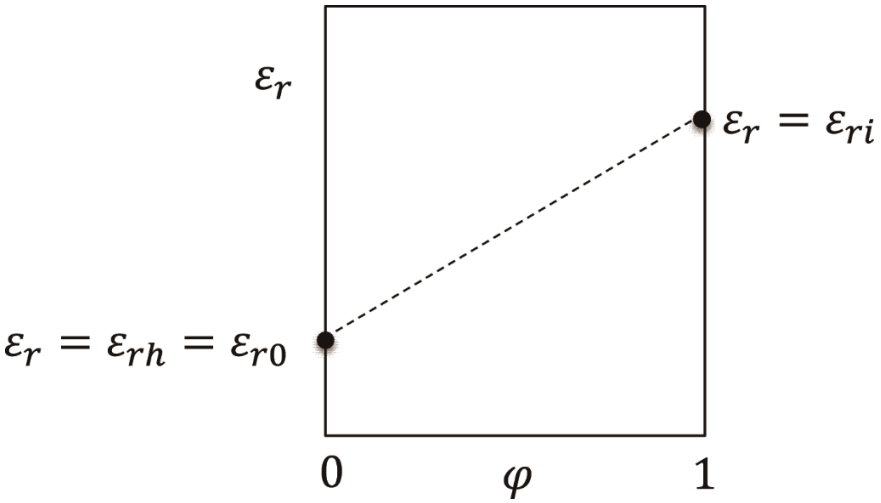

Figure 2.16. Relative permittivity ε_r as a function of particle content φ for the MGA.

Figure (2.16) is a schematic representation of the relative permittivity as a function of particle volume fraction for a MGA. When there is no inclusion in the composite , φ = 0 the permittivity value is determined by the permittivity of host. In the case of host material being the

PPS resin, the $\varepsilon_{rh} = \varepsilon_{ro} = 3$. At the percolated state $\varphi = 1$, $\varepsilon_r = \varepsilon_{ri}$, all particles are compacted.

The Maxwell Garnett mixing formula can be applied for the magnetic permeability in composite materials as well.

$$\frac{\mu_r - \mu_{rh}}{\mu_r + 2\mu_{rh}} = \varphi \frac{\mu_{ri} - \mu_{rh}}{\mu_{ri} + 2\mu_{rh}} \qquad 2.104$$

Where μ is the permeability of the composite material, μ_i the permeability of the inclusion and μ_h the permeability of the host material. The relative complex permeability is μ/μ_0 and the permeability of the host material is the same as the permeability of vacuum $\mu_h = \mu_0 = 1$. Eq. (2.104) reduces to,

$$\frac{\mu_r - 1}{\mu_r + 2} = \varphi \frac{\mu_{ri} - 1}{\mu_{ri} + 2} \qquad 2.105$$

The Eq. (2.105) yield the following mixing formulas of permeability

$$\mu_r = \frac{\mu_{ri}(1 + 2\varphi) + 2(1 - \varphi)}{\mu_{ri}(1 - \varphi) + 2(2 + \varphi)} \qquad 2.106$$

Maxwell Garnett mixing formula for permeability of the composite materials

2.8.1.2. Coherent Model Approximation for permeability (CMA)

The composite materials is considered to be composed of polycristal ferrites surrounded by a nonmagnetic grain layer as shown in schematic Fig. (2.17)

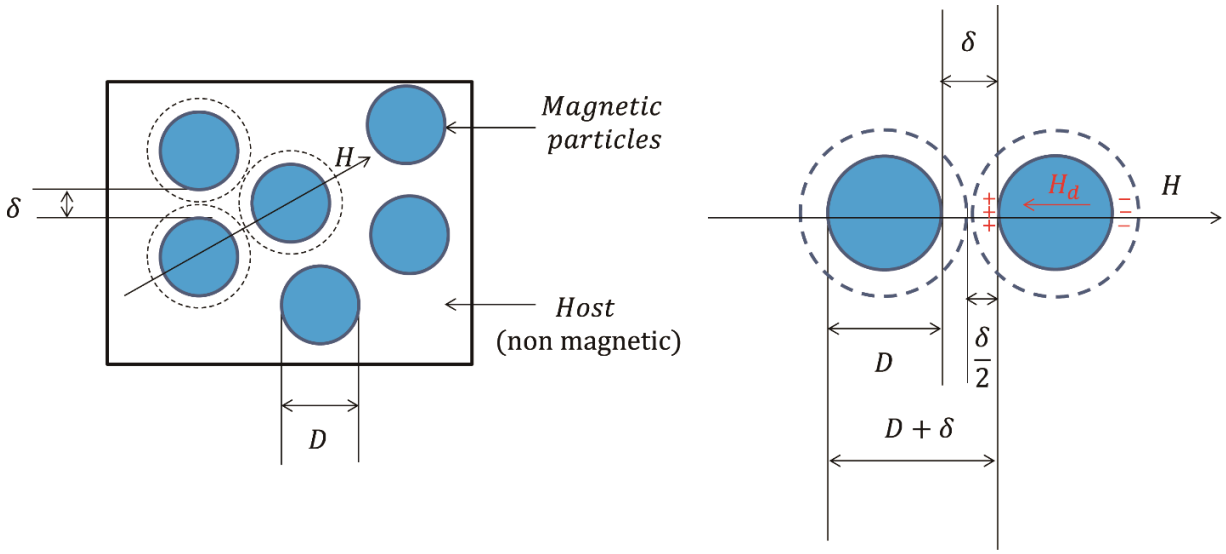

Figure 2.17. Magnetic particles embedded in a host nonmagnetic and the composite structure in one dimension

The average size of the magnetic particles is D and the average thickness of the non-magnetic layer is denoted by $\delta/2$ respectively. Applying the magnetic field H, magnetization will be produced and the H_d inside the magnetic particles will arise. The magnetic circuit in the composite is given by the Amperes integral

$$\oint Hdr = I \tag{2.107}$$

$$\oint_{comp} Hdr + \oint_{air} Hdr = I \tag{2.108}$$

$$\oint_{comp} Hdr = I - \oint_{air} Hdr = const \tag{2.109}$$

Knowing that $B = \mu H$,

$$\frac{1}{\mu}\int Bdr = const \tag{2.110}$$

Since the particle unit in the composite is the combination of average size of the magnetic particles and the average thickness of the non-magnetic layer $(D + \delta)$

$$\frac{1}{\mu}\int_{unit} Bdr = \frac{1}{\mu_B}B(D + \delta) \tag{2.111}$$

$$\frac{1}{\mu_B}B(D + \delta) = \frac{1}{\mu_B}B \cdot D + \frac{1}{\mu_0}B \cdot \delta \tag{2.112}$$

From

$\mu_r = \mu/\mu_0, \mu_{rB} = \mu_B/\mu_0$

$$\mu_r = \frac{\mu}{\mu_0} \text{ and } \mu_{rB} = \frac{\mu_B}{\mu_0} \quad 2.113$$

$$\frac{(D+\delta)}{\mu_r} = \frac{D}{\mu_{rB}} + \delta \quad 2.114$$

Where μ_r and μ_{rB}, are the effective permeability of the composite material and permeability of the magnetic particles respectively. Equation (2.114) is one dimensional CMA mixing equation, in other words, in the equation only the resistivity of the non-magnetic particles is used. The parameters D and δ do not change with frequency.

$$\mu_r = \frac{\mu_{rB}(D+\delta)}{D + \mu_{rB}\delta} \quad 2.115$$

Dividing the Eq.(2.115) by D, we get

$$\mu_r = \frac{\mu_{rB}(1 + {}^{\delta}/_{D})}{1 + \mu_{rB}\left({}^{\delta}/_{D}\right)} \quad 2.116$$

The ratio δ/D is related to the density of magnetic composite materials. From Eq. (2.116), when, the ratio δ/D tends to zero, $\delta = 0$, μ_r will be the bulk of the embedded magnetic particles. If

δ/D tends to infinite, that means $D = 0$, the relative permeability will be that of the host particles.

The percolation φ in the composite is defined as

$$\varphi = \frac{D}{(D+\delta)} \qquad 2.117$$

Assuming that the magnetic particles are uniformly distributed in the composite materials, homogeneous distribution, and the tridimensional mixing equation φ is then

$$\varphi = \frac{D^3}{(D+\delta)^3} \qquad 2.118$$

$$\varphi^{-1/3} - 1 = \frac{\delta}{D} \qquad 2.119$$

From Eq.(2.115), the relative permeability of the composite can be rewrite as,

$$\mu_r = \frac{\mu_{rB}}{(1-\mu_{rB})\varphi^{1/3} + \mu_{rB}} \qquad 2.120$$

2.8.2. Effective cluster model (ECM)

Granular composite materials contain various clusters and insolated particles. Doyles and Jacobs investigates the change of dielectric to metallic properties in the suspension of conducting

spheres using ECM based on the Clausius-Mossotti relation [9] and evaluate the dielectric enhancement in the metal granular composite [10].

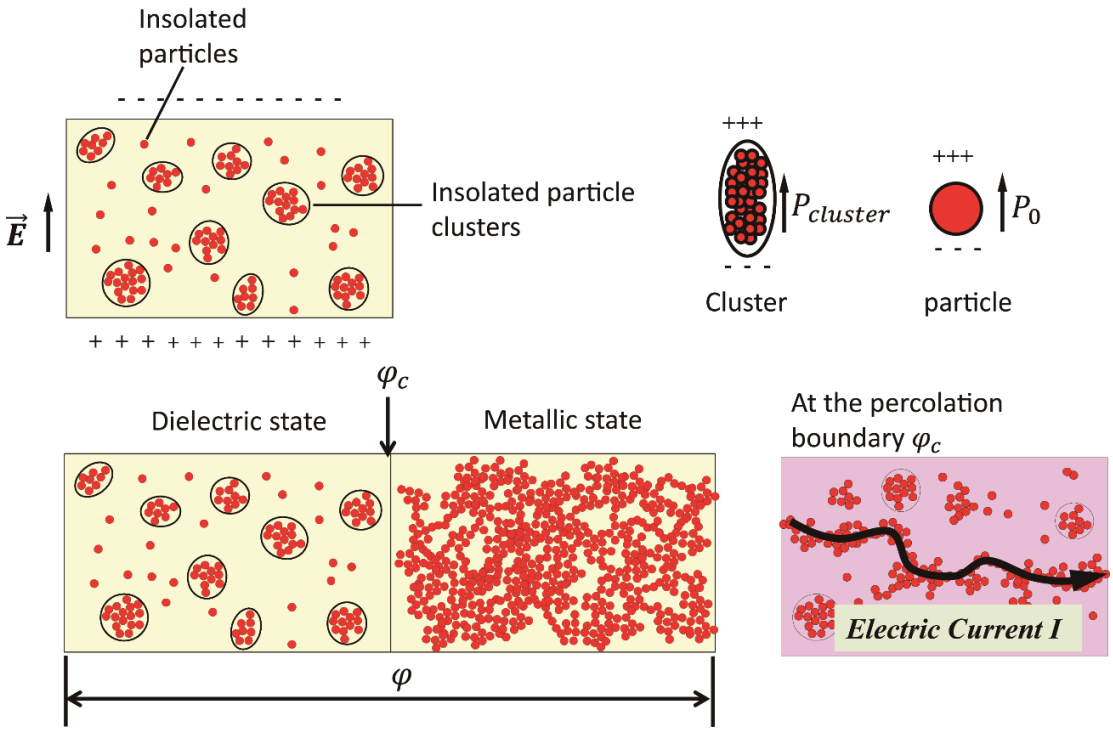

Figure 2.18. Conducting particles embedded in a host non conducting material. At lower content the composite materials contain various clusters and insolated particles. As the volume content of inclusions increases, the Metallica state is achieved at high particle content. At the percolation state φ_c, the boundary between dielectric to metallic there is the coexistence of isolated particle clusters and percolated cluster. The LFP state can be achieved in this region.

The volume fraction of clusters in embedded particles is guiven by

$$\varphi_{clust} = f\varphi \qquad 2.121$$

Where φ is the arbitrary content and f volume fraction of isolated clusters to the total particles volume. The volume fraction of embeded isolated particles is,

$$\varphi_0 = (1 - f)\varphi \qquad 2.122$$

Then,

$$\varphi = \varphi_{clust} + \varphi_0 \qquad 2.123$$

Increasing φ the percolation state is achieved at φ_c. At $\varphi = \varphi_c$, the transition from dielectric to metalic state occures and a percolated cluster is formed

$$\varphi_{cluster} = f\varphi_c \qquad 2.124$$

$$\varphi_0 = (1 - f)\varphi_c \qquad 2.125$$

When $f = 1$, $\varphi_{clust} = \varphi_c$ and $\varphi_0 = 0$.

The effective polarization P_a and isolated polarization P_0 of particles can be defined as $P_a = \varphi$ and $P_0 = \varphi_0 = (1 - f)\varphi$ and the isolated particle cluster polarizability $P_{cluster} = \varphi_{cluster}$, then,

$$P_{cluster} = \frac{\varphi_{cluster}}{\varphi_c} = \frac{1}{\varphi_c} f\varphi \qquad 2.126$$

The effective polarization can be expressed as,

$$P_a = P_0 + P_{clustet} \tag{2.127}$$

$$P_a = (1-f)\varphi + \frac{1}{\varphi_c} f\varphi \tag{2.128}$$

$$P_a = \left[1 + f\left(\frac{1}{\varphi_c} - 1\right)\right]\varphi \tag{2.129}$$

At $\varphi = \varphi_c$, $f = 1$,

$$P_a = \left[1 + \frac{\varphi}{\varphi_c}\left(\frac{1}{\varphi_c} - 1\right)\right]\varphi \tag{2.130}$$

All particles make a largest cluster at the percolation threshold φ_c. Doyles and Jacobs inserted the effective polarization Eq. (2.131) into the Clausius-Mossotti equation Eq. (2.130) and derived the formula to describe the variation of permittivity with particle content [10].

$$\frac{\varepsilon_r + 1}{\varepsilon_r + 2} = P_a \tag{2.131}$$

$$\frac{\varepsilon_r + 1}{\varepsilon_r + 2} = \left[1 + \frac{\varphi}{\varphi_c}\left(\frac{1}{\varphi_c} - 1\right)\right]\varphi \tag{2.132}$$

According to the Eq. (2.132), the permittivity will shows a large increase near the percolation threshold φ_c as indicated in Fig. 2.18. ε_{r0} is the permittivity of host material.

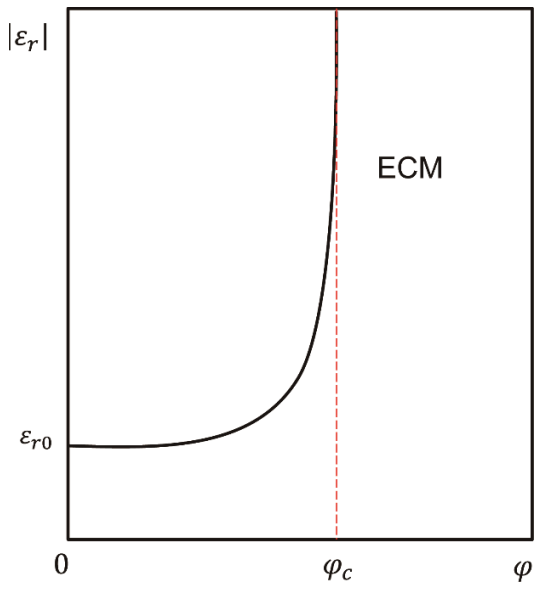

Figure 2.19. Schematic representation of normalized permittivity $|\varepsilon_r|$as a function of particle content φ. The permittivity shows a large increase near the percolation threshold φ_c

References

[1] R.M. Walser, Electromagnetic metamaterials, in: International Symposium on Optical Science and Technology, SPIE, 2001, pp. 15.

[2] J.B. Pendry, A.J. Holden, D.J. Robbins, W.J. Stewart, Magnetism from conductors and enhanced nonlinear phenomena, IEEE Transactions on Microwave Theory and Techniques, 47 (1999) 2075-2084.

[3] J.B. Pendry, A.J. Holden, D.J. Robbins, W.J. Stewart, Low frequency plasmons in thin-wire structures, J Phys-Condens Mat, 10 (1998) 4785-4809.

[4] R.A. Shelby, D.R. Smith, S. Schultz, Experimental verification of a negative index of refraction, Science, 292 (2001) 77-79.

[5] T. Tsutaoka, Frequency dispersion of complex permeability in Mn-Zn and Ni-Zn spinel ferrites and their composite materials, J Appl Phys, 93 (2003) 2789-2796.

[6] T. Tsutaoka, T. Kasagi, K. Hatakeyama, M.Y. Koledintseva, Analysis of the Permeability Spectra of Spinel Ferrite Composites Using Mixing Rules, in: IEEE International Symposium on Electromagnetic Compatibility, , IEEE, Denver, 2013, pp. 545 - 550.

[7] J.C.M. Garnett., XII. Colours in metal glasses and in metallic films, Philosophical Transactions of the Royal Society of London. Series A, Containing Papers of a Mathematical or Physical Character, 203 (1904) 385-420.

[8] J.C.M. Garnett., VII. Colours in metal glasses, in metallic films, and in metallic solutions.—II, Philosophical Transactions of the Royal Society of London. Series A, Containing Papers of a Mathematical or Physical Character, 205 (1906) 237-288.

[9] A.R. Von Hippel, Dielectrics and waves, Wiley, 1954.

[10] W.T. Doyle, I.S. Jacobs, Effective cluster model of dielectric enhancement in metal-insulator composites, Physical review. B, Condensed matter, 42 (1990) 9319-9327.

Chapter 3: Experimental Method

The granular composite metamaterial samples were prepared by mixing ferromagnetic particles, metallic particles with Polyphenylene Sulfide (PPS) resin powder. The mixture was melting at 300^0 C and pressing at pressure of 620 MPa in the cooling process down to the room temperature. Toroidal samples with inner diameter 3 mm and outer diameter of 7 mm were prepared which were used to collect the relative permittivity and permeability spectra data. For the electrical conductivity measurement, rectangular samples with 2 mm thickness were prepared.

The complex relative permittivity ε_r and μ_r of the composite materials were measured by the transmission/reflection method using a coaxial line cell and a network analyzer (Agilent E5071C) in the frequency range from 10 MHz to 20 GHz. The electrical conductivity of composite materials was measured by the two terminal method using an impedance analyzer (HP4194A) in the frequency range from 1 kHz to 40 MHz.

3.2. Sample Preparation

Commercially available ferromagnetic Permalloy FeNi ($Fe_{53}Ni_{47}$), Permendur FeCo ($Fe_{50}Co_{50}$); Ferrite Ni-Zn ($Ni_{0.24}Zn_{0.65}Fe_{2.04}O_4$), Mn-Zn ($Mn_{0.55}Zn_{0.41}Fe_{2.06}O_4$) and cupper cu powder were used for granular composite materials. Particle diameter was controlled below 45 μm by sieve; the shape and size distribution of the embedded particles were examined using a scanning electron microscope (SEM). The Cu particles are coagulated having the arborized shape of several tens μm in length which consist of semi-spherical small sized particles with mean particle diameter of about 10 μm [1]. The shapes of Fe53Ni47 particles are spherical; the

mean particle diameter which was estimated by the lognormal distribution function, was found to be 7.07 μm [2]. The $Fe_{50}Co_{50}$ have a mean particle diameter of about 2.08 μm [3]. Meanwhile the mean particle diameters of Ni-Zn and Mn-Zn are 3.24 μm and 2.51 μm respectively [4].

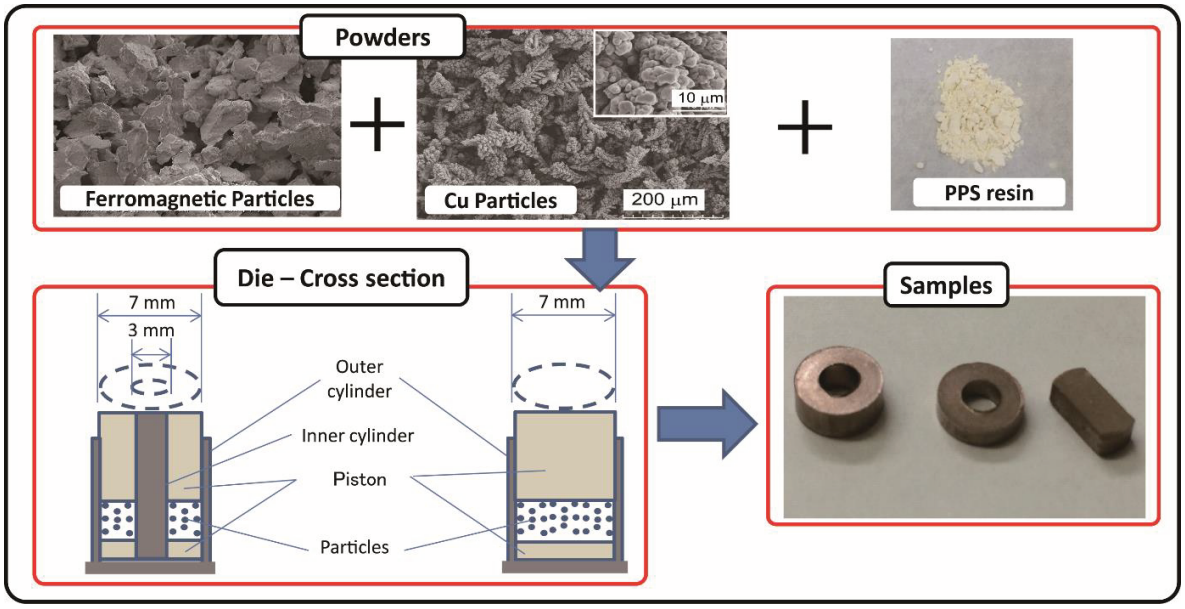

Figure 3.1. The process of sample preparation: ferromagnetic, metallic and PPS resin powders, are mixed together to form hybrid mixture. The powder is inserted in between pistons in a cylinder to form toroidal and disc shaped samples.

The samples preparation is illustrated in Fig. (3.1). Ferromagnetic powder was mixing together with Cu powder and polyphenylene sulphide (PPS) resin powder forming hybrid composite materials. The particles were grid and then inserted in between two metallic cylinders which has the inner diameter of 3 mm and the outer diameter of 7 mm and cylinder with diameter of 7 mm. The mixture was then taken to the furnace at 300^0C for 20 min to melting the resin powder. After melting the resin, the mixture was compressed by pressing the piston at a pressure of 620 MPa at the process of cooling down to the room temperature. Toroidal samples

with inner diameter of 3 mm and outer diameter of 7 mm were produced and disc samples with diameter of 7mm. the thickness of samples were controlled to 1mm to 2 mm; the disc samples were then cut into rectangular shape.

3.3.Volume content of the hybrid composite materials

When manufacturing a composite material, fillers particles are impregnated with resin. The volume filler fraction can be calculated using a combination of weights density and volumes of the matrix (resin + filler).

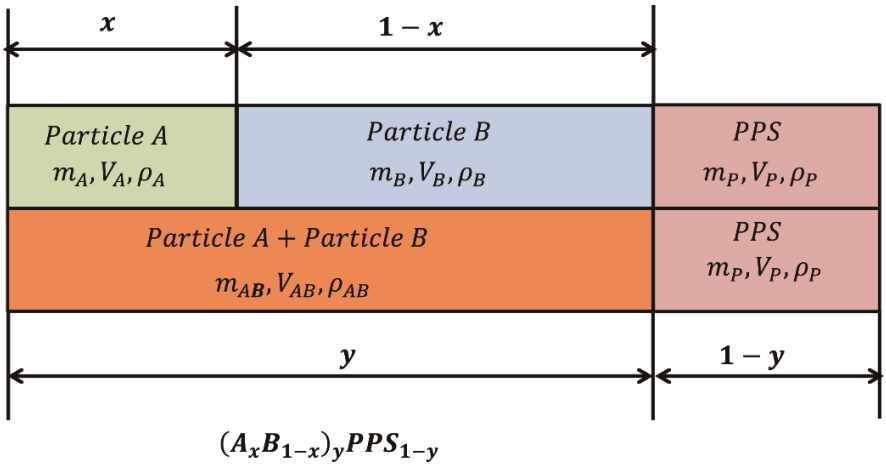

Figure 3.2. Schematic diagram of the volume distribution in hybrid composite materials

Considerer a hybrid composite material which is manufacturing by mixing particle A which has mass m_A, volume V_A and density ρ_A, and particle B with mass m_B, volume V_B and density ρ_B embedded in a host resin with mass m_P, volume V_P and density ρ_P Fig. (3.2). The expression to calculate the volume fraction of particles x and the volume concentration of dispersed particles in the composite y can be deducted. Starting from the expression of density,

$$\rho = \frac{m}{V} \tag{3.1}$$

where V, m and ρ are the volume, mass and density of the hybrid composite. The density is then

$$\rho = \frac{m_{AB} + m_P}{V_{AB} + V_P} = \frac{\rho_{AB} V_{AB} + \rho_P V_P}{V} = \frac{\rho_{AB} yV + \rho_P (1-y)V}{V}$$

$$\rho = \rho_{AB} y + \rho_P (1-y) \tag{3.2}$$

and the average density of A-B particles is defined as

$$\rho_{AB} = \frac{m_A + m_B}{V_{AB}} = \frac{\rho_A V_A + \rho_B V_B}{V_{AB}} = \frac{\rho_A x V_{AB} + \rho_B (1-x) V_{AB}}{V_{AB}}$$

$$\rho_{AB} = x\rho_A + (1-x)\rho_B \tag{3.3}$$

replacing ρ_{AB} in Eq. (3.2), we then get the expression to calculate *x y*:

$$\rho = xy(\rho_A - \rho_B) + y(\rho_B - \rho_P) + \rho_P$$

$$xy = \frac{(\rho - \rho_P) - y(\rho_B - \rho_P)}{\rho_A - \rho_B} \qquad 3.4$$

when $x = 1$, the composite material is the mix of particles A and PPS resin

$$y = \frac{\rho - \rho_P}{\rho_A - \rho_P} \qquad 3.5$$

when $y = 1$, the composite material is the mix of particles A and B without the PPS resin

$$x = \frac{\rho - \rho_B}{\rho_A - \rho_B} \qquad 3.6$$

The samples were prepared by mixing together metallic Cu particles with ferromagnetic particles in a host PPS resin forming hybrid composite materials. Since the hybrid composite materials contain two particles having different densities, the volume fraction of mixed particles in the host resin was estimated by use of the effective density of the hybrid particles which was calculated using the each density and the prepared volume ration. The volume fraction of Cu metallic particles φ_A in the composite was determined by the following equation:

$$\varphi_A = \frac{V_A}{V_A + V_B + V_P} \qquad 3.7$$

Where

$$\mathrm{V}_{AB} = yV \qquad 3.8$$

$$V_A = xV_{AB} = xyV \qquad 3.9$$

$$V_B = (1 - x)V_{AB} = (1 - x)yV \qquad 3.10$$

$$V_P = (1 - y)V \qquad 3.11$$

Therefore

$$\varphi_A = \frac{xyV}{xyV + (1 - x)yV + (1 - y)V} \qquad 3.12$$

$$\varphi_A = \mathrm{xy} \qquad 3.13$$

So that

$$\varphi_A = \mathrm{xy} = \frac{(\rho - \rho_P) - y(\rho_B - \rho_P)}{\rho_A - \rho_B} \qquad 3.14$$

From the Eq. (3.14), if the volume fraction of the dispersed particles y is known, the volume fraction of metallic particles A in the composite is determined and consequently the volume fraction B of ferromagnetic particles can also be determined.

3.4. Experimental measurements

3.4.1. Relative complex permittivity and permeability spectra

The complex relative permittivity and magnetic permeability are quantities that are not directly measurable, they are obtained from the measurement of sensor reflection coefficient or scattering parameters, which can be obtained with a different number of techniques proposed and developed over the last decades. Some of these techniques are open ended coaxial probe, cavity resonator, free space measurement parallel plate capacitors and transmission line techniques; they may be in time domain or frequency domain and make use of probes with one or two ports. However, some techniques have a very limited frequency band of operation. The transmission line technique, Transmission/Reflection or coaxial method gives accurate results and allows measurement in very wide frequency range [5, 6]. The transmission line technic comprises two kind of methods, 1-port call or short circuit coaxial line method and 2-port call or open coaxial line method.

The 1-port method, the sample is loaded at the end of short circuited transmission line as showed in Fig. (3.3) and the reflection coefficients are measured. This method is used to measure high frequency complex permeability values. On the other hand the 2-port method, the sample is loaded at the middle of transmission line Fig. (3.4) and the S-parameters of scattering parameters

as a function of the complex relative permittivity and magnetic permeability have to be found. This is achieved by expressing the scattering parameters S11 and S21 measured by a vector network analyzer as a function of the reflection coefficient (Γ) of the air sample interface and transmission coefficient (T) respectively.

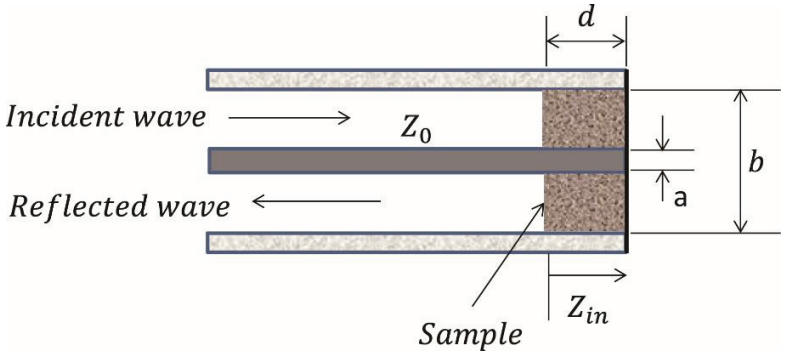

Figure 3.3. Cross sectional view of short-circuit coaxial line with filled material

The complex permeability can be calculated by the difference between the impedance of holder loaded with and without toroidal sample:

$$\mu_r = 1 + \chi = 1 + \frac{Z - Z_{air}}{jd\mu_0 f ln\left(\frac{b}{a}\right)} \qquad 3.15$$

Where *a* and *b* denotes the inner and outer diameter of the toroidal sample respectively, *d* the height of the sample and f is the frequency of applied *ac* electromagnetic field.

The vector analysis measures the complex reflection coefficient, which is calculated to the input impedance of the cell according to the follow equation:

$$Z_{in} = Z_0 \frac{1+\Gamma}{1-\Gamma} \qquad 3.16$$

with $Z_0 = 50\Omega$, characteristic impedance of the 7 mm test port. The resistance R_{in} and reactance X_{in} values of the input impedance of the cell is given by:

$$Z_{in} = R_{in} + jX_{in} \qquad 3.17$$

$$R_{in} = Z_0 \frac{1-\Gamma'^2-\Gamma''^2}{(1-\Gamma')^2+\Gamma''^2} \qquad 3.18$$

$$X_{in} = Z_0 \frac{2\Gamma''}{(1-\Gamma')^2+\Gamma''^2} \qquad 3.19$$

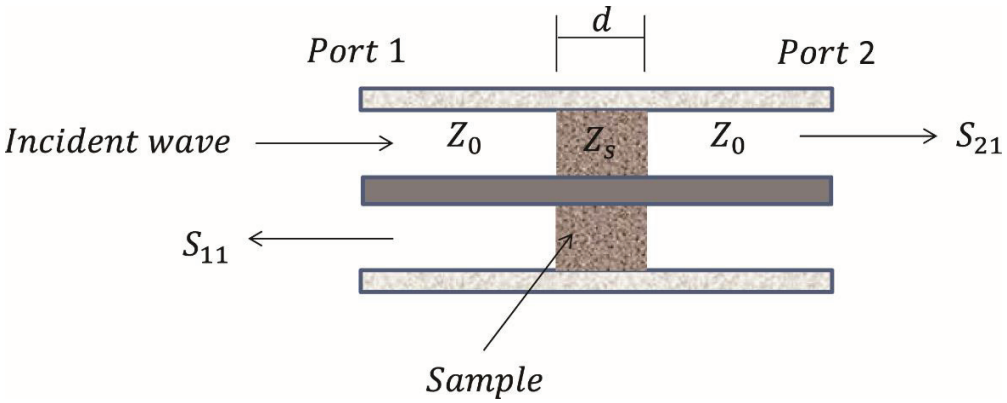

Figure 3.4. Cross sectional view of open circuited coaxial line with filled material and S-Parameter notation.

The relationship between S-parameters of scattering parameters as a function of the complex relative permittivity (μ_r) and magnetic permeability (ε_r) are determining by using the Nicolson-

Ross-Weir (NRW) method using measurements of the reflection coefficient (S_{11}) and the transmission coeficiente (S_{21}) [7].

$$S_{11} = \frac{(1 - T^2)\Gamma}{1 - T^2\Gamma^2} \quad 3.20$$

$$S_{21} = \frac{(1 - \Gamma^2)\Gamma}{1 - T^2\Gamma^2} \quad 3.21$$

$$\Gamma = \mathrm{K} \pm \sqrt{K^2 - 1} \quad 3.22$$

Where

$$\mathrm{K} = \frac{{S_{11}}^2 + {S_{21}}^2 + 1}{2S_{11}} \quad 3.23$$

The transmission coefficient,

$$\mathrm{T} = \frac{S_{11} + S_{21} - \Gamma}{1 - (S_{11} + S_{21})\Gamma} \quad 3.24$$

The complex dielectric constant and permeability can be determinate from Γ and T:

$$\Gamma = \frac{Z_s - Z_0}{Z_s + Z_0} = \frac{\sqrt{\frac{\mu_r}{\varepsilon_r}} - 1}{\sqrt{\frac{\mu_r}{\varepsilon_r}} + 1} \quad 3.25$$

$$\mathrm{T} = e^{-i\frac{2\pi}{\lambda_0}\sqrt{\varepsilon_r \mu_r d}} \quad 3.26$$

From Eq. (3.25) and (3.26) we can define x and y as follows:

$$\frac{\mu_r}{\varepsilon_r} = \left(\frac{1+\Gamma}{1-\Gamma}\right)^2 = x \quad 3.37$$

$$\mu_r \varepsilon_r = -\left(\frac{\lambda_0}{2\pi d} ln \frac{1}{T}\right)^2 = y \quad 3.38$$

$$\mu_r = \sqrt{xy} \quad 3.39$$

$$\varepsilon_r = \sqrt{\frac{y}{x}} \quad 3.40$$

For measurement using the wave guide sample holder, the equations can be written as follows

$$\mu_r = \frac{1+\Gamma}{\Lambda(1-\Gamma)\sqrt{\frac{1}{\lambda_0{}^2} - \frac{1}{\lambda_c{}^2}}} \quad 3.41$$

$$\varepsilon_r = \frac{\left(\frac{1}{\Lambda^2} + \frac{1}{{\lambda_c}^2}\right){\lambda_0}^2}{\mu_r} \qquad 3.42$$

Where λ_0 is free space wavelength, λ_c is the cutoff wavelength of the waveguide and $\frac{1}{\Lambda^2} = -\left(\frac{1}{2\pi d} ln \frac{1}{T}\right)^2$

3.4.1.1. Experimental set up for data collection, relative complex permittivity and permeability spectra

The relative complex permittivity ε_r and permeability μ_r data were collected by the conventional *S*-parameter method using a coaxial transmission line and a network analyzer Agilent E5071C from 10 MHz to 20 GHz.

Toroidal samples with inner diameter of 3 mm outer diameter of 7 mm; 1 and 2 mm thickness are inserted in a coaxial sample holder. The thickness of samples was controlled about 1mm to 2mm in order to avoid the dimensional resonance of the electromagnetic wave in the coaxial line. It is important that the sample be uniform and fills completely the guide in the transmission line sample holder to avoid the measurement errors; the sample should be fit tightly in the holder. To avoid the air gap and ensure the connection between the sample and sample holder, a conductive Ag paste was used during the measurements.

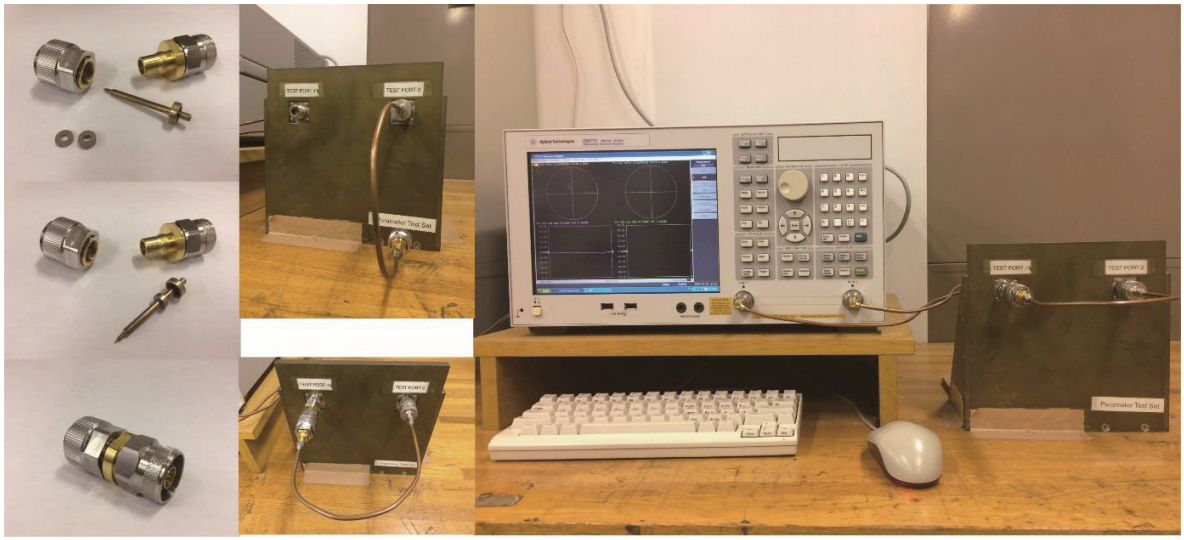

Figure 3.5. Experimental set up for data collection of relative permittivity ε_r and permeability μ_r spectra.

Under computer network control, network analyzer system calibration and measurement are obtained at the reference planes port 1 and port 2 indicated in Fig. (3.5). The measured scattering parameters are normalized to the characteristic impedance Z_0 of the transmission line section. The reflections coefficients S_{11} at the air to the sample surface, and transmission coefficient S_{21} through the sample, are found at reference planes port 1 and 2. From complex reflection and transmission coefficients, the computer associated with the network analyzer determines the real and imaginary parts of the permittivity and permeability.

3.4.2. Electrical resistivity and conductivity

The amount of electrical current that flows in a material is restricted by amount of resistance of the material. The electrical resistivity ρ of a material is a measure of how strongly the material opposes the flow of the electric current and it's given by the following expression:

$$\rho = A\frac{R}{L}[\Omega.m] \tag{3.43}$$

Where R is the electrical resistance of a uniform specimen of the material measured in ohms, L the length of the piece of material measured in meters and A the cross-sectional area of the specimen measured in meters square. The resistivity is given ohms per meter, $\Omega.m$

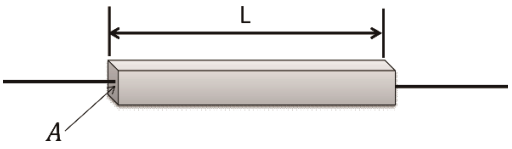

Figure 3.6. Piece of resistive material with electrical contact in both terminals

Resistivity of a material depends upon on the physical nature of the materials being used. Different types of conductors can be compared to one another as a good conductor or not regardless to their resistivity.

While both the electrical resistance R and resistivity ρ, are a function of the physical nature of the material being used and of its physical shape and size expressed by its length L and its sectional area A, conductivity relates to how ease the electric current flow through the material.

The electrical conductivity is the inverse on resistivity and is measured in Siemens per meter S/m:

$$\sigma = \frac{1}{\rho}[S/m] \qquad 3.44$$

Conductivity is the reciprocal of resistivity. Therefore a material or conductor with high resistivity will have a low conductivity, and vice versa.

3.4.2.1.Experimental set up for data collection, electrical resistivity and conductivity

The ac electrical conductivity σ_{ac} of the samples was obtained from the electrical resistivity measurement by the two-terminal method with an impedance analyzer HP4194A from 100 Hz to 40 MHz Fig. (3.7).

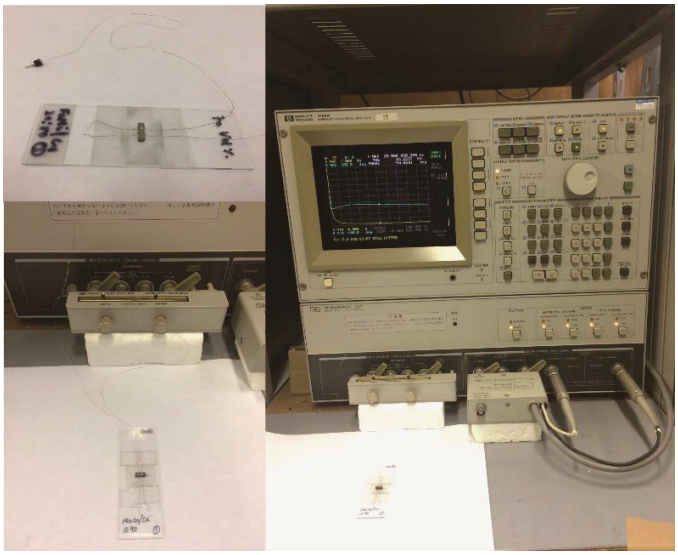

Figure 3.7. Electrical set up for data collection of electrical resistivity and conductivity

The electrical properties of the samples were obtained by measuring the resistance R and reactance X. The terminals of sample are connected to a sample holder which is connected to the HP4194A. The R and X were collected using a computer program connected to the HP4194A. From the resistance measurement and measurement of the length L and calculation of the cross-sectional area of samples the electrical conductivity ρ of the samples was calculated.

References

[1] T. Tsutaoka, T. Kasagi, S. Yamamoto, K. Hatakeyama, Low frequency plasmonic state and negative permittivity spectra of coagulated Cu granular composite materials in the percolation threshold, Applied Physics Letters, 102 (2013) 181904.

[2] Herieta Massango, T. Tsutaoka, T. Kasagi, Electromagnetic properties of Fe53Ni47 nd Fe53Ni47/Cu granular composite materials in the microwave range, Mater. Res. Express, 3 (2016).

[3] T. Kasagi, T. Tsutaoka, K. Hatakeyama, Electromagnetic properties of Permendur granular composite materials containing flaky particles, J Appl Phys, 116 (2014) 153901.

[4] T. Tsutaoka, T. Kasagi, K. Hatakeyama, M.Y. Koledintseva, Analysis of the Permeability Spectra of Spinel Ferrite Composites Using Mixing Rules, in: IEEE International Symposium on Electromagnetic Compatibility, , IEEE, Denver, 2013, pp. 545 - 550.

[5] V. Radonic, N. Blaz, L. Zivanov, Measurement of Complex Permeability Using Short Coaxial Line Reflection method, Acta Physics Polonica, 117 (2009) 820-824.

[6] S. Takeda, T. Hotchi, S. Motomura, H. Suzuki, Theoretical Consideration on Short- & Open-circuited Transmission Line for Permeability & Permittivity Measurement, Journal of Magnetic Society of Japan, (2015).

[7] A.M. Nicolson, G.F. Ross, Measurement of the Intrinsic Properties of Materials by Time-Domein Techniques, IEEE Transactions on Instrumentation and Measurement, IM-19 (1970) 377-382.

Chapter 4: Results and Discussion

4.1. Electrical conductivity of granular composite materials

When a polymer matrix having a conductivity σ_p is filled with dispersed filled particles having a conductivity σ_f, the composite prepared gains a conductivity value σ. When the volume filler fraction φ reaches a critical value φ_c, (percolation threshold) an infinite conductivity cluster is formed and, consequently, the composite becomes conductive. The conductive phase is formed by dispersed conductive fillers.

Two types of hybrid composite samples have been prepared by incorporated ferromagnetic, ferrite and Cu particles in a polymer PPS resin forming the combinations, FeNi/Cu, FeCo/Cu, NiZnF/Cu and MnZnF/Cu as mentioned in chapter 3.

The designation x in Fig. (4.1a), (4.2a), (4.3a) and (4.4a) have been employed to indicate the fraction of Cu fillers in the composite and to differentiate with the fraction of filled particle φ in Fig. (4.1b), (4.2b), (4.3b) and (4.4b). The FeNi/Cu and FeCo/Cu composites are considered to have a double metallic system since the ferromagnetic particles combined with Cu particles contributes to the electrical properties. While in the case of NiZnF/Cu and MnZnF/Cu, the ferrite particles have low conductivity, the electrical properties of the composites are determined mainly by the Cu particles content against the total volume. The combination (FeNi+ Cu and FeCo + Cu) are treated as a single particle system in the host PPS resin and the combination of (NiZn + PPS and MnZn + PPS) has a host system for Cu particles. Considering the volume fraction of particles by φ, the particle content of Cu can be defined by Eq. (3.13). The electrical properties of FeCo and FeNi have been investigated. The percolation threshold φ_c was defined as 0.76 for FeCo and 0.61 for FeNi composites materials. The 85 vol. % of FeCo and FeNi only are in the

percolate state but cannot produce the LFP state with negative permittivity [1, 2] . The electrical properties of Cu granular composite materials have been studied [3] and the percolation threshold was found at $\varphi_c = 0.16$. The composition of the selected hybrid granular composites is denoted by $(A_xB_{1-x})_yPPS_{1-y}$, where x is the volume fraction of A in the AB hybrid particle and y indicates the total volume fraction of embedded particles y = 0.85 in the case of FeCo/Cu and FeNi/Cu and 0.80 for NiZnF/Cu and MnZnF/Cu granular composite materials.

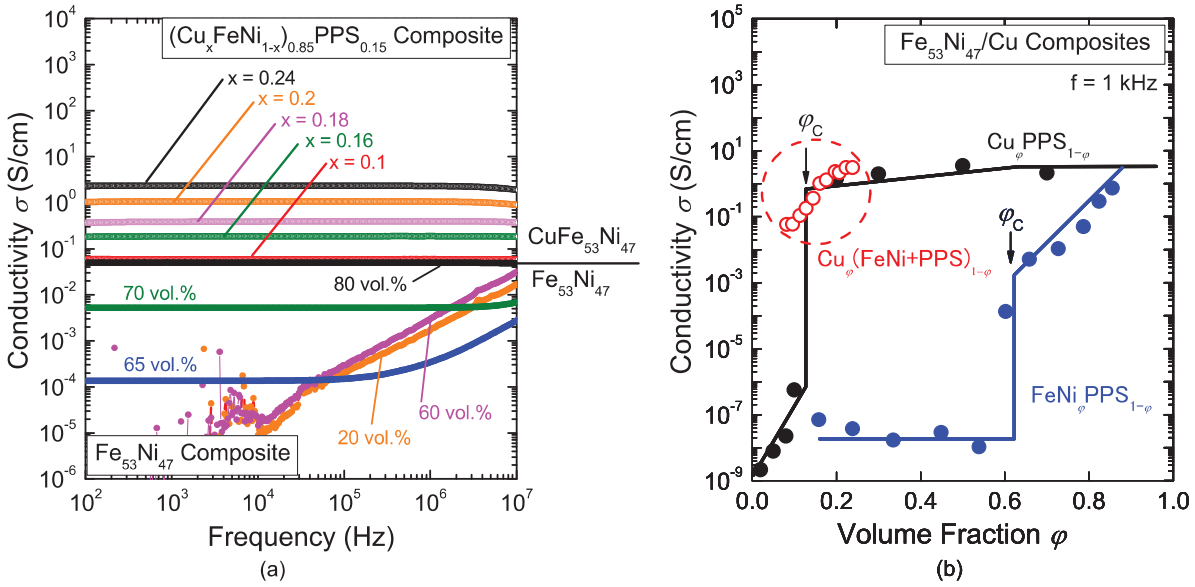

Figure 4.1. Electrical conductivity spectra of FeNi/Cu granular composite materials as a function of frequency (a) and the electrical conductivity at 1 KHz as a function of the volume fraction φ (b)

The electrical conductivity σ_{ac} of the FeNi/Cu hybrid composite material is shown in Fig. 4.1(a) as a function of frequency. The conductivity shows no frequency dependence up to about 10 MHz for all Cu particle content. The σ_{ac} at 1 kHz of Cu, FeNi and FeNi/Cu granular composites is summarized in Fig. 4.1(b) as a function of φ. The σ_{ac} of $(Cu_xFeNi_{1-x})_{0.85}PPS_{0.15}$ is located at about 0.1 S/m at x = 0.10, increases with increasing x, and reaches the same value as

that of Cu/PPS composite at around x = 0.2. The $(Cu_xFeNi_{1-x})_{0.85}PPS_{0.15}$ hybrid composites is already in percolated state even at the lowest particle content.

Since the results of FeNi/PPS composite material at φ = 0.85 shows that the metallic connection is already established with conductivity value around 0.1 S/cm. Hence, the $(Cu_xFeNi_{1-x})_{0.85}PPS_{0.15}$ composite materials at volume fraction y = 0.85 is already in the percolated state; the conductivity being enhanced by increasing Cu particles. Decreasing the volume fraction y, the expectation is that the composite materials would show some dielectric properties in the low Cu particle content. The results of FeNi/Cu measurement at y = 0.70 are showed in the Appendix A. The Cu particle content up to x = 0.10 showed in fact dielectric properties with the conductivity below 0.1 S/cm. The conductivity not only depends on the Cu particles content in the composite materials but also on the volume fraction of inclusions y.

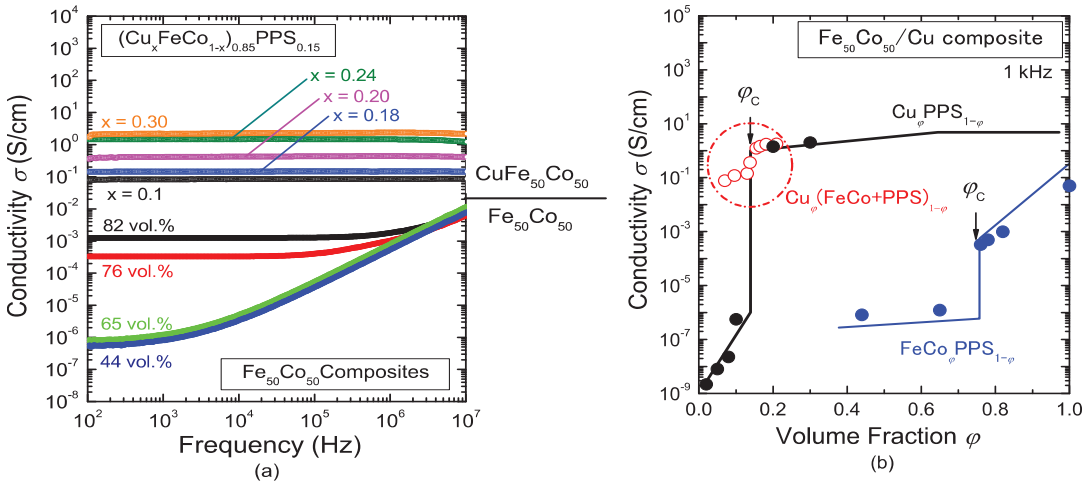

Figure 4.2. Electrical conductivity spectra of FeCo/Cu granular composite materials as a function of frequency (a) and the electrical conductivity at 1 KHz as a function of the volume fraction φ (b)

As in the case of FeNi/Cu, the FeCo/Cu granular composite materials show no dependence with frequency up to about 10 MHz, Fig. 4.2(a). The σ_{ac} at 1 kHz is shown in Fig. 4.2(b) as a function of the Cu and FeCo particle volume fraction φ. The FeCo/Cu hybrid composites have larger conductivity than FeCo; the σ_{ac} value is about 0.1 S/cm even at the Cu particle volume fraction $\varphi = 0.05$. This high conductivity is attributed to the combination of surface oxidized metallic FeCo and Cu particles. An abrupt increase of σ_{ac} can be seen at about φ = 0.15; the σ_{ac} value becomes more than 1.0 S/cm.

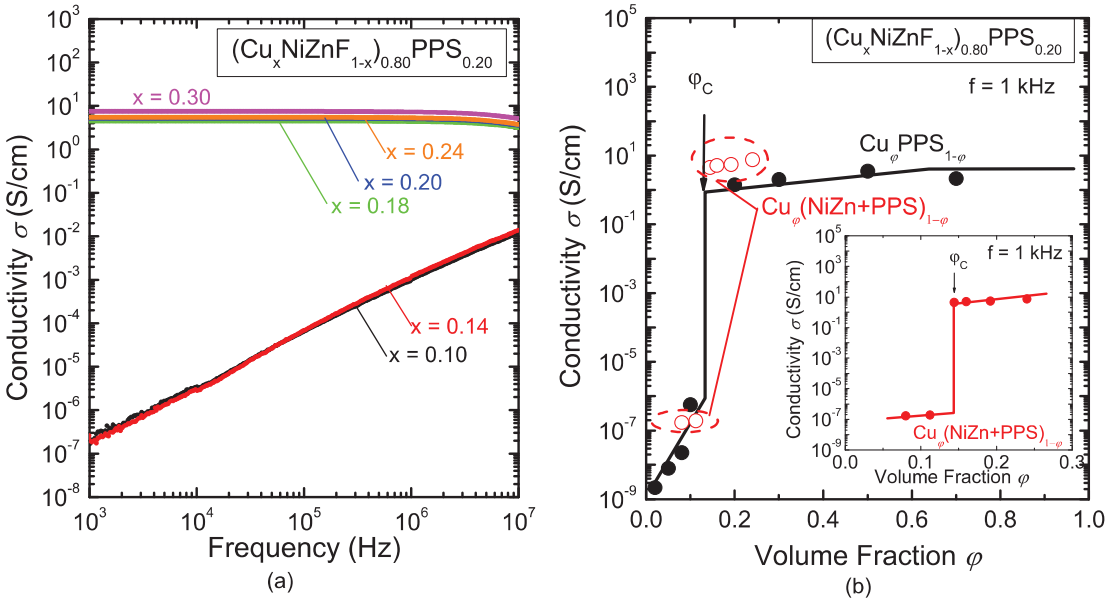

Figure 4.3. Electrical conductivity spectra of NiZnF/Cu granular composite materials as a function of frequency (a) and the electrical conductivity at 1 KHz as a function of the volume fraction φ (b). The inset in (b) is the expanded NiZnF/Cu and its respective φ_c.

The ac electrical conductivity σ_{ac} spectra of NiZnF/Cu hybrid composite materials as a function of frequency is shown in Fig.4.3(a). The low composite samples x = 0.10 and 0.14 shows very low conductivity in the order of 10^{-7} S/cm at 1 kHz; the conductivity σ_{ac} rapidly

increases with frequency up to around 10^{-1} S/cm at 40 MHz. Meanwhile, from x = 0.18 to x = 0.3, samples have relatively large conductivity value of 2 to 8 S/cm and shows almost no frequency dependence in the whole measurement frequency range. Since a large conductivity difference can be seen between x = 0.14 and x = 0.18, the electrical percolation is considered to take place at around x = 0.18 particle content. The conductivity σ_{ac} of NiZnF/Cu composite materials at 1 kHz is shown in Fig.4.3(b) as a function of Cu particle volume fraction φ. The conductivity σ_{ac} is in the order of 10^{-7} S/cm up to φ = 0.11; a large jump of σ_{ac} is observed between φ = 0.11 and 0.14. Thus, we defined the electrical percolation threshold φ_C = 0.14 for NiZnF/Cu composites. At φ = 0.14 and above it, the composite is in the metallic state with the conductivity value of more than 1.0 S/cm.

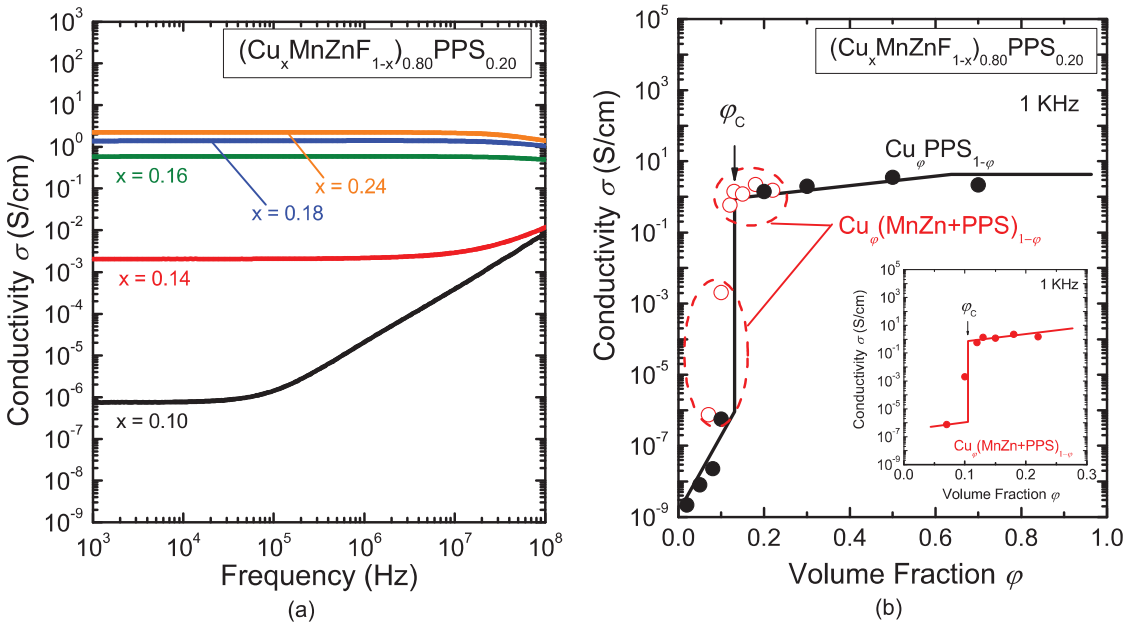

Figure 4.4. Electrical conductivity spectra of MnZnF/Cu granular composite materials as a function of frequency (a) and the electrical conductivity at 1 KHz as a function of the volume fraction (b). The inset in (b) is the expanded MnZnF/Cu and its respective φ_c.

The ac electrical conductivity σ_{ac} spectra of MnZnF/Cu hybrid composite materials as a function of frequency are shown in Fig.4.4(a). The low composite samples x = 0.10 and 0.14 shows low conductivity around 10^{-6} and 10^{-3} S/cm at 1 kHz; the conductivity σ_{ac} of x = 0.10 is constant up to 100 KHz and rapidly increases with frequency up to 10^{-2} S/cm at 40 MHz and x = 0.14 sample, σ_{ac} is constant up to about 10 MHz and slightly increases to 10^{-2} S/cm at 40 MHz Meanwhile, from x = 0.16 to x = 0.3, samples have relatively large conductivity value of 0.5 to 2 S/cm and shows almost no frequency dependence in the whole measurement frequency range. A large conductivity difference can be seen between x = 0.10 and x = 0.14 and also between 0.14 and 0.16, the electrical percolation is considered to take place at around x = 0.16 particle content. The conductivity $\sigma_{ac}$of MnZnF/Cu composite materials at 1 kHz is shown in Fig.4.4(b) as a function of Cu particle volume fraction φ. A large jump of σ_{ac} is observed between φ = 0.08 and 0.13 with φ = 0.11 as a mid-point. Thus, we defined the electrical percolation threshold φ_C = 0.11 for NiZnF/Cu composites. At φ = 0.13 and above it, the composite is in the metallic state with the conductivity value of more than 1.0 S/cm. The electrical connection among the Cu particle chains can produce the electric current along the percolated clusters and the low frequency plasmonic state can be induced.

4.2. Complex permittivity

The complex permittivity spectra $\varepsilon_r = \varepsilon_r' - j\varepsilon_r''$ as a function of frequency of FeNi/Cu, FeCo/Cu, NiZnF/Cu and MnZnF/Cu are shown in Fig. 4.5(a), 4.6(a), 4.7(a) and 4.8(a) real parts and imaginary parts Fig. 4.5(b), 4.6(b), 4.7(b) and 4.8(b). The permittivity spectrum can be

separated into dielectric frequency dispersion permittivity with positive value and in the plasmonic permittivity dispersion with the negative ε_r' below the characteristic frequency f_0 which is associated to the plasma frequency of the conduction electrons. The plasma oscillation of conduction electrons is induced in metal particle cluster by the electric current flowing in the percolated composite structure. Since the plasma oscillation is produced by the conduction electrons moving along the percolated cluster only, the low carrier density state can be established in metal granular composites.

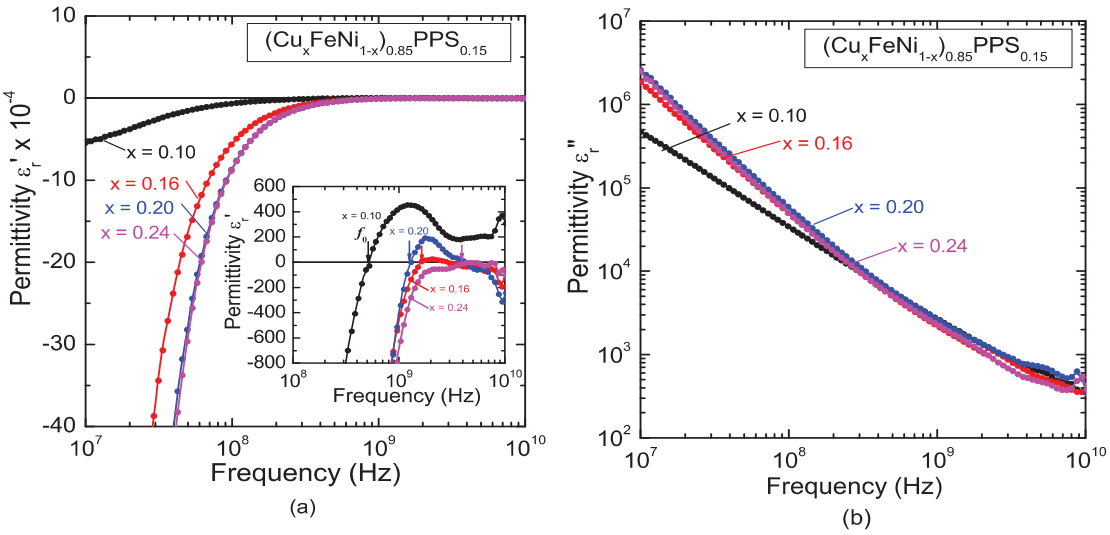

Figure 4.5. Relative complex permittivity spectra of FeNi/Cu granular composite materials: ((a) real part ε_r' and (b) imaginary part ε_r'')). The inset of the (a) is the expansion of the ε_r'

The real part ε_r', Fig.4.5(a) of $(Cu_xFeNi_{1-x})_{0.85}PPS_{0.15}$ hybrid granular shows negative value in the low frequency and increases with increasing frequency and across the zero at a characteristic frequency f_0 . Simultaneously, the imaginary part ε_r'' Fig.4.5 (b) shows a large positive value in the low frequency range and rapidly decreases with frequency. This negative

permittivity dispersion is observed even at x = 0.10. Thus the $(Cu_{0.1}FeNi_{0.9})_{0.85}PPS_{0.15}$ is already in a plasmonic state.

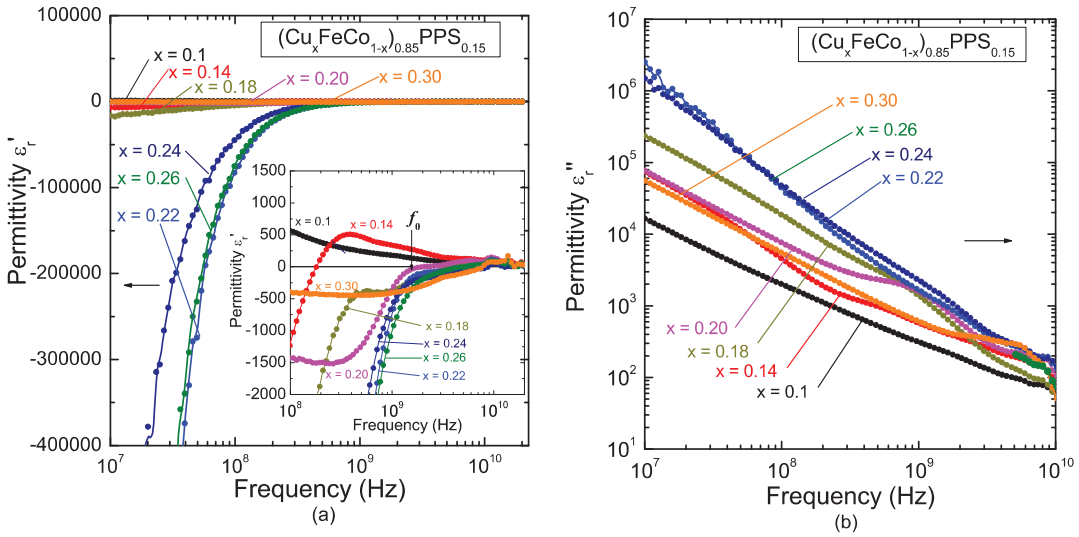

Figure 4.6. Relative complex permittivity spectra of FeCo/Cu granular composite materials: ((a) real part ε_r' and (b) imaginary part ε_r'')). The inset of the (a) is the expansion of the ε_r'

At x = 0.1, as shown in Fig. 4.6. a typical dielectric permittivity spectrum with positive ε_r' was observed in $(Cu_xFeCo_{1-x})_{0.85}PPS_{0.15}$ materials. The ε_r' is around 1200 at 10 MHz and decreases with frequency reaching almost unity at 10 GHz. The imaginary part ε_r'' for the same particle content shows a relatively low permittivity compared to the other particle content indicating low dielectric loss. Meanwhile, at x = 0.14, the FeCo/Cu composite shows a plasmonic permittivity dispersion with a large negative ε_r' value; the ε_r' crosses the zero at a characteristic frequency f_0 and becomes positive above it. With the increase of Cu particle content x, the negative permittivity is enhanced; the characteristic frequency f_0 shifts to the

higher frequency. Simultaneously, higher Cu content leads to the increase of ε_r'' caused by the conductivity loss.

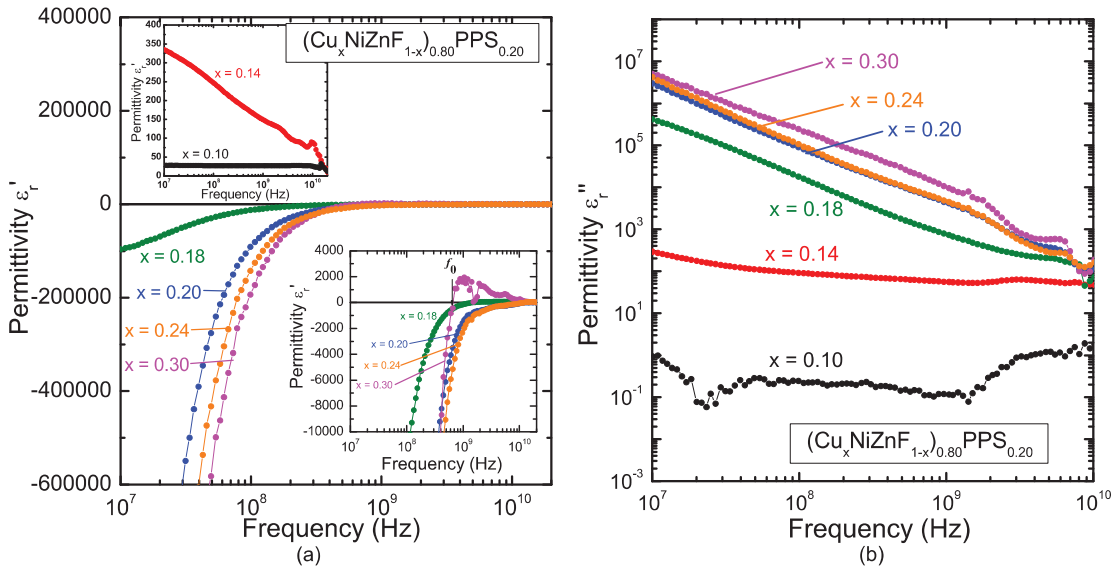

Figure 4.7. Relative complex permittivity spectra of NiZnF/Cu granular composite materials: ((a) real part ε_r' and (b) imaginary part ε_r'')). The inset of the (a) is the expansion of the ε_r' at low Cu volume fraction x = 0.10 and x = 0.14 and the expanded figure of the ε_r' at plasmonic state

The real part permittivity ε_r' of $(Cu_xNiZnF_{1-x})_{0.80}PPS_{0.20}$ at x = 0.10 and 0.14, a typical dielectric permittivity spectrum with positive ε_r' was observed as show in in Fig. 4.7. The ε_r' is around 25 at 10 MHz and is constant up to 20 GHz at x = 0.1 particle content as shown in the inset of Fig.4.7(a). Meanwhile, at x = 0.14 particle content, ε_r' is around 325 and decreases with frequency reaching almost unity at 10 GHz. The imaginary part ε_r'' Fig.4.7(b) for the same particle content shows a relatively low permittivity compared to the other particle content

indicating low dielectric loss. The x = 0.18 composite and above show a plasmonic permittivity dispersion with a large negative ε_r' value.

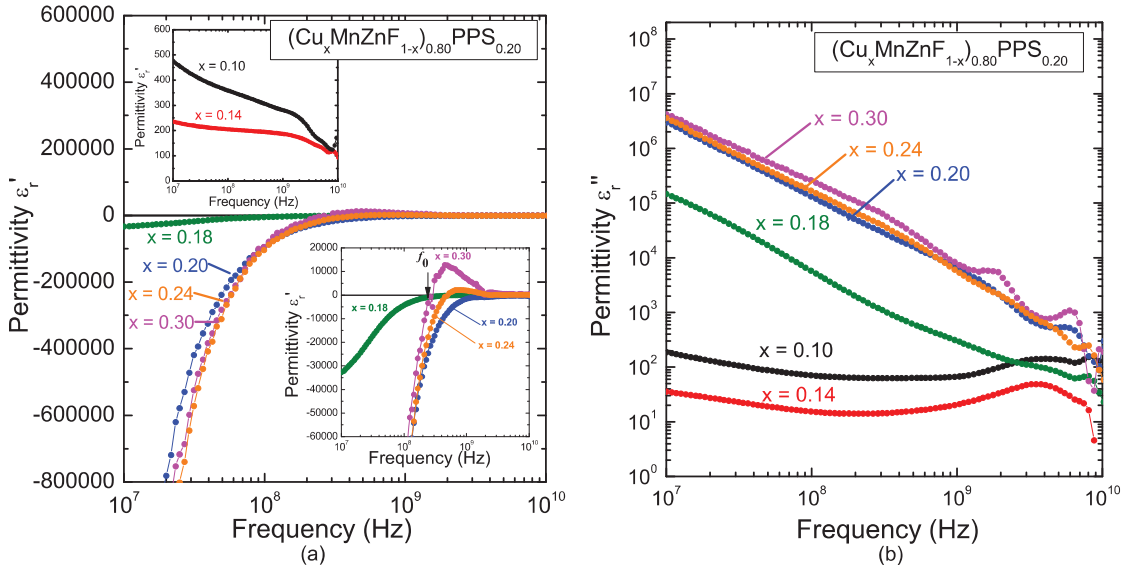

Figure 4.8. Relative complex permittivity spectra of MnZnF/Cu granular composite materials: ((a) real part ε_r' and (b) imaginary part ε_r'')). The inset of the (a) is the expansion of the ε_r' and a low Cu volume fraction x = 0.10 and x = 0.14 and the expanded figure of the ε_r' at plasmonic state

For $(Cu_xMnZnF_{1-x})_{0.80}PPS_{0.20}$ the x = 0.10 and 0.14 particle real permittivity ε_r' shows a typical dielectric permittivity spectrum with positive ε_r'. The ε_r' is around 250 and 450 at 10 MHz and decreases up to 100 at 20 GHz at x = 0.10 and 0.14 respectively as shown in the inset of Fig.4.8(a). However, from x = 0.18 particle content and above it the composite shows a plasmonic behavior with negative ε_r'. The imaginary part ε_r'' Fig.4.8(b) x = 0.10 and 0.14 particle content shows low permittivity around 200 and 40 respectively and it is almost constant up to 10

GHz. As the Cu particle content increase the loss also increases at low frequency; ε_r'' decreases with frequency reaching almost unity at 10 GHz.

With the increase of Cu particle content, the negative permittivity is enhanced; the characteristic frequency f_0 shifts to the higher frequency. Simultaneously, higher Cu content leads to the increase of ε_r'' caused by the conductivity loss. The imaginary parts ε_r'' at low Cu particle content of ferrite composite materials NiZnF/Cu and MnZnF/Cu shows a relatively low permittivity compared to these of FeNi/Cu and FeCo/Cu composite materials indicating a relatively low dielectric loss. The same tendency in complex permittivity spectra was observed in the other hybrid composite materials containing combination of metallic and magnetic particles [3-5]

The negative permittivity ε_r' spectrum in metallic materials having conductive loss can be described by the Drude model $\varepsilon_r = 1 - \frac{\omega_{pe}^2}{\omega^2 + j\omega\Gamma_e}$ (2.51), the plasma frequency of conduct electrons from (2.44), $f_p = \frac{1}{2\pi}\sqrt{\frac{n_0 e^2}{m\varepsilon_0}}$. In the absence of damping, $f_0 = f_p$; however when damping exists, $f_0 = \sqrt{\omega_p^2 - \Gamma_e^2}/2\pi$ shifts to the lower frequency from f_p. When the damping is small ε_r' below f_0 diverges to negative infinite in the low frequency limit. Meanwhile, the high damping condition gives the constant negative ε_r' value in the low frequency limit. Hence the samples with x = 0.20 and 0.30 in Fig. 4.6(a) are considered to have high damping properties.

4.3. Complex permittivity fitting

The frequency dispersion of permittivity was evaluated by the numerical fitting of the measuring ε_r' using Drude model for metals and Lorentz model for dielectrics. The fitting results

of FeNi/Cu, FeCo/Cu, NiZnF/Cu and MnZnF/Cu composite materials are shown in Fig. 4.9, 4.10, 4.11 and 4.12. The frequency dispersion parameters for the plasma oscillation and dielectric resonance can be evaluated by the non-linear least mean square fitting of measured data. The imaginary part ε_r'' was calculated using the fitted parameters obtained from the ε_r' spectrum. The f_{0_cal} was calculated by the formula $f_0 = \sqrt{\omega_p^2 - \Gamma_e^2}/2\pi$ using fitted parameters.

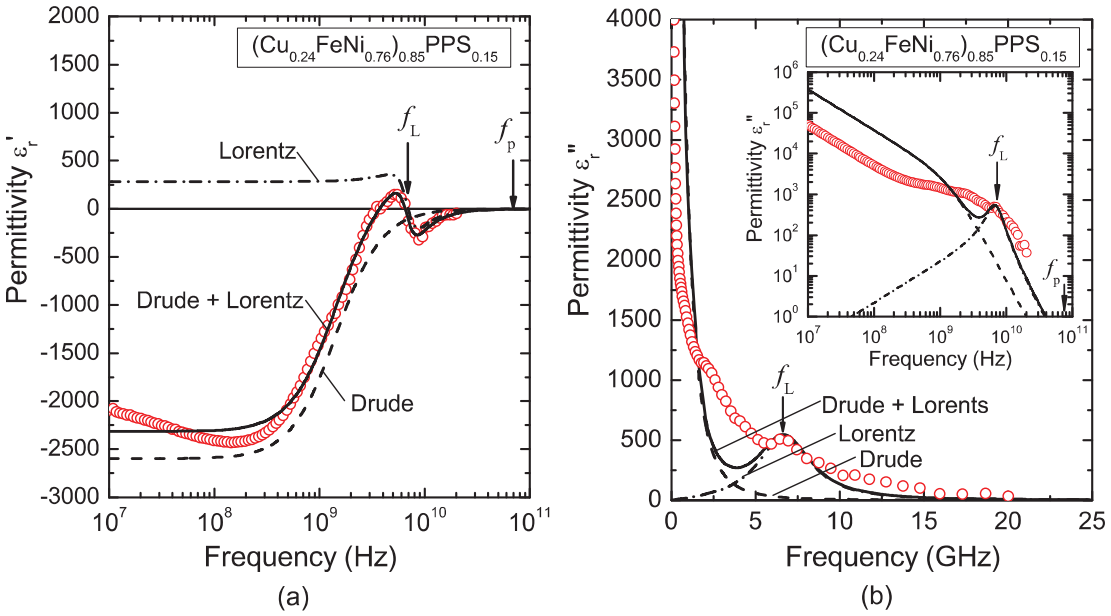

Figure 4.9. The numerical fitting of complex permittivity spectra of $(Cu_{0.24}FeNi_{0.76})_{0.85}PPS_{0.15}$ composite material ((a) real part, (b) imaginary part)). Solid, dashed and dash-doted lines are the calculation curves by the Drude and Lorentz models. The f_L and f_p denote the dielectric resonance frequency and the plasma frequency, respectively. The inset of figure (b) is the logarithmic plot of ε_r''.

The complex permittivity spectrum of $(Cu_{0.24}FeNi_{0.76})_{0.85}PPS_{0.1}$ composite material is shown in Fig. 4.9(a) for the real part and 4.9(b) the imaginary part. The dispersion curve shows a

maximum above the characteristic frequency. Although the composite sample is in percolated state, the permittivity spectrum cannot be explained only by the Drude model. The dispersion curve seems to include the Lorentz dispersion curve, a dielectric resonance caused by isolated metallic particle clusters can be considered [6]. By taking into account the combination of Drude and Lorentz models, the following equation combining Eq. (2.43) and Eq. (2.51) was derived,

$$\varepsilon_r = 1 - \frac{\omega_p^2}{\omega^2 + j\omega\Gamma_D} + \frac{\chi\omega_L^2}{\omega_L^2 - \omega^2 + j\omega\Gamma_L} \qquad 4.1$$

where ω_L is the dielectric resonance angular frequency, Γ_L is the damping constant of the resonance and χ is the electric susceptibility given by Eq.(2.41). The reliability factor R^2 was 0.99058 for the fitting of the ε_r' curve. Obtained plasma frequency f_p is 73.8 GHz; the damping factor Γ_D and characteristic frequency f_0 are 1.44 GHz and 73.6 GHz, respectively. Furthremore, the dielectric resonance frequency f_L is 6.94 GHz, the damping of the resonance Γ_L is 3.71GHz, and the dc dielectric susceptibility is 283. From the obtained damping constant Γ_D, it suggests that the damping of the plasma oscillation is not so large in the $(Cu_{0.24}FeNi_{0.76})_{0.85}PPS_{0.15}$ composite. In the numerical calculation curves, the dashed line indicates the plasmonic oscillaiton (Drude) component and the dash-dotted line shows the dielectric resonance (Lorentz) one. The combined data is indicated by the solid line. The calculated curve using the fitted parameters shows a fairly good aggreement with measured data in the microwave range above 1 GHz. Hence the observed microwave ε_r' spectrum can be explained by the superposition of the Drude and Lorentz type frequency dispersion curves. The observed Lorentz type dielectric resonance mignt be originated by the induced electric dipole in the isolated Cu and FeNi particle

clusters. The isolated metal particle clusters might behave as a dielectric resonator, which was observed in the metal-dielectric composite containing isolated metallic fibers[7].

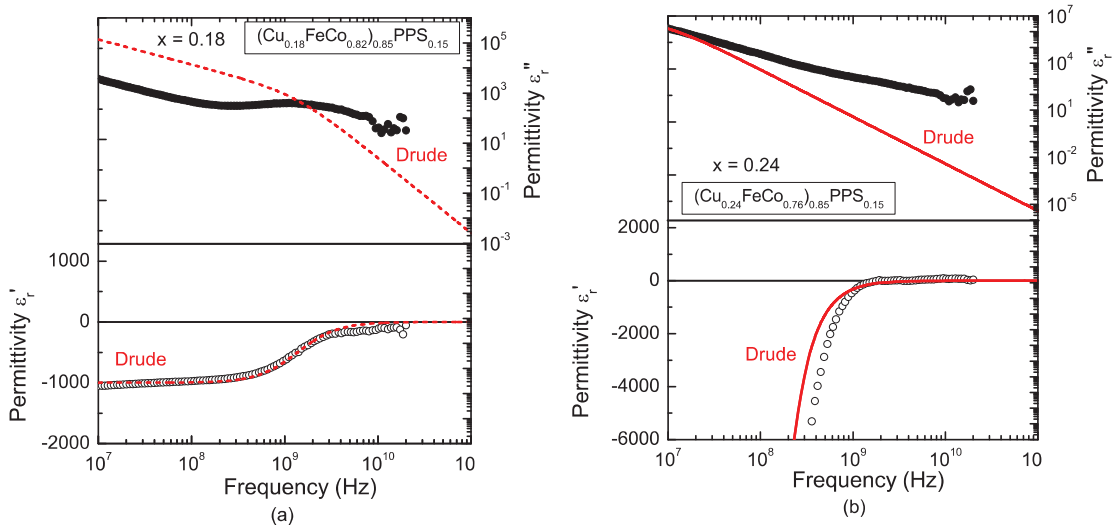

Figure 4.10. The numerical fitting of complex permittivity of $(Cu_xFeCo_{1-x})_{0.85}PPS_{0.15}$ in the plasmonic state for x = 0.18 and x = 0.24. the open and filled circles indicates the real and imaginary parts of relative permittivity the solid dashed red lines are the calculation curves by the Drude mdel.

The fitting results of $(Cu_xFeCo_{1-x})_{0.85}PPS_{0.15}$ for x = 0.18 and 0.24 are shown in Fig.4.10(a) and 4.10(b) respectively. The open and filled circles indicate the real and imaginary parts of the experimental data, respectively. The dashed red lines indicate the real and imaginary parts calculated by the Drude model. There is a fairly good agreement between the numerical and experimental data in the ε_r' spectrum but a relatively large discrepancy exists between calculated and measured data in the imaginary part ε_r''. The observed microwave permittivity in the $(Cu_xFeCo_{1-x})_{0.85}PPS_{0.15}$ composite can be qualitatively explained by the Drude type frequency

dispersion mechanisms. The obtained plasma frequency f_p is 43.4 GHz; the damping factor Γ_D and characteristic frequency f_0 are 1.37 GHz and 6.91 GHz, respectively and the reliability factor R^2 is 0.978 for x = 0.18. The f_p is 17.9 GHz; Γ_D is 11.9 MHz and f_0 is 2.89 GH for x = 0.24 samples. The reliability factor R^2 is 0. 997 shows the consistency of the fitting results.

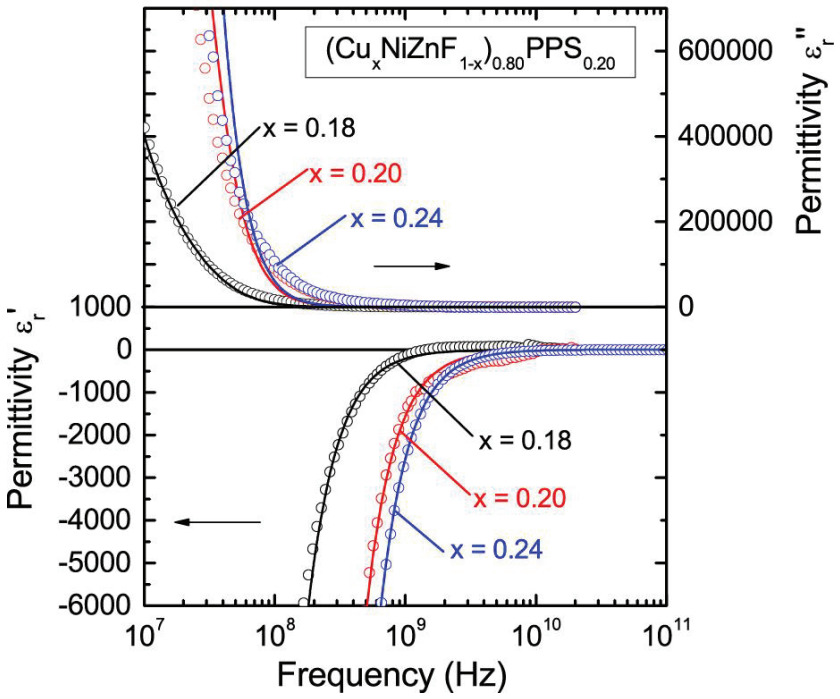

Figure 4.11. The numerical fitting of complex permittivity of $(Cu_xNiZnF_{1-x})_{0.80}PPS_{0.20}$ in the plasmonic state for x = 0.18, x = 0.20 and x = 0.24. The open circles indicate the real and imaginary parts of the experimental data; the solid lines indicate the real and imaginary parts calculated by the Drude model.

The fitting results of $(Cu_xNiZnF_{1-x})_{0.80}PPS_{0.20}$ samples x = 0.18, 0.20 and 0.24 are shown in Fig.4.11. The open circles indicate the real and imaginary parts of the experimental data; the solid lines indicate the real and imaginary parts calculated by the Drude model. A fairly good

agreement was found between the numerical and experimental data in ε_r' spectra. The obtained frequency dispersion parameters f_p, Γ_D, and f_0 are listed in table 1. Reliability factor R^2 indicates more than 0.90 for all samples showing the consistency of the fitting result. From table 4.1, the plasma frequency f_p, increases with increasing the Cu particle content from 14.5 GHz at x = 0.18 to 50.4 GHz at x = 0.30. Further, the damping constant Γ_D shows almost the same value at x = 0.18 and 0.20. However, x = 0.24 shows a small damping Γ_D.

Table 4.1. Frequency dispersion parameters for the permittivity spectrum of NiZnF/Cu for x = 0.18, 0.20 and 0.24 obtained by the numerical fitting

	Drude Model Parameters		Reliability Factor	Characteristic Frequency (Hz)	
x	f_p (Hz)	Γ_D	R^2	f_{0_Cal}	f_{0_Obs}
0.18	9.75 x 10^9	3.05 x 10^7	0.957	1.55 x 10^9	1.41 x 10^9
0.20	3.94 x 10^{10}	3.69 x 10^7	0.940	3.94 x 10^{10}	1.17 x 10^{10}
0.24	5.04 x 10^{10}	9.59 x 10^6	0.902	5.04 x 10^{10}	1.28 x 10^{10}

The characteristic frequency f_0 also increases with x, but the discrepancy between the $f_{0\_cal.}$ and $f_{0\_obs.}$ becomes large with increasing x. As discussed above in the case of FeNi/Cu composite, it is considered that the contribution of the dielectric resonance caused by the isolated Cu particle chain to the permittivity spectrum cannot be ignored when the Cu particle content increase in the percolated state. Hence the discrepancy between the fitted and observed ε_r'' spectrum at x = 0.20 and 0.24 as shown in Fig.4.11 might be attributed to this effect.

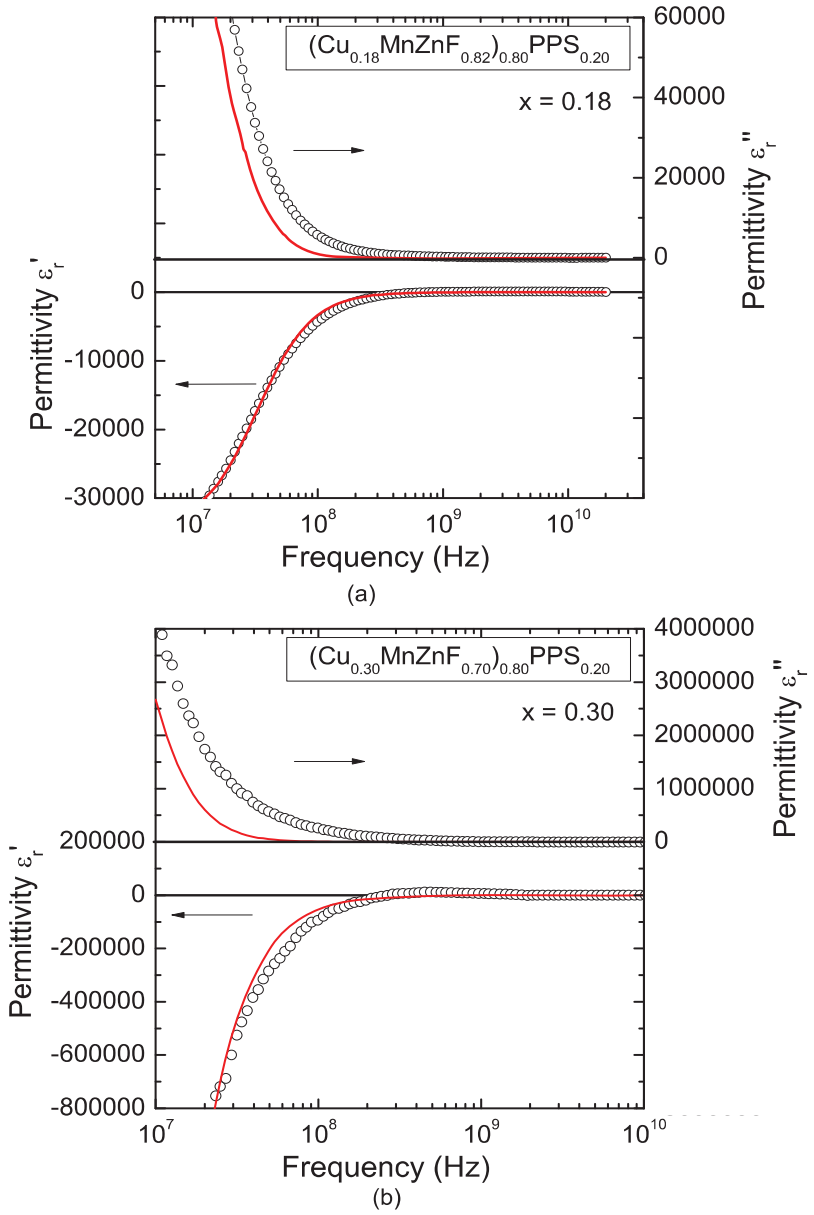

Figure 4.12. The numerical fitting of complex permittivity of $(Cu_xMnZnF_{1-x})_{0.80}PPS_{0.20}$ in the plasmonic state for x = 0.18 and x = 0.30. The open circles indicate the real and imaginary parts of the experimental data; the solid lines indicate the real and imaginary parts calculated by the Drude model.

The fitting results of $(Cu_xMnZnF_{1-x})_{0.80}PPS_{0.20}$ for x = 0.18 and 0.30 are shown in Fig.4.12(a) and 4.12(b) respectively. The open circles indicate the real and imaginary parts of the experimental data. The red solid lines indicate the real and imaginary parts calculated by the Drude model. The obtained frequency dispersion parameters f_p, Γ_D, and f_0 are listed in table 4.2. As shown in Fig. 4.12., there is a fairly good agreement between the numerical and experimental data in the ε_r' spectrum but a relatively large discrepancy exists between calculated and measured data in the imaginary part ε_r'' especially in the x = 0.30 sample. The reliability factor R^2 is 0.992 for x = 0.18 and 0.998 for x = 0.30 indicating a fairly good agreement between the numerical and experimental data in ε_r' spectra.

Table 4.2. Frequency dispersion parameters for the permittivity spectrum of MnZn/Cu for x = 0.18 and x = 0.24 obtained by the numerical fitting

	Drude Model Parameters		Reliability Factor	Characteristic Frequency (Hz)	
x	f_p (Hz)	Γ_D	R^2	f_{0_Cal}	f_{0_Obs}
0.18	6.09 x 10^9	3.29 x 10^7	0.992	9.70 x 10^8	7.38 x 10^8
0.30	2.33 x 10^{10}	1.22 x 10^7	0.998	3.71 x 10^9	2.75 x 10^9

The frequency dispersion of permittivity analysis of FeNi/Cu, FeCo/Cu, NiZnF/Cu and MnZn/Cu hybrid composite materialsthere by Drude and Lorentz models shows a fairly good agreement between numerical and experimental data in the ε_r' spectrum but a relatively large discrepancy exists between calculated and measured data in the imaginary part ε_r''. This indicates that the Kramers-Kroinig relations are not fulfiled. The Kramers-Kroining relations are

bidirectioal functions that connet the real and imaginary parts of an complex analytic function and the Kamers-Kroning relation of the usual plasma model do not take into account the dissipation. The origin of the discrepancy is not clear in this stage, but it might be attributed to the other dielectric energy dissipation process in the metal composite structure. The same situation of discrepancy between calculated and measured data in imaginary parte ε_r'' was reported[8]. The discrepancy was attributed to the large relative uncertainty error in the measurement of the imaginary permittivity. We also believe that the discrepancy in our date may be attributed to the measurement error uncertainty added to the fact that the ε_r'' spectrum was calculated using fitted parameters from real permittivity ε_r'.

4.4. Evaluation of low permittivity of NiZnF/Cu hybrid composite materials by Effective Cluster Model (ECM)

The variation of the low frequency permittivity of NiZnF/Cu composites with particle content was evaluated by the Effective Cluster Model (ECM) which was introduced by W.T. Doyle and I.S. Jacobs [9] using the Eq. (2.132). Fig.4.13 shows the absolute value of permittivity ε_r measured at 1 kHz as a function of volume fraction φ of NiZnF/Cu particles.

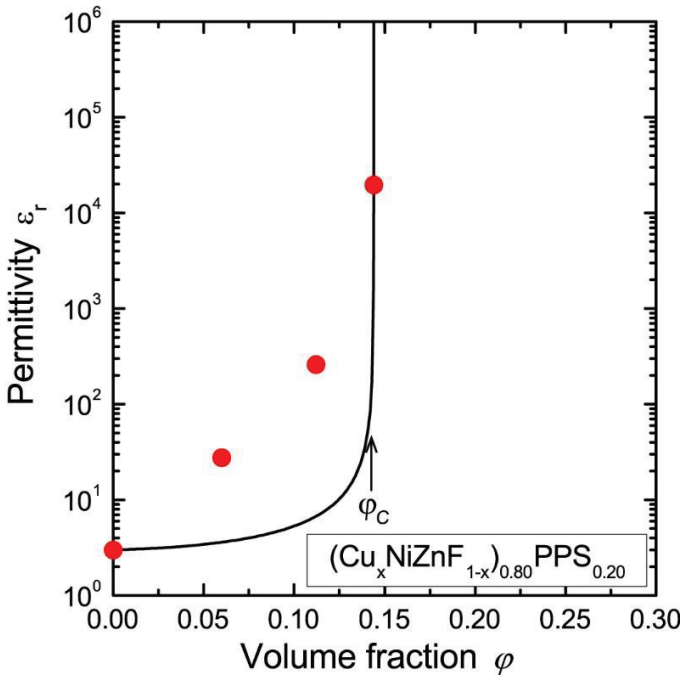

Figure 4.13. The absolute permittivity at 1 KHz of $(Cu_xNiZnF_{1-x})_{0.80}PPS_{0.20}$ as a function of particle content. Solid line indicates the calculatio curve obtained by the ECM

As shown in this figure, the ε_r shows a rapid increase near the percolation threshold φ_c indicating the insulator to metal transition. However, a relatively large discrepancy between experimental and numerical data is observed at φ = 0.06 and φ = 0.12. Since the ECM model used here is based on the spherical metal particle distribution in the host materials, the shape anisotropy of embedded particle should be taken into account [2, 10]. However, the qualitative variation of dielectric constant with particle content can be described by the ECM model for the NiZnF/Cu composite materials.

4.5.Complex permeability

The complex permeability spectra $\mu_r = \mu_r' - j\mu_r''$ as a function of frequency of FeNi/Cu, FeCoPPS/Cu, NiZnF/Cu and MnZnF/Cu hybid granular composite materilas are shown in Fig. 4.14(a), 4.15(a), 4.16(a) and 4.17(a) real parts μ_r' and imaginary parts μ_r'', Fig. 4.14(b), 4.15(b), 4.16(b) and 4.17(b).

The negative permeability spectrum in ferromagnetic materials can be realized by the Magnetic Resonance (MR) originated from Domain Wall Vibration (DWV) or Gyro Spin Rotation (GSR). Generally, the GSR in the alloy takes place in the X-band range about 6 to 9 GHz; DW resonance frequency is located below 1 GHz [11].

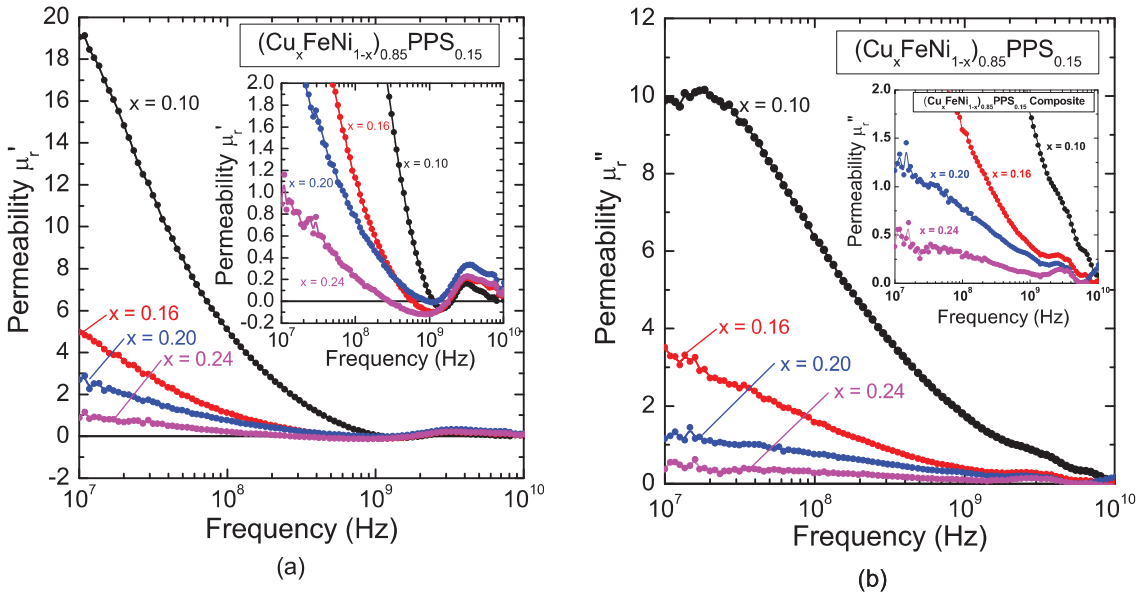

Figure 4.14. Relative complex permeability spectra of FeNi/Cu granular composite materials: ((a) real part μ_r' and (b) imaginary part μ_r'')). The insets is the expansion of the μ_r' and μ_r'' respectively.

Complex permeability spectra μ_r of the $(Cu_xFeNi_{1-x})_{0.85}PPS_{0.15}$ hybrid composite materials are shown in Fig.4.14.(a) real part μ_r' and 4.14(b) imaginary part μ_r''. The real part μ_r' at x = 0.10 is about 19 at 10 MHz and its imaginary part μ_r'' shows a maximum at around 25 MHz. Both μ_r' and μ_r'' decrease with increasing frequency. With the increase of Cu particle content x, which indicates the decrease of the $Fe_{53}Ni_{47}$ one, the permeability spectrum is suppressed by the eddy current effect; a rapid decrease in both μ_r' and μ_r'' can be observed at low frequency from 19 and 10 to 5 and 3.5 for x = 0.10 and x = 0.16. MNG spectrum in the frequency range from 200 MHz to 2.3 GHz in the percolated state takes place. Since the MNG property was observed at around 4 GHz in $Fe_{53}Ni_{47}$ composite materials [1], the negative permeability dispersion in FeNi/Cu composite materials below 1 GHz may be attributed mainly to the DWV mechanism. As shown in the inset of Fig.4.14(a), it seems that the negative μ_r' is enhanced in the plasmonic state by the increase of Cu fraction ratio; simultaneously, the negative μ_r' frequency range tends to shift lower from several GHz to several 100 MHz. This type of the MNG property was reported in the Fe/Al_2O_3 composites in RF rang [12].

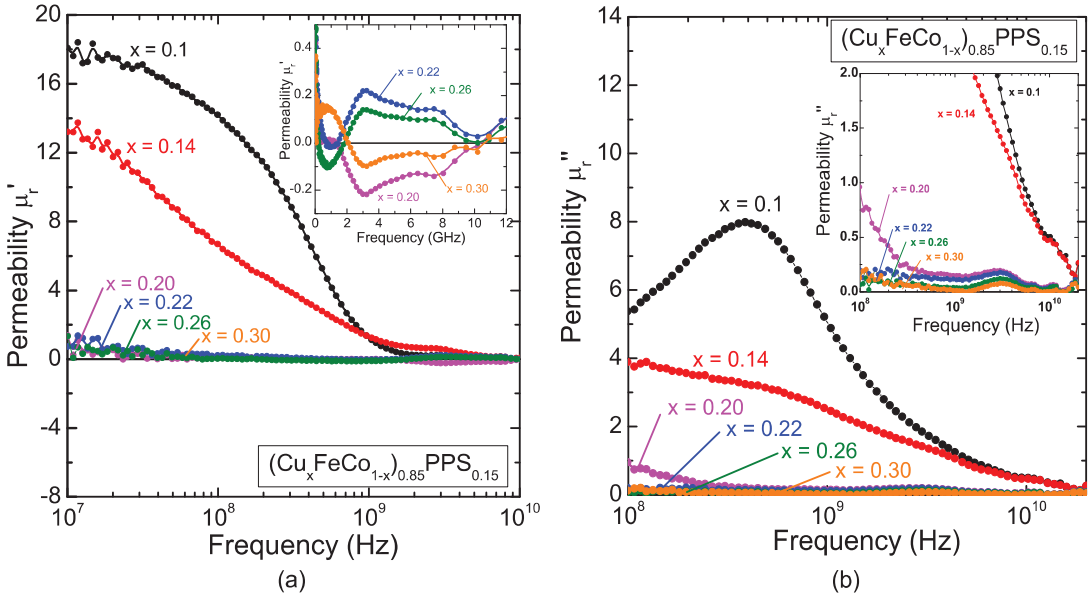

Figure 4.15. Relative complex permeability spectra of FeCo/Cu granular composite materials: ((a) real part μ_r' and (b) imaginary part μ_r'')). The insets is the expansion of the μ_r' and μ_r'' respectively.

Complex permeability spectra μ_r of the $(Cu_xFeCo_{1-x})_{0.85}PPS_{0.15}$ hybrid composite materials are shown in Fig.4.15.(a) real part μ_r' and 4.15(b) imaginary part μ_r''. The real part μ_r' shows broad frequency dispersion above 10 MHz and decreases with frequency. The low frequency μ_r' shows an abrupt decrease between x = 0.14 and 0.20 caused by the eddy current effect. The μ_r' spectrum shows a small negative permeability in the LFP state from x = 0.20 to 0.30 in the RF from 200 MHz to10 GHz. The imaginary part μ_r''. shows a broad maximum at 400 MHz for the x = 0.1 and 0.14, respectively. In the LFP state, both the μ_r' and μ_r''. are suppressed in the high frequency range. The negative frequency dispersion of permeability is attributed to the magnetic resonance caused by DWV and GRS in the ferromagnetic FeCo particles.

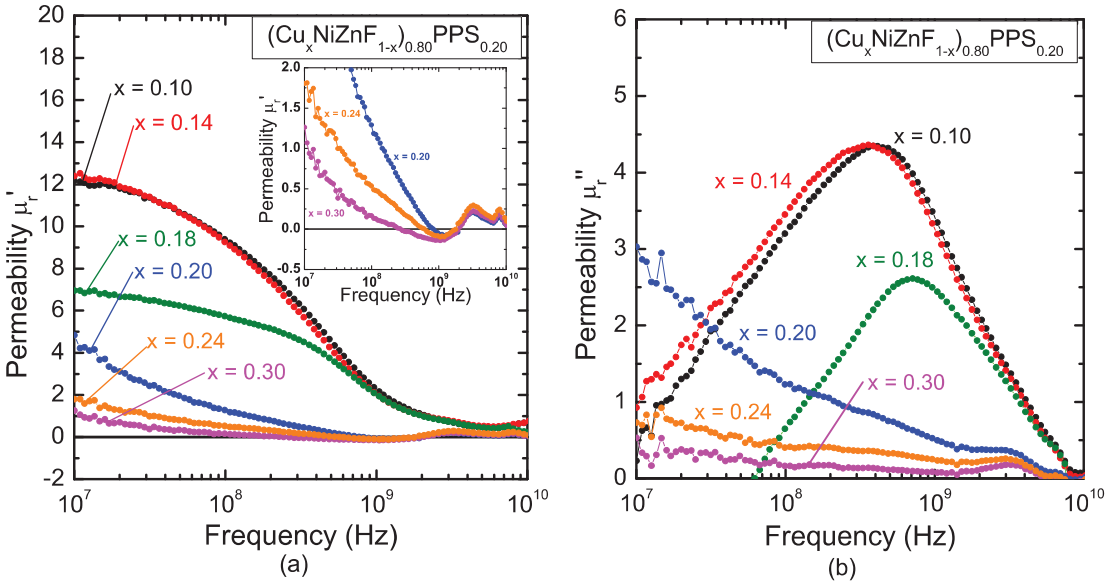

Figure 4.16. Relative complex permeability spectra of NiZnF/Cu granular composite materials: ((a) real part μ_r' and (b) imaginary part μ_r'')). The insets in (a) is the expansion of the μ_r' at percolated state.

Complex permeability spectra of NiZnF/Cu composite materials are shown in Fig.4.16, ((a) real part and (b) imaginary part). The real part μ_r' at 10 MHz is around 12 at x = 0.10 and x = 0.14; the imaginary part μ_r'' shows a broad maximum at around 400 MHz for the same Cu particle contents. The low frequency part of μ_r' decreases at the percolation threshold x = 0.18 and is entirely suppressed at x = 0.20 by the eddy current effect. The μ_r' decreases with frequency and shows a small negative value from x = 0.20 to 0.30 from 300MHz to 2 GHz frequency range. In the LFP state, both the μ_r' and μ_r'' are suppressed in the high frequency range. The negative frequency dispersion of permeability is attributed to the magnetic resonance caused by domain wall vibration and gyromagnetic spin rotation in the ferromagnetic NiZn ferrite particles [13, 14]. Since the second small frequency dispersion of permeability μ_r' can be recognized in several

GHz from the inset of Fig.4.16(a), this dispersion can be caused by GSR; a DW resonance is considered to take a role for the negative permeability dispersion around 1 GHz.

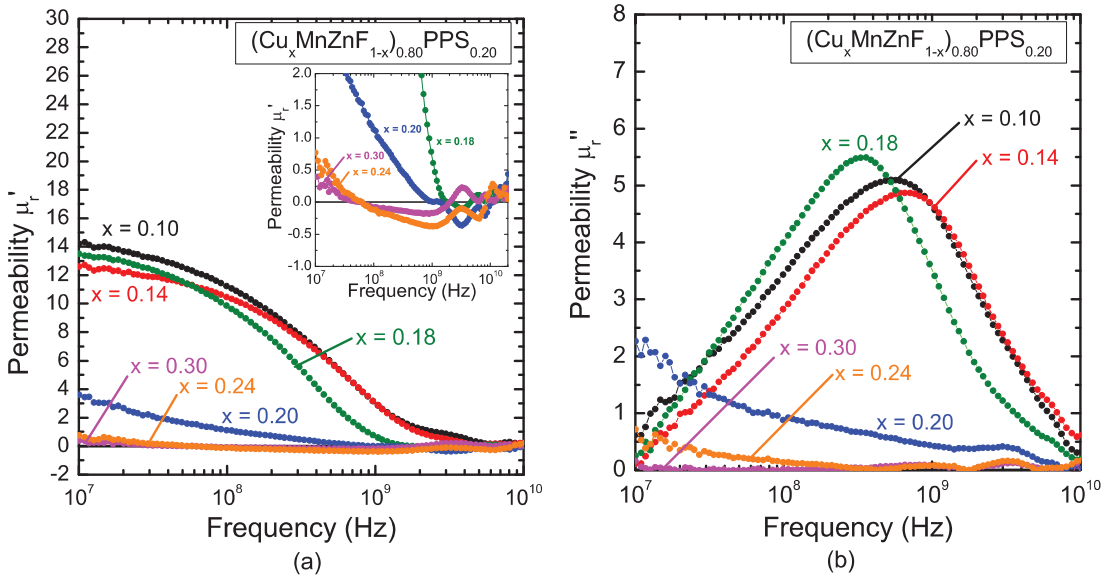

Figure 4.17. Relative complex permeability spectra of NiZnF/Cu granular composite materials: ((a) real part μ_r' and (b) imaginary part μ_r'')). The insets in (a) is the expansion of the μ_r' at percolated state.

Complex permeability spectra of MnZnF/Cu composite materials are shown in Fig.4.17, ((a) real part μ_r' and (b) imaginary part μ_r''). The real part μ_r' at 10 MHz shows a large value around 14 at x = 0.10, x = 0.14 and x = 0.18 composite samples; the imaginary part μ_r'' of permeability shows a broad maximum at around 350 MHz for x = 0.18 and 600 MHz for x = 0.10 and x = 0.14 samples. Above x = 0.14 Cu content the eddy current effect takes place and both μ_r' and μ_r'' rapidly decrease up to 0.25 for μ_r' and μ_r'' is almost zero at x = 0.30. The μ_r' shows a small negative value from x = 0.18 to 0.30 at 70 MHz to 10 GHz frequency range. In the MnZn/Cu

composite material both the μ_r' andμ_r'' are suppressed in the high frequency range. The negative frequency dispersion of permeability is attributed to the magnetic resonance caused by domain wall vibration and gyromagnetic spin rotation in the ferromagnetic NiZn ferrite particles [14].

The μ' and μ'' vary with frequency if some kind of resonance is induced at frequency f_0. Generally permeability drops off and magnetic loss increases in a very high frequency region because of the occurrence of a magnetic resonance. In ferrite with high permeability tends to have its permeability decrease at relatively low frequency. Snoek explains this fact in terms of the natural resonance or the resonance of rotation magnetization under the action of the anisotropy field. The anisotropy plays a relevant role in ferromagnetic, without it the materials is super paramagnetic.

The magnetic loss in NiFe/Cu and FeCo/Cu is higher compare to the loss in NiZnF/Cu and MnZn/Cu. The magnetic loss can be attributed to the Eddy current effect. The eddy current loss is high in magnetic metals and alloys than in the ferrite. The inclusion of Fe particles results in a decrease in resistivity associated the fact that the composites are mixed with metallic Cu particles, results in increase of eddy current loss

The negative frequency dispersion of permeability of FeNi/Cu composite materials is attributed to the DWV of ferromagnetic particles since is located below 1 GHz and DWV and GRS of ferromagnetic particles in FeCo/Cu, and MnZnF/Cu particles since the negative permeability is located above 1 GHz [15-17]. Interestingly, where the composite materials shows a negative permeability μ_r' spectrum, the μ_r'' spectra for the same content indicate a small maximum in this same frequency range.

.

4.6. DNG Characteristic

From the complex permittivity and permeability spectra indicated in Fig.4.5, 4.6, 4.7, 4.8 and Fig. 4.14, 4.15, 4.16, 4.17, the DNG property where ε_r' and μ_r' are overlapped, was observed in the FeNi/Cu, FeCo/Cu, NiZnF/Cu and MnZn/Cu hybrid granular composites materials

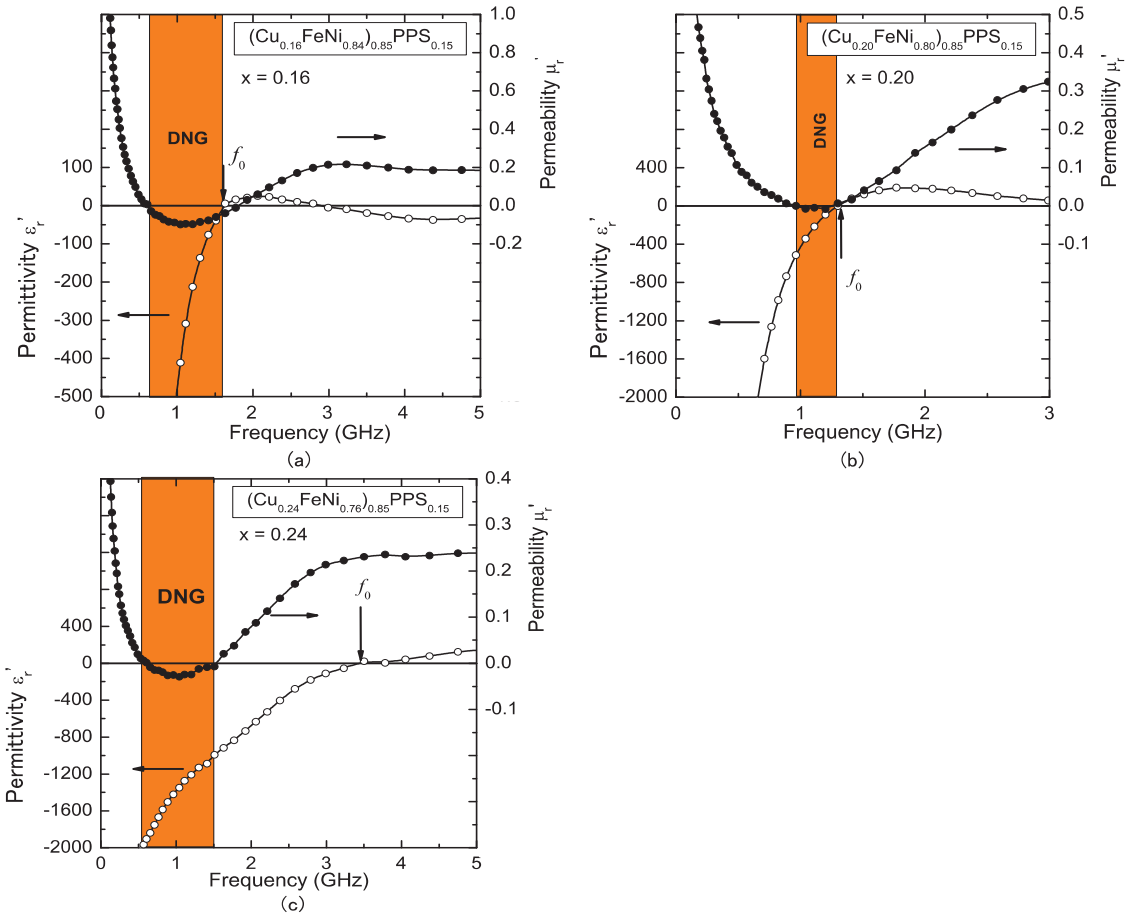

Figure 4.18. Real part of the relative complex permittivity and permeability spectra of the $(Cu_xFeNi_{1-x})_{0.85}PPS_{0.15}$ composite materials and the DNG characteristic

The DNG spectra ε_r' and μ_r' are summarized in Fig.4.18. For the x = 0.16 sample, Fig.4.18(a), $(Cu_{0.16}FeNi_{0.84})_{0.85}PPS_{0.15}$, the ENG character is obtained below f_0 = 1.6 GHz; simultaneously the MNG range locates between 600 MHz and 2 GHz. Hence, the DNG property

is realized in the frequency range from 600 MHz to 1.6 GHz. In the $(Cu_{0.20}FeNi_{0.80})_{0.85}PPS_{0.15}$ composite, x = 0.2 the characteristic frequency f_0 locates at 1.25 GHz; the MNG frequency range is from 0.95 to 1.25 GHz. Thus the DNG band is from 0.95 to 1.25 GHz which is narrow. Further, the $(Cu_{0.24}FeNi_{0.76})_{0.85}PPS_{0.15}$ composite (x = 0.24) shows the DNG property in the frequency range from 550 MHz to 1.5 GHz. Since the f_0 locates at 3.5 GHz in this composition, the whole MNG range is in the DNG state. The DNG characteristic can be realized in the sub microwave frequency range from 500 MHz to 1.6 GHz in the FeNi/Cu composite materials.

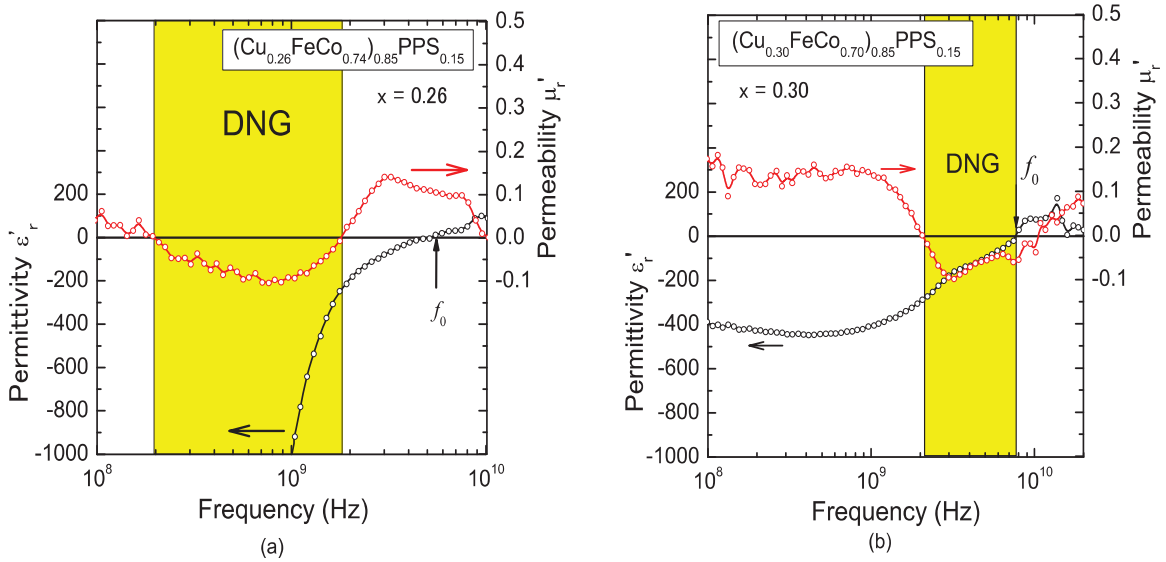

Figure 4.19. Real part of the relative complex permittivity and permeability spectra of the composite material $(Cu_xFeCo_{1-x})_{0.85}PPS_{0.15}$ and the DNG characteristic

The DNG property of the FeCo/Cu hybrid composites x = 0.26 and 0.30 are shown in Fig.4.19. From the ε_r' and μ_r' spectra of $(Cu_{0.26}FeCo_{0.74})_{0.85}PPS_{0.15}$ composite, the ENG characteristic was observed below f_0 = 5.12 GHz; simultaneously the MGN range locates between 195 MHz to 1.77 GHz. In the $(Cu_{0.30}FeCo_{0.70})_{0.85}PPS_{0.15}$ composite, the ENG

characteristic is located below f_0 = 7.45 GHz; the MNG characteristic appears between 2.06 GHz and 8.03 GHz; the DNG is located in frequency range from 2.06 GHz to 7.45 GHz. Hence the DNG characteristic is realized in the sub microwave and X-band range in the FeCo/Cu hybrid composite materials.

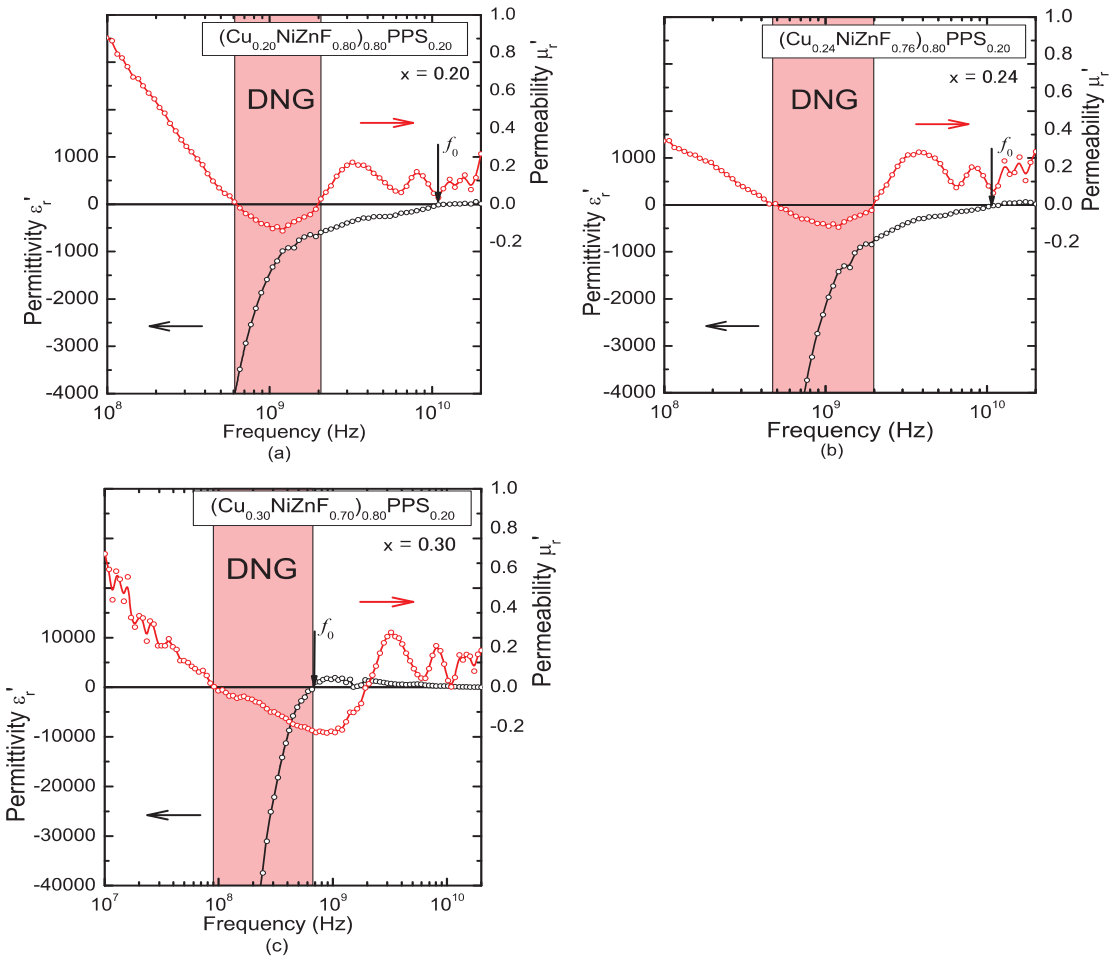

Figure 4.20. Double negative (DNG) permittivity and permeability spectra of $(Cu_xNiZn_{1-x})_{0.80}PPS_{0.20}$

Double negative electromagnetic property of the NiZnF/Cu hybrid composites at x = 0.20, 0.24 and 0.30 are shown in Fig.4.20. From the ε_r' and μ_r' spectra, the composites have negative

values of both ε_r' and μ_r' in the DNG band from 610 MHz to 2 GHz for the ($Cu_{0.20}$ NiZn-$F_{0.80}$)$_{0.80}$$PPS_{0.20}$, from 544 MHz to 1.98 GHz for the ($Cu_{0.24}$ $NiZnF_{0.76}$)$_{0.80}$$PPS_{0.20}$ and from 105 to 686 MHz for ($Cu_{0.30}$ $NiZnF_{0.70}$)$_{0.80}$$PPS_{0.20}$ composite materials, respectively. The DNG characteristic can be realized in the sub microwave for NiZn/Cu hybrid composite materials.

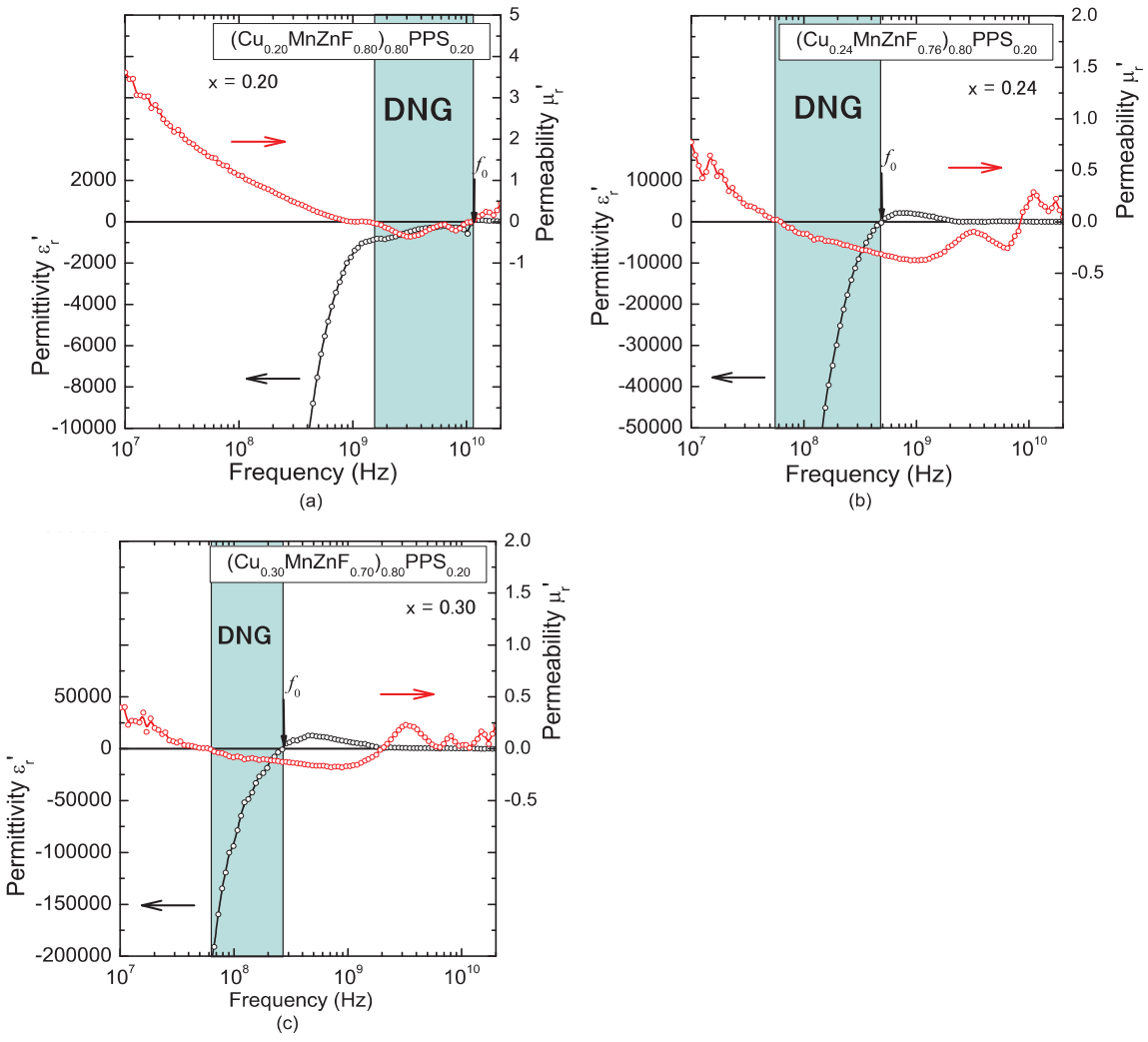

Figure 4.21. Double negative (DNG) permittivity and permeability spectra of (Cu_xNiZn_{1-x})$_{0.80}$$PPS_{0.20}$

Double negative electromagnetic property of the MnZnF/Cu hybrid composites at x = 0.20, 0.24 and 0.30 are shown in Fig.4.21. The $(Cu_{0.20}$ NiZn-$F_{0.80})_{0.80}PPS_{0.20}$, x = 0.20 shows the DNG charecteristic in the frequency range from 1.41 GHz to 10.9 GHz, from 57.8 MHz to 527 MHz for the $(Cu_{0.24}$ $NiZnF_{0.76})_{0.80}PPS_{0.20,}$ x = 0.24 and from 62 MHz to 285 MHz for $(Cu_{0.30}$ $NiZnF_{0.70})_{0.80}PPS_{0.20,}$ x = 0.30 composite materials, respectively. Hence the DNG characteristic is realized in the sub microwave and X-band range in the MnZnF/Cu hybrid composite materials.

Since the ENG spectrum is realized by the low frequency plasma oscillation of conduction electrons in the percolated Cu cluster chain, ENG can be obtained in the wide frequency range below f_0 and the negative ε_r' value can become large in the low frequency range. Meanwhile, since the MNG spectrum is obtained by the magnetic resonance in the ferromagnetic particle, the negative μ_r' band is narrow and its value is relatively small. There is a possibility to control the DNG band by changing the Cu and ferromagnetic particles content ratio in the granular composite structure.

References

[1] H. Massango, T. Tsutaoka, T. Kasagi, Electromagnetic properties of Fe53Ni47 nd Fe53Ni47/Cu granular composite materials in the microwave range, Mater. Res. Express, 3 (2016).

[2] T. Kasagi, T. Tsutaoka, K. Hatakeyama, Electromagnetic properties of Permendur granular composite materials containing flaky particles, J Appl Phys, 116 (2014) 153901.

[3] T. Tsutaoka, T. Kasagi, S. Yamamoto, K. Hatakeyama, Low frequency plasmonic state and negative permittivity spectra of coagulated Cu granular composite materials in the percolation threshold, Applied Physics Letters, 102 (2013) 181904.

[4] T. Tsutaoka, K. Fukuyama, H. Kinoshita, T. Kasagi, S. Yamamoto, K. Hatakeyama, Negative permittivity and permeability spectra of Cu/yttrium iron garnet hybrid granular composite materials in the microwave frequency range, Applied Physics Letters, 103 (2013) 261906.

[5] Z.-d. Zhang, R.-h. Fan, Z.-c. Shi, S.-b. Pan, K.-l. Yan, K.-n. Sun, J.-d. Zhang, X.-f. Liu, X.L. Wang, S.X. Dou, Tunable negative permittivity behavior and conductor–insulator transition in dual composites prepared by selective reduction reaction, Journal of Materials Chemistry C, 1 (2013) 79.

[6] S.T. Chui, L. Hu, Theoretical investigation on the possibility of preparing left-handed materials in metallic magnetic granular composites, Physical Review B, 65 (2002) 144407.

[7] A.N. Lagarkov, S.M. Matytsin, K.N. Rozanov, A.K. Sarychev, Dielectric properties of fiber-filled composites, J Appl Phys, 84 (1998) 3806-3814.

[8] L.Liu, S. Matitsine, Y. B. Gan, L. F. Chen, L.B. Kong, Frequency dependence of effective permittivity of carbon nanotube composites, J Appl Phys, 101 (2007).

[9] W.T. Doyle, I.S. Jacobs, Effective cluster model of dielectric enhancement in metal-insulator composites, Physical review. B, Condensed matter, 42 (1990) 9319-9327.

[10] W.T. Doyle, I.S. Jacobs, The Influence of Particle-Shape on Dielectric Enhancement in Metal-Insulator Composites, J Appl Phys, 71 (1992) 3926-3936.

[11] T. Kasagi, T. Tsutaoka, K. Hatakeyama, Negative permeability spectra in Permalloy granular composite materials, Applied Physics Letters, 88 (2006) 172502.

[12] K. Sun, R.H. Fan, Z.D. Zhang, K.L. Yan, X.H. Zhang, P.T. Xie, M.X. Yu, S.B. Pan, The tunable negative permittivity and negative permeability of percolative Fe/Al2O3 composites in radio frequency range, Applied Physics Letters, 106 (2015) 172902.

[13] T. Nakamura, T. Tsutaoka, K. Hatakeyama, Frequency dispersion of permeability in ferrite composite materials, J Magn Magn Mater, 138 (1994) 319-328.

[14] T. Tsutaoka, T. Kasagi, K. Hatakeyama, M.Y. Koledintseva, Analysis of the Permeability Spectra of Spinel Ferrite Composites Using Mixing Rules, in: IEEE International Symposium on Electromagnetic Compatibility, , IEEE, Denver, 2013, pp. 545 - 550.

[15] T. Tsutaoka, T. Kasagi, K. Hatakeyama, Permeability spectra of Yittrium Iron Garnet and its granular composite materials under dc magnetic field, J Appl Phys, 110 (2011) 053909.

[16] Teruhiro Kasagi, Takanori Tsutaoka, A. Tsurunaga, High-frequency Permeability of Fe-Co and Co Composite Materials, Journal of the Korean Physical Society, 62 (2013) 2113 - 2117.

[17] T. Tsutaoka, T. Ono, A. Tsurunaga, T. Kasagi, K. Hatakeyama, M.Y. Koledintseva, High Frequency Permeability of Fe-Al-Si Granular Compopsite Materials, in: IEEE International Symposium on Electromagnetic Compatibility, IEEE EMC Society, Long beach, USA, 2011, pp. 78-83.

[18] Z.-c. Shi, R.-h. Fan, K.-l. Yan, K. Sun, M. Zhang, C.-g. Wang, X.-f. Liu, X.-h. Zhang, Preparation of Iron Networks Hosted in Porous Alumina with Tunable Negative Permittivity and Permeability, Advanced Functional Materials, 23 (2013) 4123-4132.

[19] Z.C. Shi, R.H. Fan, Z.D. Zhang, K.L. Yan, X.H. Zhang, K. Sun, X.F. Liu, C.G. Wang, Experimental realization of simultaneous negative permittivity and permeability in Ag/Y3Fe5O12 random composites, Journal of Materials Chemistry C, 1 (2013) 1633-1637.

[20] X.-a. Wang, Z.-c. Shi, M. Chen, R.-h. Fan, K.-l. Yan, K. Sun, S.-b. Pan, M.-x. Yu, Tunable Electromagnetic Properties in Co/Al2O3 Cermets Prepared by Wet Chemical Method, J Am Ceram Soc, 97 (2014) 3223-3229.

[21] K. Sun, Z.-d. Zhang, R.-h. Fan, M. Chen, C.-b. Cheng, Q. Hou, X.-h. Zhang, Y. Liu, Random copper/yttrium iron garnet composites with tunable negative electromagnetic parameters prepared by in situ synthesis, RSC Adv., 5 (2015) 61155-61160.

Chapter 5: Conclusion

In this study, the electromagnetic properties of FeNi ($Fe_{53}Ni_{47}$), FeCo ($Fe_{50}Co_{50}$); Ferrite Ni-Zn ($Ni_{0.24}Zn_{0.65}Fe_{2.04}O_4$), Mn-Zn ($Mn_{0.55}Zn_{0.41}Fe_{2.06}O_4$) combining with cupper powder Cu forming a hybrid composite materials were investigated in the microwave frequency range up to 20 GHz. The composition of the selected hybrid granular composites is denoted by $(A_xB_{1-x})_yPPS_{1-y}$, where x is the volume fraction of A in the AB hybrid particle and y indicates the total volume fraction of embedded particles $y = 0.85$ in the case of FeCo/Cu and FeNi/Cu and 0.80 for NiZnF/Cu and MnZnF/Cu granular composite materials. Toroidal samples with inner diameter of 3 mm and 7 mm of outer diameter were prepared. The relative complex permittivity ε_r and permeability μ_r of the composite materials were measured by the two port call, transmission/reflection method using a coaxial line cell and a network analyzer (Agilent E5071C) in the frequency range from 10 MHz to 20 GHz [1]. The electrical conductivity of was measured by the two terminal method using an impedance analyzer (HP4194A) in the frequency range from 1 kHz to 40 MHz.

From the electrical conductivity measurements, FeNi/Cu and FeCo/Cu shows metallic properties even in the lowest Cu particle content with conductivity above 1 S/cm indicading that the composite is in the percolated state. The electrical conductivity is determined by the combination of Cu and ferromagnetic particl. However since the ferrite particles NiZn and MnZn have insolate electric properties the hybrid composites NiZnF/Cu and MnZnF/Cu, showed dielectric properties at low Cu particle content increasing with Cu particles. Hence, the electrical conductivity of these composite materials is determined by Cu content.

From the permittivity analysis, the plasmonic state with ENG was achieved in all combination of granular composite materials. With the increase of Cu particle content, the negative permittivity was enhanced; the characteristic frequency shifts to the higher frequency. Simultaneously, higher Cu content leads to the increase of imaginary part of the permittivity caused by the conductivity loss. The frequency dispersion of permittivity was evaluated by the numerical fitting of the measuring complex permittivity using Drude model for metals and Lorentz model for dielectrics. A fairly good agreement between numerical and experimental data in the real part of the permittivity dspersion was found but a relatively large discrepancy exists between calculated and measured data in the imaginary part. The variation of the low frequency permittivity of NiZnF/Cu composites with particle content was evaluated by the Effective Cluster Model by W.T. Doyle and I.S. Jacobs[2]. The relative complex permittivity showed a rapid increase near the percolation threshold as predicted by the model.

A typical frequency dispersion was observed in the magnetic permeability spectrum; a broad maximum of the imaginary part of permeability indicates the existence of the magnetic resonance by the domain wall vibration and gyromagnetic spin rotation. The MNG spectrum due to magnetic resonance was also realized in all combination of granular composite materials. The composites showed magnetic loss due to the eddy current effect. The loss is high in magnetic metals and alloys than in the ferrite.

The DNG characteristic was realized in the absence of external magnetic field from the sub microwave range to about 1.6 GHz and 2 GHz in the FeNi/Cu and NiZnF/Cu hybrid composite materials respectively. While the DNG characteristic was realized in the sub microwave and X-band range in the FeCo/Cu and MnZnF/Cu hybrid composite materials in frequency range up to 10 GHz. The DNG characteristic was realized in the absence of external magnetic field. The

DNG characteristic has also been observed in other metal ferromagnetic hybrid granular composites materials, where the DNG band locates in sub microwave range up to 1 GHz [3-7].

The composite materials in this study have relatively high conductive loss (imaginary part of permittivity shows a large value) in the percolation-induced LFP state in around the DNG band. Electromagnetic wave energy can be easily dissipated in these materials. This indicates that the transmission of the electromagnetic wave through the composite at the DNG band can become small. Hence, the negative permittivity characteristic can be utilized for the construction of meta-surface with the frequency selective transmission property [8]; The electromagnetic wave shielding or absorbing applications can be considered to use these DNG composites as well as the negative refraction materials. The quasi-isotropic Negative Refractive Index (NRI) or Zero Index Material (ZIM) can be realized using the DNG granular composite materials[7, 9]. The calculated NRI spectrum for the x = 0.24 in $(Cu_xFeNi_{1-x})_{0.85}PPS_{0.15}$ composite is presented in Appendix B.

References

[1] A.M. Nicolson, G.F. Ross, Measurement of the Intrinsic Properties of Materials by Time-Domein Techniques, IEEE Transactions on Instrumentation and Measurement, IM-19 (1970) 377-382.

[2] W.T. Doyle, I.S. Jacobs, Effective cluster model of dielectric enhancement in metal-insulator composites, Physical review. B, Condensed matter, 42 (1990) 9319-9327.

[3] Z.-c. Shi, R.-h. Fan, K.-l. Yan, K. Sun, M. Zhang, C.-g. Wang, X.-f. Liu, X.-h. Zhang, Preparation of Iron Networks Hosted in Porous Alumina with Tunable Negative Permittivity and Permeability, Advanced Functional Materials, 23 (2013) 4123-4132.

[4] Z.C. Shi, R.H. Fan, Z.D. Zhang, K.L. Yan, X.H. Zhang, K. Sun, X.F. Liu, C.G. Wang, Experimental realization of simultaneous negative permittivity and permeability in Ag/Y3Fe5O12 random composites, Journal of Materials Chemistry C, 1 (2013) 1633-1637.

[5] X.-a. Wang, Z.-c. Shi, M. Chen, R.-h. Fan, K.-l. Yan, K. Sun, S.-b. Pan, M.-x. Yu, Tunable Electromagnetic Properties in Co/Al2O3 Cermets Prepared by Wet Chemical Method, J Am Ceram Soc, 97 (2014) 3223-3229.

[6] K. Sun, Z.-d. Zhang, R.-h. Fan, M. Chen, C.-b. Cheng, Q. Hou, X.-h. Zhang, Y. Liu, Random copper/yttrium iron garnet composites with tunable negative electromagnetic parameters prepared by in situ synthesis, RSC Adv., 5 (2015) 61155-61160.

[7] T. Tsutaoka, K. Fukuyama, H. Kinoshita, T. Kasagi, S. Yamamoto, K. Hatakeyama, Negative permittivity and permeability spectra of Cu/yttrium iron garnet hybrid granular composite materials in the microwave frequency range, Applied Physics Letters, 103 (2013) 261906.

[8] N.I. Landy, S. Sajuyigbe, J.J. Mock, D.R. Smith, W.J. Padilla, Perfect metamaterial absorber, Phys Rev Lett, 100 (2008) 207402.

[9] T. Tsutaoka, H. Massango, T. Kasagi, S. Yamamoto, K. Hatakeyama, Double negative electromagnetic properties of percolated Fe53Ni47/Cu granular composites, Applied Physics Letters, 108 (2016) 191904.

Appendix A: Electromagnetic properties of FeNi/Cu composite materials at y = 0.70

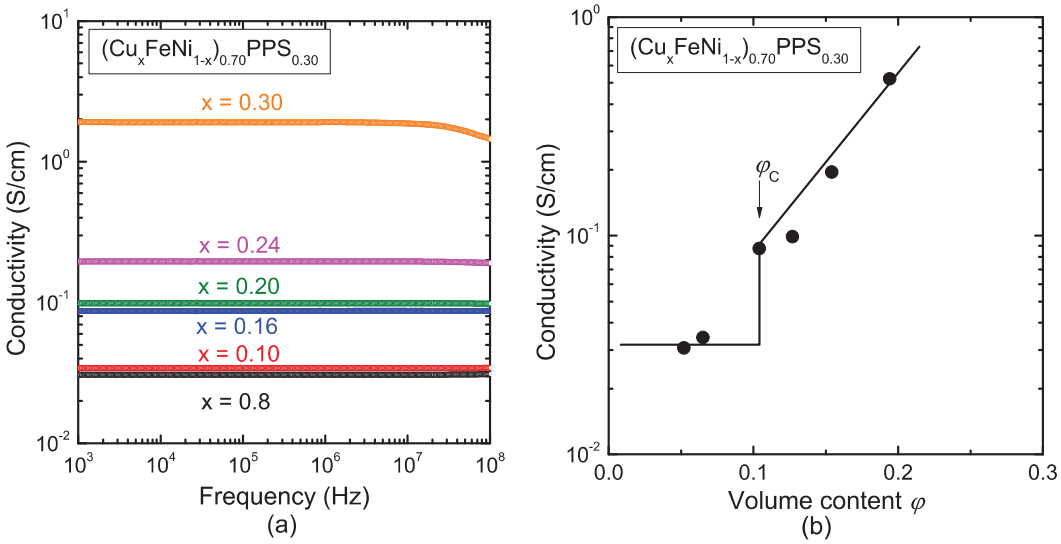

Electrical conductivity spectra of FeNi/Cu granular composite materials as a function of frequency (a) and the electrical conductivity at 1 KHz as a function of the volume fraction φ (b)

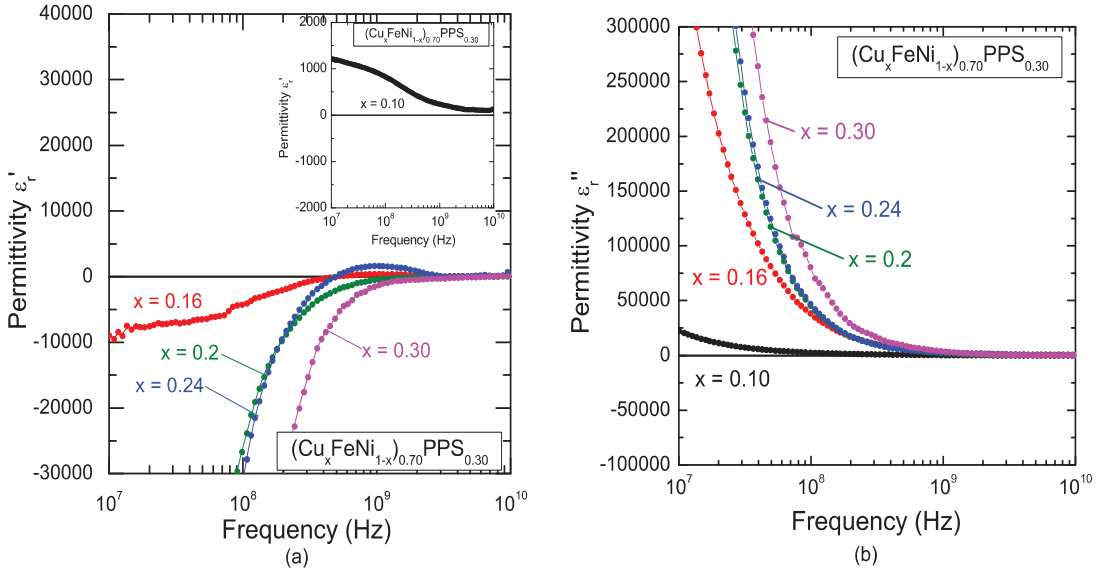

Relative complex permittivity spectra of FeCo/Cu granular composite materials: ((a) real part ε_r' and (b) imaginary part ε_r''). The inset of the (a) is the expansion of the ε_r'

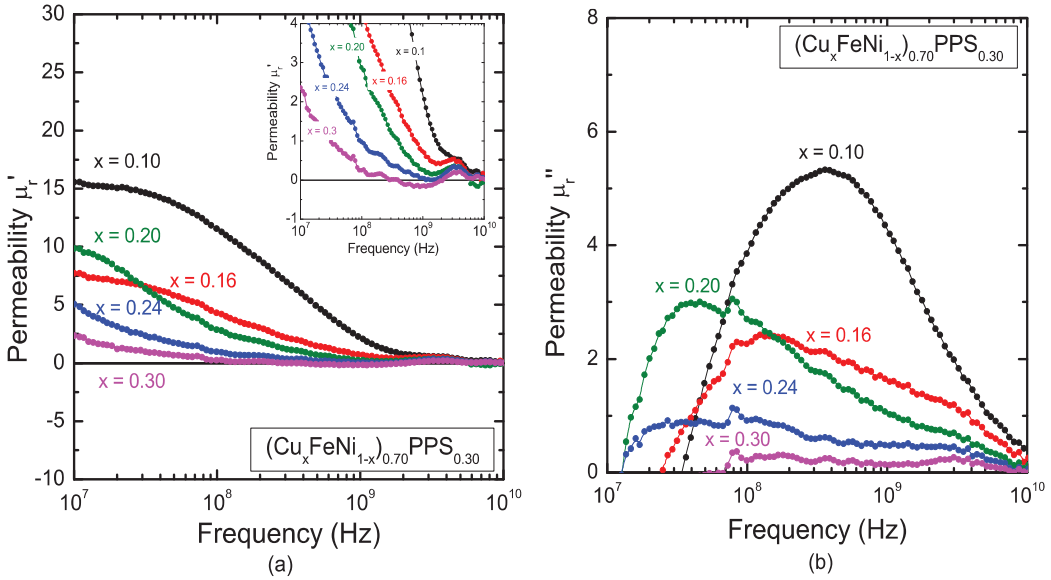

Relative complex permeability spectra of FeNi/Cu granular composite materials: (a) real part μ_r' and (b) imaginary part μ_r''. The inset is the expansion of the μ_r'

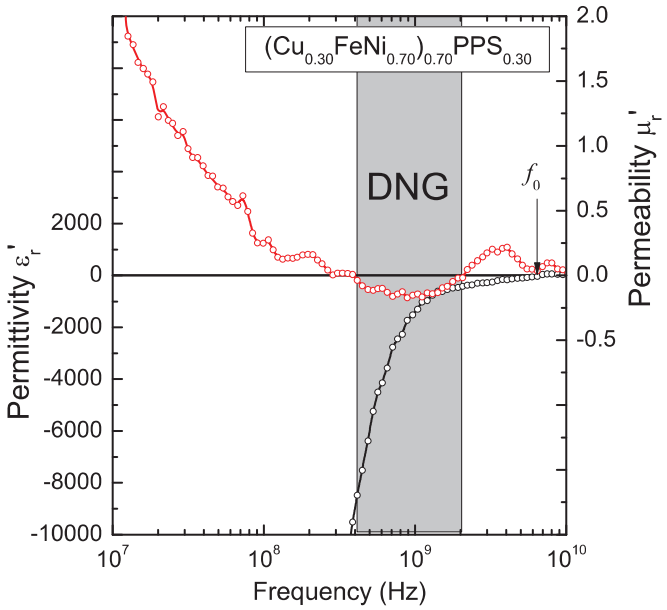

Real part of the relative complex permittivity and permeability spectra of the $(Cu_xFeNi_{1-x})_{0.85}PPS_{0.15}$ composite materials and the DNG characteristic

Appendix B: Relative refractive index n_r of FeNi/Cu Composite materials

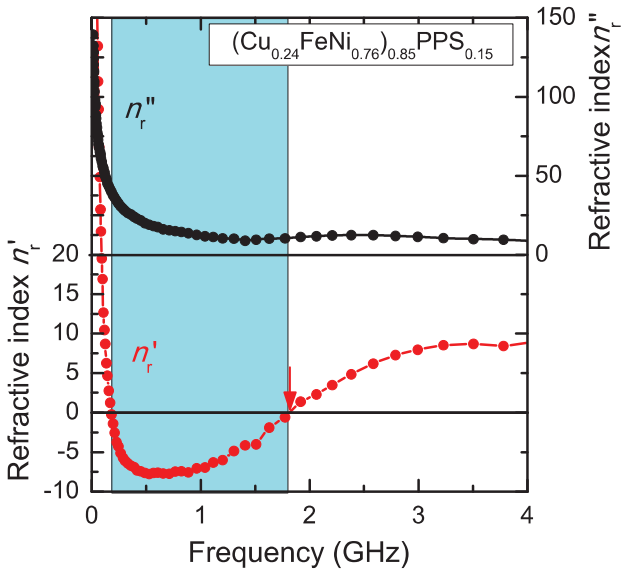

$$n = \sqrt{\varepsilon_r \mu_r} = \sqrt{(\varepsilon_r' - j\varepsilon_r'')(\mu_r' - j\mu_r'')}$$

$$n = \sqrt{(\varepsilon_r'\mu_r' - \varepsilon_r''\mu_r'') - j(\varepsilon_r'\mu_r'' - \varepsilon_r''\mu_r')}$$

Putting

$$a = \varepsilon_r'\mu_r' - \varepsilon_r''\mu_r''$$

$$n = \sqrt{a + jb}$$

$$b = \varepsilon_r'\mu_r'' - \varepsilon_r''\mu_r'$$

We can get,

$$n = n_r' - n_r''$$

$$n = \pm\left(\frac{\sqrt{a+\sqrt{a^2+b^2}}}{\sqrt{2}} - \frac{\sqrt{-a+\sqrt{a^2+b^2}}}{\sqrt{2}}\right)$$